

Electronic Thesis and Dissertation Repository

---

8-20-2014 12:00 AM

## Factors Affecting Bed Agglomeration in Bubbling Fluidized Bed Biomass Boilers

Alejandro Montes, *The University of Western Ontario*

Supervisor: Dr Chunbao (Charles) Xu, *The University of Western Ontario*

A thesis submitted in partial fulfillment of the requirements for the Master of Engineering Science degree in Chemical and Biochemical Engineering

© Alejandro Montes 2014

Follow this and additional works at: <https://ir.lib.uwo.ca/etd>

 Part of the [Chemical Engineering Commons](#)

---

### Recommended Citation

Montes, Alejandro, "Factors Affecting Bed Agglomeration in Bubbling Fluidized Bed Biomass Boilers" (2014). *Electronic Thesis and Dissertation Repository*. 2325.  
<https://ir.lib.uwo.ca/etd/2325>

This Dissertation/Thesis is brought to you for free and open access by Scholarship@Western. It has been accepted for inclusion in Electronic Thesis and Dissertation Repository by an authorized administrator of Scholarship@Western. For more information, please contact [wlsadmin@uwo.ca](mailto:wlsadmin@uwo.ca).

FACTORS AFFECTING BED AGGLOMERATION IN BUBBLING FLUIDIZED BED  
BIOMASS BOILERS

(Thesis format: Integrated Article)

by

Alejandro Montes

Graduate Program in Chemical and Biochemical Engineering

A thesis submitted in partial fulfillment  
of the requirements for the degree of  
Master of Science

The School of Graduate and Postdoctoral Studies  
The University of Western Ontario  
London, Ontario, Canada

© Alejandro Montes 2014

## Abstract

Agglomeration of bed materials at high temperature is one of the most important and challenging problems for fluidized-bed biomass boilers for thermal/power generation. Inorganic alkali components from the fuel can be problematic as they form low-melting alkali compounds. In the present study, the critical amount of liquid (molten ash in real biomass boiler operations) that would result in severe bed agglomeration and defluidization was studied in two small pilot-scales bubbling fluidized bed (BFB) rigs, one operated at room temperature using glycerol-water to simulate molten ash and the other operated at elevated temperatures using low melting-point salt (KOH) to simulate molten ash. It was found that in the fluidization systems studied the critical liquid amount causing bed agglomeration is likely 0.2-0.5 wt% (in relation to the weight of bed material loaded) and 0.7-0.8 wt% would cause severe channeling and very poor fluidization conditions.

**Keywords:** *fluidization, agglomeration, bed material, biomass, bubbling fluidized bed.*

## Co-Authorship Statement

### Chapter 3

<b>Article Title:</b> Study on the critical amount of liquid for bed materials agglomeration in a bubbling fluidized bed
<b>Authors:</b> Alejandro Montes, Majid Hamidi, Cedric Briens, Franco Berruti, Chunbao (Charles) Xu and Honghi Tran.
<b>Status:</b> To be submitted to Chemical Engineering Science journal
<b>Contribution:</b> Experimental work and data analysis were performed by Alejandro Montes and Majid Hamidi. Majid Hamidi developed all the capacitance sensors system. Chunbao (Charles) Xu, Honghi Tran, Cedric Briens and Franco Berruti provided general guidance, consultation regarding experimental work and interpretation of results. The manuscript draft was written and revised by Alejandro Montes, and reviewed by Chunbao (Charles) Xu and Honghi Tran.

### Chapter 4

<b>Article Title:</b> Study of bed materials agglomeration in a heated bubbling fluidized bed (BFB) using silica sand as the bed material and KOH to simulate molten ash
<b>Authors:</b> Alejandro Montes, Chunbao (Charles) Xu and Honghi Tran
<b>Status:</b> To be submitted to AIChE Journal
<b>Contribution:</b> Experimental work and data analysis were performed by Alejandro Montes. Chunbao (Charles) Xu, and Honghi Tran provided general guidance, consultation regarding experimental work and interpretation of results. The manuscript draft was written and revised by Alejandro Montes, and reviewed by Chunbao (Charles) Xu and Honghi Tran.

## Chapter 5

<b>Article Title:</b> Fusion behavior of synthetic and real biomass ashes – Effects of potassium
<b>Authors:</b> Alejandro Montes, Chunbao (Charles) Xu and Honghi Tran
<b>Status:</b> To be submitted to Applied Energy
<b>Contribution:</b> Experimental work and data analysis were performed by Alejandro Montes. Chunbao (Charles) Xu, and Honghi Tran provided general guidance, consultation regarding experimental work and interpretation of results. The manuscript draft was written and revised by Alejandro Montes, and reviewed by Chunbao (Charles) Xu and Honghi Tran.

## Acknowledgments

I would like to express my deepest appreciation to my supervisors, Dr Chunbao (Charles) Xu and Dr. Honghi Tran, for their excellent guidance, encouragement and continuous support during my studies. Their research experience and mentorship has been crucial to successfully complete this master program. I would like to thank Majid Hamidi, Malaya Nanda and Melissa Price (University of Windsor) for all their help, support and all their valuable technical advices in some part of my experimental work.

I would like to acknowledge the industrial support from various pulp and paper companies and the Natural Sciences and Engineering Research Council of Canada (NSERC) via the Discovery Grants, for their financial support for this project and my master studies.

I also want to extend my gratitude to the faculty and staff of Institute for Chemical and Fuels from Alternative Resources (ICFAR) and Chemical and Biochemical Engineering Department for providing support and education during my studies.

Many thanks to Dr. Dimitre Karamanev, Dr. Anand Prakash and Dr. Liyang Jiang for kindly serving on my thesis examination committee, and for reviewing my thesis.

Special thanks to my lovely wife and my son for their support, constant encouragement and understanding when I was busy working. Finally, I would like to thank my family and friends for their support and encouragement.

# Table of Contents

Abstract.....	ii
Co-Authorship Statement.....	iii
Acknowledgments.....	v
Table of Contents.....	vi
List of Tables.....	x
List of Figures.....	xi
Nomenclature.....	xv
Preface.....	xvi
Chapter 1.....	1
1 INTRODUCTION.....	1
1.1 Biomass boilers in pulp and paper industry.....	3
1.2 Agglomeration in BFB biomass boilers.....	3
1.3 Thesis objectives.....	4
1.4 Thesis structure.....	5
1.5 References.....	7
Chapter 2.....	9
2 LITERATURE REVIEW.....	9
2.1 Fluidized bed biomass boilers.....	9
2.1.1 Minimum fluidization velocity.....	11
2.2 Biomass and ash chemistry.....	14
2.2.1 Biomass classification.....	15
2.2.2 Biomass as a Fuel.....	16
2.3 Agglomeration.....	17

2.3.1	Basics of agglomeration in BFB biomass boilers .....	18
2.3.2	Alkali metals .....	20
2.3.3	Effect of operating parameters .....	24
2.3.4	Mitigation.....	25
2.4	Summary .....	26
2.5	References .....	27
Chapter 3	.....	32
3	Study on the critical amount of liquid for bed materials agglomeration in a bubbling fluidized bed.....	32
3.1	Introduction.....	32
3.2	Experimental apparatus and methods .....	34
3.2.1	Facility description.....	34
3.2.2	Methods.....	35
3.3	Results and Discussion .....	39
3.3.1	Capacitance and pressure analysis .....	39
3.3.2	Analysis of bed material samples .....	43
3.4	Conclusions.....	44
3.5	References.....	45
Chapter 4	.....	47
4	Study of bed materials agglomeration in a heated bubbling fluidized bed (BFB) using silica sand as the bed material and KOH to simulate molten ash .....	47
4.1	Introduction.....	47
4.2	Experimental Materials and methods.....	51
4.2.1	Facility description.....	51
4.2.2	Methods.....	52
4.3	Results and Discussion .....	55



4.3.1	Temperature and pressure measurements .....	55
4.3.2	Particle size distribution analysis of the bed materials after the BFB tests .....	65
4.4	Conclusions.....	69
4.5	References.....	70
Chapter 5	.....	73
5	Fusion behavior of synthetic and real biomass ashes – Effects of potassium.....	73
5.1	Introduction.....	73
5.1.1	Biomass ash composition.....	73
5.1.2	Agglomeration detection methods .....	75
5.2	Materials and methods .....	77
5.2.1	Materials .....	77
5.2.2	Apparatus .....	77
5.2.3	Preparation of test samples .....	79
5.2.4	Experimental procedure .....	80
5.3	Results and Discussion .....	82
5.3.1	Heating stage calibration.....	82
5.3.2	Fusion tests of mixtures of synthetic ash compounds and silica sand particles.....	83
5.3.3	Fusion tests of the mixture of pure KOH and silica sand particles.....	87
5.3.4	Fusion tests of the mixture of the real biomass fly ash and silica sand particles.....	89
5.4	Conclusions.....	91
5.5	References.....	92
5.6	Appendix 5-1 .....	95
Chapter 6	.....	96
6	CONCLUSIONS AND RECOMMENDATIONS .....	96

6.1 Conclusions.....	96
6.2 Recommendations.....	98
Appendices.....	99
A Bubbling fluidized bed reactor description, modifications and operation procedures.	99
A.1 Facility description.....	99
A.2 Modification of the gas distributor .....	103
A.3 Fluidization air supply and flow rate control.....	107
A.1.1 Minimum fluidization velocity .....	107
A.4 Reactor Heating and Insulation.....	110
A.5 Operation Procedures.....	114
A.6 References.....	117
A.7 Distributor Dimensions.....	118
Curriculum Vitae .....	119

## List of Tables

Table 2-1: Different values for C1 and C2 .....	13
Table 2-2: Alkali melting points .....	23
Table 3-1: Viscosities of glycerol-water mix (30% v/v) at various temperatures measured following the ASTM D445 Standard.....	36
Table 4-1: Summary of the tests .....	53
Table 5-1: Composition of a real fly ash sampled from a biomass boiler in a Canadian pulp mill .....	77
Table 5-2: Wood/woody biomass ash composition wt% (Vassilev et al. 2010). .....	79
Table 5-3: Summary of the tests and the test samples composition <sup>1</sup> .....	80
Table 5-4: Heating stage calibration .....	82
Table A-1: Air flow rates vs. superficial gas velocities ( $U_g$ ).....	107
Table A-2: $U_{mf}$ calculated with different correlations based in Ergun's equation.....	109

## List of Figures

Figure 1-1: Two main types of process to convert biomass to bioenergy (Basu, 2010).....	2
Figure 1-2: Agglomeration process in Bubbling Fluidized Biomass (BFB) boilers .....	4
Figure 2-1: Fluidization regimes including fixed bed, bubbling, fast fluidization regimes ...	10
Figure 2-2: $\Delta P$ vs $U_g$ for uniformly sized sharp sand (Kunii & Levenspiel, 1991) .....	14
Figure 2-3: Classification solids fuels by their H/C and O/C ratios (Basu, 2010).....	17
Figure 2-4: Coating-Induce mechanism (1) and melt induce mechanism (2).....	19
Figure 2-5: (A) sand particle surrounded by a rich potassium layer, (B) agglomerates formatted by binding material rich in potassium SEM/EDX analysis (Khan, et al., 2009)....	22
Figure 3-1: Schematic diagram of the small pilot-scale cold BFB test rig used.....	35
Figure 3-2: Bubble frequency in a fluidized bed divided into three different sections under different fluidizing conditions.....	37
Figure 3-3: Standard deviation of bubble frequency vs. injected amount of glycerol-water (30% v/v) (wt% in relation to the bed material loaded into the bed).....	39
Figure 3-4: Variation of the fluidized state inside the BFB at $U_g$ of 0.14m/s (or $4U_{mf}$ ) with the glycerol-water liquid injection amount increasing from 0 to 1.4 wt% .....	41
Figure 3-5: Effect of the glycerol-water (30% v/v) (wt% in relation to the bed material loaded into the bed), injection and superficial gas velocities on the average pressure drop of the bed (a), and the slope of the bed pressure drop versus the liquid injection amount (b) .....	42
Figure 3-6: Samples of bed materials after fluidization at different glycerol-water (30% v/v) injection amounts .....	43

Figure 3-7: SEM image of sand particles from the BFB at 0.0wt% (a) and 1.4wt% (b) liquid injection, respectively .....	44
Figure 4-1: Agglomeration, segregation and de-fluidization in a BFB (Lin & Dam-Johansen, 1997) .....	48
Figure 4-2: Saturation states in liquid-solid agglomerates. (a) Pendular state, (b) Funicular state, and (C) Capillary state (adapted from Pietsch, 2002) .....	50
Figure 4-3: Schematic diagram of the bubbling fluidized-bed system at Western Research Park, Sarnia. ....	52
Figure 4-4: Temperature and pressure measurements in the blank test with 0.0 wt% KOH in the bed material at $3.9U_{mf}$ (A) and $5.9 U_{mf}$ (B).....	56
Figure 4-5: Temperature and pressure measurements in the BFB tests at $3.9U_{mf}$ with different amounts of KOH in the bed material, 0.0wt% (A), 0.2wt% (B), 0.5wt% (C) and 0.8wt% (D) .....	58
Figure 4-6: Temperature and pressure measurements in the BFB tests at $5.9U_{mf}$ with different amounts of KOH in the bed material, 0.0wt% (A), 0.2wt% (B), 0.5wt% (C) and 0.8wt% (D) .....	59
Figure 4-7: Cumulative of particle size distribution for the silica sand particles used as the bed material in this study .....	65
Figure 4-8: Cumulative distribution wt% of agglomerates with a particle size $\geq 0.6$ mm obtained from the BFB tests at $3.9U_{mf}$ with different KOH loading (0.2, 0.5 and 0.8 wt% of the bed material).....	66
Figure 4-9: Cumulative distribution of agglomerates with a particle diameter $\geq 0.6$ mm from the fluidization tests at $5.9 U_{mf}$ with different KOH loading (0.2, 0.5 and 0.8 wt%) .....	67
Figure 4-10: Agglomerates obtained in the BFB tests with 0.8 wt% KOH in the bed material at $3.9U_{mf}$ .....	68

Figure 5-1: Three-step agglomeration mechanism (Ohman & Nordin, 2000) .....	74
Figure 5-2: Picture of Wild Leitz Microscope Heating Stage 1350 and Microscope.....	78
Figure 5-3: Close-up of the heating stage .....	81
Figure 5-4: Heating stage calibration curve.....	82
Figure 5-5: Microscopic photos of the mixture of synthetic ash compounds and silica sand particles in which $K_2O$ accounts for 10.75 wt% of the total ash (Test# K-1) at various temperatures .....	83
Figure 5-6: Microscopic photos taken at various temperatures during the repeated experiment with the same test sample (Test # K-1).....	84
Figure 5-7: Microscopic photos of the mixture of silica sand particles with synthetic ash compounds containing a larger amount of $K_2O$ (29 wt% of the total ash) (Test# K-2) at various temperatures. ....	86
Figure 5-8: Microscopic photos of a mixture of silica sand particles with synthetic ash compounds containing a 0 wt% $K_2O$ (Test# K-3) at various temperatures.....	87
Figure 5-9: Microscopic photos of a mixture of pure KOH (10 wt%) and silica sand particles (90 wt%) at various temperatures .....	88
Figure 5-10: Microscopic photos of a mixture of the real biomass fly ash (10 wt%) and silica sand particles (90 wt%) at various temperatures .....	89
Figure A-1: Schematic diagram of the bubbling fluidized-bed reactor system for biomass combustion, gasification or pyrolysis studies at the Industrial Bioproducts Lab in Western Research Park (Sarnia).....	100
Figure A-2: Photo of the feeding system .....	101
Figure A-3: Data acquisition software developed for the BFB system .....	103
Figure A-4: Original gas distributor .....	104

Figure A-5: A set of perforated cones used for the gas distributor.....	105
Figure A-6: Wind box blocked with bed materials particles (silica sand).....	105
Figure A-7: New gas distributor design.....	106
Figure A-8: Picture of the new gas distributor.....	106
Figure A-9: Experimental measurement of $U_{mf}$ .....	110
Figure A-10: Bed temperature measured without insulation.....	111
Figure A-11: Bed temperature measured with glass fiber insulation material .....	112
Figure A-12: Bed material temperature measurement.....	113
Figure A-13: Bed material temperature with ceramic insulation and fluidization air temperature at the exit of the small furnace.....	114

## Nomenclature

<p><math>\rho_g</math>: Gas density.</p> <p><math>\mu_g</math>: Gas viscosity.</p> <p><math>\rho_p</math>: Particle density.</p> <p><math>d_p</math>: Particle diameter.</p> <p><math>g</math>: Gravity.</p> <p><math>U_{mf}</math>: Minimum fluidization velocity.</p> <p><math>\varepsilon</math>: Bed voidage.</p> <p><math>\varepsilon_{mf}</math>: Bed voidage at minimum fluidization conditions.</p> <p><math>\emptyset_s</math>: Sphericity of the solid particles.</p> <p><math>U_g</math> : Superficial gas velocity.</p> <p><math>W_{\text{bed particles}}</math> : Net bed weight of the particles.</p> <p><math>A_t</math>: Bed cross sectional area.</p> <p><math>L_{bed}</math>: Bed height.</p> <p><math>\Delta P_{bed}</math>: Bed pressure drop.</p> <p><math>A_r</math>: Archimides number.</p>	<p><math>Re_{mf}</math>: Reynolds number at minimum fluidization conditions.</p> <p><math>\rho_b</math>: Bulk density of the bed.</p>
--	---



## Preface

*"Look deep into nature and then you will understand everything better" – Albert Einstein*

*To my wife and son*

## Chapter 1

### 1 INTRODUCTION

The increasing global energy demand, the decreasing fossil fuels reserves, the rising prices and deterioration of the environment have resulted in an increasing interest for alternative energy resources which are renewable, sustainable and eco-friendly (Alauddin, et al., 2010). This is why in the last decade the use of renewable energy had been steadily growing, and it has been reported that approximately 19% of the global energy consumption in 2012 was provided by renewable energy, and continued to grow in 2013 (REN21, 2014).

Among all the renewable resources, biomass has received a great deal of attention and is considered an important source of renewable energy to contribute to the energy needs in developed and developing countries (Bridgwater, 2004). It is the only renewable source of carbon, that can provide, through different conversion processes, liquid, gaseous and solid fuels, which produces lower emission (in comparison with fossil fuels) of environmentally detrimental gases (Alauddin, et al., 2010). In order to diminish the heavy dependence on fossil fuels, conversion of biomass to fuels and chemicals can play a key role. Governments around the world have formulated new legislation and policies to incentivize biomass use (Dautidis, et al., 2013). Biomass can be defined as all the organic materials derived from living material that are combustible in nature (Panwar, et al., 2012), usually the concept refers to all organic materials derived from plant or plant-based materials as a result of photosynthesis, but food processing wastes, sewage sludge, the organic components of municipal solid waste and pulping by-products (black liquor) are also considered biomass (Zhang, et al., 2010). The main biomass sources are wood, energy crops, agricultural and forest residues.

Biomass can be converted to biofuel via two main types of process thermo-chemical and bio-chemical (Figure 1-1), Bio-chemical conversion is much slower than thermochemical conversion (several days, weeks or even longer vs. a few seconds or minutes) but does not requires much external energy (Basu, 2010).

Three main products can be derived from bioenergy: power/heat, transportation fuels, and chemical feedstock. Combustion, gasification, liquefaction and pyrolysis are the major routes for thermochemical conversion of biomass, whereas that fermentation and digestion are the major routes for bio-chemical conversion (Zhang, et al., 2010; McKendry, 2002). For an overview of the different thermochemical conversion routes as well as bio-chemical conversion routes, see the publications of (Zhang, et al., 2010; McKendry, 2002; Faaij, 2006).

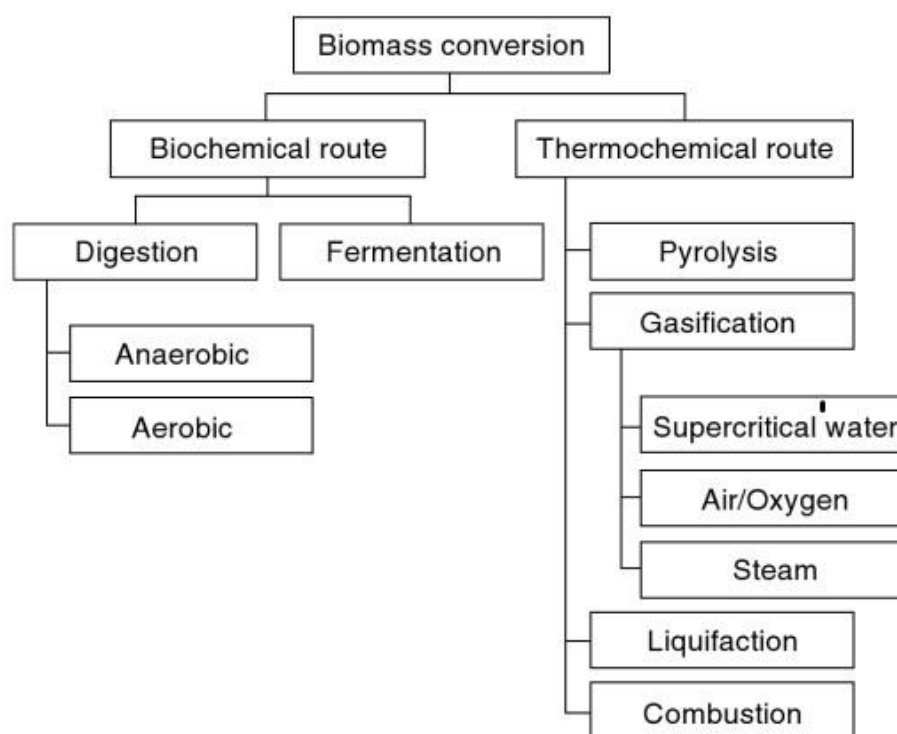


**Figure 1-1: Two main types of process to convert biomass to bioenergy (Basu, 2010)**

Among the technologies that can be used to burn (combustion/gasification) biomass for thermal/power generation, fluidized bed are emerging as one of the most promising techniques due to their flexibility in dealing with different range of fuels (different sizes, shapes, moisture contents and heating values), high efficiency and low environmental impact (Khan, et al., 2009).

## 1.1 Biomass boilers in pulp and paper industry

The pulp and paper and the sawmill industries are the greatest users of bio-energy in Canada are (Islam, et al., 2004).

High pressure steam and electric power are needed in pulp and paper mills, for many processes including drying pulp and paper products, heating water and process liquors, and concentrating spent cooking liquor (e.g., black liquor). Burning concentrated black liquor in recovery boilers contributes about 60 to 70% of the energy requirement in the mills, while the remaining 30 to 40% is generated by biomass combustion in biomass boilers. Fossil fuels are also co-fired in biomass boilers or in dedicated boilers and the consumption vary from mill to mill depending mainly on different mill technologies.

Bubbling fluidized bed (BFB) and stoker grate are the two main types of biomass boilers currently used in pulp and paper mills.

There are about 300 large biomass boilers in pulp and paper mills in North America; along with a large number of smaller units operated in lumber mills, tissue mills, plywood mills, etc. In Canada most of the biomass boilers are stoker grate boilers (vibrating grates, traveling grates, reciprocating grate, pinhole grates). In Scandinavia and South America where mills are generally newer, larger and more efficient, biomass boilers are mostly bubbling fluidized beds.

Despite its broad application, biomass combustion/gasification in fluidized bed processes still has some technical difficulties. Bed material agglomeration is a major operational problem, as discussed in details in the following section (Bartels, et al., 2008).

## 1.2 Agglomeration in BFB biomass boilers

Biomass is found and utilized everywhere around the world. However, the diversity of biomass makes it a complex and difficult fuel to utilize because of the heterogeneities in chemical composition and especially ash composition (Vassilev, et al., 2010).

Pietsch (2002) defined agglomeration as “ the formation of larger entities from particulate solids by sticking particles together by short range physical forces between the particles

themselves or through binders, substances that adhere chemically or physically to the solid surfaces and form a material bridge between the particles”

There is a common agreement between many researchers that the agglomeration process in BFB boilers is the result of stickiness (van der Waals and electrostatic forces and/or the presence of a liquid (melt) phase) or adhesiveness of bed material produced by alkali compounds derived from the biomass ash.

The alkali compounds, mainly potassium (K) and sodium (Na) can be problematic as they form low-melting alkali compounds and may also react with the bed material, usually silica sand, forming low-melting alkali silicates. These low-melting compounds characterized by low melting temperatures, coated the sand particles with a “sticky” layer. This makes sand particles agglomerate upon collisions and grow larger with time. This eventually leads to partial or complete defluidization of the reactor, which in turn results in a lengthy and expensive unscheduled shutdown (Bartels, et al., 2008).

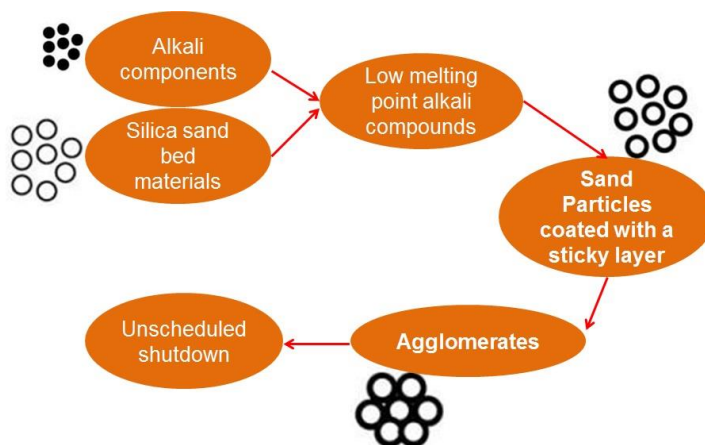


**Figure 1-2: Agglomeration process in Bubbling Fluidized Biomass (BFB) boilers**

Agglomeration will be further discussed in Chapter 2 “Literature Review”, as the focus of this thesis is on factors affecting bed agglomeration in BFB biomass boilers.

### 1.3 Thesis objectives

This investigation is part of the project “FUNDAMENTAL STUDIES OF DRYING, COMBUSTION AND ASH PROPERTIES OF BIOMASS, AND IMPACTS ON

BOILER AND PULP AND PAPER MILL OPERATIONS” that is being conducting by The University of Toronto Pulp & Paper Centre and supported by NSERC CRD grant and ten pulp and paper related companies. The main objective of this project lead by The University of Toronto is to obtain fundamental data on drying, combustion and ash properties of biomass mixtures and to use this information to develop viable control strategies and new technologies to improve biomass boiler and mill operations.

The research program consists of four main tasks (Tasks A through D); each task involves several projects. This thesis project (“Factors affecting Bed Agglomeration in BFB Boilers”) is a part of Task A (Combustion and Ash behavior).

The main objectives of this MEng thesis project were to:

1. Investigate and determine the critical amount of liquid (molten ash) that would result in severe bed agglomeration and defluidization in BFB biomass boilers.
2. Investigate the ash fusion behavior on bed agglomeration.
3. Install, commission and upgrade a small pilot-scale BFB reactor located at Western Research Park (Sarnia). Experiments presented in Chapter 4 were performed in this reactor. A new MEng student will continue with high temperature bed materials agglomeration studies using this reactor.

The research for objective 1 is summarized in two manuscripts presented in Chapters 3 and 4; furthermore objective 2 is summarized in Chapter 5, and objective 3 in Appendix A.

## 1.4 Thesis structure

Chapter 1 briefly describes the importance of the renewable energy resources for the future energy security, making special focus on the importance of biomass. Then the key role of biomass in the pulp and paper mill industry is explained together with the main operational problem in BFB boilers, agglomeration. Finally the objectives and structure of this thesis are described.

Chapter 2 describes some basic concepts of fluidized beds and fluidization. Then biomass ash characteristics and ash related problems are described. Afterwards, provides an overview of current research efforts and a comprehensive literature review on agglomeration in fluidized bed.

Chapter 3 and 4 presents the studies and results on the critical amount of liquid for bed material agglomeration in a bubbling fluidized bed. These experiments were carried out in two small pilot-scales bubbling fluidized bed (BFB) rigs, one operated at room temperature which is located at Institute for Chemicals and Fuels from Alternative Resources (ICFAR) at Western University using glycerol-water to simulate molten ash (Chapter 3) and the other operated at elevated temperatures located at Western Research Park at Sarnia using low melting-point salt (KOH) to simulate molten ash (Chapter 4).

Chapter 5 presents the results on ash fusion behavior of biomass ash or simulated ash.

Chapter 6 provides overall conclusions for the whole thesis research.

Appendix A provides a detailed description of the facility, operating procedures and all the modifications performed to the small pilot-scale BFB located at Sarnia.

## 1.5 References

- Alauddin, Z., Lahijani, P., Mohammadi, M., & Mohamed, A. (2010). Gasification of lignocellulosic biomass in fluidized beds for renewable energy development: A review. *Renewable and Sustainable Energy Reviews*(14), 2852-2862.
- Bartels, M., Lin, W., Nijenhuis, J., Kapteijn, F., & Ommen, J. (2008). Agglomeration in fluidized beds at high temperatures: Mechanisms, detection and prevention. *Energy and Combustion Science*(34), 633-666.
- Basu, P. (2010). *Biomass Gasification and Pyrolysis: Practical design and Theory* (First ed.). Burlington: Academic Press.
- Bridgwater, A. (2004). Biomass fast pyrolysis. *Thermal Science*(2), 21-49.
- Dautidis, P., Marvin, W., Rangarajan, S., & Torres, A. (2013). Engineering biomass conversion processes: A system perspective. *AIChE Journal*(1), 3-18.
- Faaij, A. (2006). Modern biomass conversion technologies. *Mitigation and Adaptation strategies for Global Change*(11), 343-375.
- Islam, M., Fartaj, A., & Ting, D. (2004). Current utilization and future prospects of emerging renewable energy applications in Canada. *Renewable and Sustainable Energy Reviews*(8), 493-519.
- Khan, A., Jong, W., Jansens, P., & Spliethoff, H. (2009). Biomass combustion in fluidized bed boilers: Potential problems and remedies. *Fuel Processing Technology*(90), 21-50.
- McKendry, P. (2002). Energy production from biomass (part 2): conversion technologies. *Bioresource Technology*(83), 47-54.



- Panwar, N., Kothari, R., & Tyagi, V. (2012). Thermo chemical conversion of biomass - Eco friendly energy routes. *Renewable and Sustainable Energy Reviews*(16), 1801-1816.
- Pietsch, W. (2002). *Agglomeration Process: Phenomena, Technologies, Equipment* (First ed.). Weinheim: Wiley-VCH.
- REN21. (2014). *Renewables 2014 Global Status Report*. Accessed on June 2014, <http://www.ren21.net/REN21Activities/GlobalStatusReport.aspx>
- Vassilev, S., Baxter, D., Andersen, L., & Vassileva, C. (2010). An overview of the chemical composition of biomass. *Fuel*(89), 913-933.
- Zhang, L., Xu, C., & Champagne, P. (2010). Overview of recent advances in thermo-chemical conversion of biomass. *Energy Conversion and Management*(51), 969-982.

## Chapter 2

### 2 LITERATURE REVIEW

This chapter aims to describe some basic concepts of fluidized bed biomass boilers and fluidization, as well as biomass ash characteristics and ash related problems, and provides an overview of current research efforts and a comprehensive literature review on agglomeration in fluidized bed biomass boilers.

#### 2.1 Fluidized bed biomass boilers

Fluidized beds are used for a wide range of applications in many industrial processes, for instance, drying of solids (e.g. pharmaceutical powders), catalytic cracking of petroleum, coal combustion and incineration of a wide range of waste (e.g. sewage sludge, crop residues, and paper industry biomass waste) (Bartels, et al., 2008).

In fluidized bed biomass boilers usually the reactor is a lined chamber in the form of a vertical cylinder with a granular material such as silica sand, limestone, ceramic material or alumina as a bed material, which acts as a heat reservoir and heat transfer medium (Chandler & Group, 1997). The most commonly used is silica sand. The fuel is added to the fluidized bed of inert solid material, in a relative low ratio, in the order of a few percent in comparison to the bed material (Bartels, et al., 2009).

The bed material is supported by a distributor, which allows the bed to become fluidized by a fluidizing gas. The fluidization gas could be introduced mainly through two different kind of distributors: perforated plates or spargers. The main purpose of the distributor is to uniformly distribute the fluidizing gas into the bed (Niessen, 2002). The biomass fuel can be fed into the bed pneumatically, mechanically or by gravity from the top or side. In the fluidized bed drying, volatilisation, ignition and combustion take place.

Freeboard is located above the bed to provide 3 to 4 seconds of residence time for the final burnout of combustible material (Niessen, 2002).

Due to the good mixing between the biomass fuel (normally fed continuously) and the bed material produced by the constant moving action of the bed material, a fluidized bed biomass boiler system generally has a uniform distribution of temperatures that result in good combustion conditions and high heat transfer rates (Chandler & Group, 1997).

There are two main types of fluidized bed biomass boilers depending on the fluidization gas velocity

Bubbling fluidized bed (BFB) biomass boiler: the fluidization gas velocity is enough to produce gas bubbles, but not too much that large amounts of solids are carried out of the combustion chamber.

Circulating fluidized bed (CFB) biomass boiler: In this equipment, the particles are carried out of the combustion chamber. The fluidization gas velocity is higher in comparison with bubbling fluidized bed. The particles are recycled back to the bed through cyclones.

The following figure shows the different regimes of fluidization as the velocity of the gas flowing through a bed of solid particles is increased:

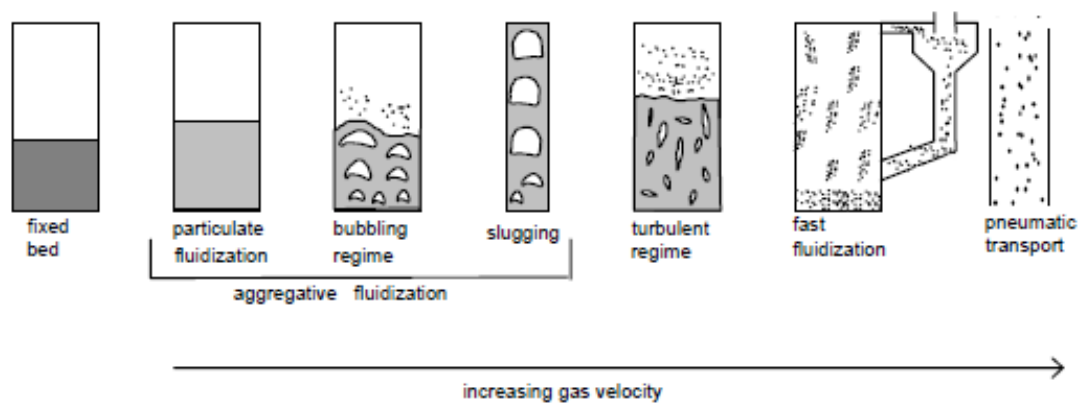


**Figure 2-1: Fluidization regimes including fixed bed, bubbling, fast fluidization regimes**

For an overview of each regime, see (Kunii & Levenspiel, 1991)

### 2.1.1 Minimum fluidization velocity

The minimum fluidization velocity (“incipient fluidization velocity”) is the superficial gas velocity at which the bed becomes fluidized; at this point the bed material behaves as a liquid, it is a crucial parameter essentially required for the design of a fluidization operation. The minimum fluidization velocity depends upon a number of factors, such as, particles shape, size, and density among others.

To find the minimum fluidizing velocity ( $U_{mf}$ ), empirical, theoretical and experimental approaches can be used.

#### 2.1.1.1 Empirical Calculation of $U_{mf}$

Leva’s correlation is the empirical correlation most commonly used (Leva, 1959)

$$U_{mf} = \frac{7.169 \times 10^{-4} g d_p^{1.82} (\rho_p - \rho_g)^{0.94}}{\rho_g^{0.06} \mu_g^{0.88}} \quad \mathbf{2-1}$$

Where (SI units)  $\rho_g$ : gas density,  $\mu_g$ : gas viscosity,  $\rho_p$ : particle density,  $d_p$ : particle diameter,  $g$ : gravity.

#### 2.1.1.2 Theoretical Calculation of $U_{mf}$

At minimum fluidization, the bed is at boundary between fixed and fluidized conditions. The frictional bed pressure drop, which is caused by the drag of the fluid on the particles, through a packed bed of height  $L$  using non-spherical particles with a mean diameter  $d_p$  has been correlated by Ergun (1952) by the equation:

$$\frac{\Delta P_{bed}}{L_{bed}} = 150 \frac{U_g \mu_g}{(\phi_s d_p)^2} \frac{(1 - \varepsilon)^2}{\varepsilon^3} + 1.75 \frac{U_g^2 \rho_g}{\phi_s d_p} \frac{(1 - \varepsilon)}{\varepsilon^3} \quad \mathbf{2-2}$$

Where  $\varepsilon$  is the voidage,  $\mu_g$  is the viscosity of the gas,  $\phi_s$  is the sphericity of the solid particles,  $U_g$  is the superficial gas velocity, and  $\rho_g$  is the gas density.

The onset of fluidization occurs when the frictional bed pressure drop becomes equal to the weight of the bed particles per unit area (Kunii & Levenspiel, 1991):

$$\Delta P_{bed} = \frac{W_{bed\ particles}}{A_t} = gL_{bed}(1 - \varepsilon_{mf})(\rho_s - \rho_g) \quad 2-3$$

Where  $W_{bed\ particles}$  is the net bed weight of the particles,  $A_t$  is the bed cross sectional area,  $\varepsilon_{mf}$  is the bed voidage at minimum fluidization conditions. The superficial velocity at minimum fluidization conditions,  $U_{mf}$ , can be found combining the last two equations (Kunii & Levenspiel, 1991). This gives a quadratic equation for  $U_{mf}$

$$\frac{d_p^3 \rho_g (\rho_s - \rho_g) g}{\mu_g^2} = \frac{1.75}{\varepsilon_{mf}^3 \phi_s} \left( \frac{d_p U_{mf} \rho_g}{\mu_g} \right)^2 + \frac{150(1 - \varepsilon_{mf})}{\varepsilon_{mf}^3 \phi_s^2} \left( \frac{d_p U_{mf} \rho_g}{\mu_g} \right) \quad 2-4$$

This equation can be written in terms of the dimensionless quantities Archimedes number (Ar) and Reynolds number ( $Re_{mf}$ ) as follow:

$$Ar = \frac{150(1 - \varepsilon_{mf})}{\varepsilon_{mf}^3 \phi_s^2} Re_{mf} + \frac{1.75}{\varepsilon_{mf}^3 \phi_s} Re_{mf}^2 \quad 2-5$$

Where:

$$Re_{mf} = \left( \frac{d_p U_{mf} \rho_g}{\mu_g} \right), Ar = \frac{d_p^3 \rho_g (\rho_s - \rho_g) g}{\mu_g^2} \quad 2-6$$

The solution for equation 2-5, in terms of Reynolds number and Archimedes number can be written in a simplified form as (Yang, 2005):

$$Re_{mf} = (C_1^2 + C_2 Ar)^{0.5} - C_1 \quad 2-7$$

With  $C_1 = 42.86 \frac{(1 - \varepsilon_{mf})}{\phi_s}$ ,  $C_2 = 0.5714 \phi_s \varepsilon_{mf}^3$

Based in experimental data, many researchers have developed empirical correlations suggesting sets of values for the constants  $C_1$  and  $C_2$ . A simplified set is shown in the following table.

**Table 2-1: Different values for C1 and C2**

Reference	C1	C2
Wen and Yu (1966)	33.7	0.0408
Richardson & St Jeronimo (1971)	25.7	0.0365
Thonglimp et al. (1894)	31.6	0.0425

Thus, the minimum fluidization velocity can be found:

- 1) If  $\phi_s$  and  $\varepsilon_{mf}$  are known,  $Re_{mf}$  and  $U_{mf}$  can be calculated directly.
- 2) If  $\phi_s$  and  $\varepsilon_{mf}$  are not known (unfortunately the usual case), correlated values for  $C_1$  and  $C_2$  must be used.

### 2.1.1.3 Experimental approach

$U_{mf}$  can be determined experimentally from  $\Delta P$  vs  $U_g$  plots. When visual observations of the bed are not possible this plots are very useful as a rough indication of the quality of the fluidization (Kunii & Levenspiel, 1991).

As can be seen in Figure 2-2 (typical for systems of uniformly sizes particles that are not too small), in a fixed bed the pressure drop increases as the flow rate is increased, the pressure drop is approximately proportional to gas velocity and follows Erguns equation 2-2. The pressure drop usually reaches a maximum  $\Delta p_{max}$ , which is higher than the static pressure drop of the bed, as the fluid velocity is further increased from this point ( $\Delta p_{max}$ ), the bed expands and the porosity increases from  $\varepsilon$  to  $\varepsilon_{mf}$ , resulting in a decrease in pressure drop to a value which is independent of fluid velocity (static pressure drop of the bed). If the process is reversed and the gas velocity is decreased, the particles settle down to form a loose fixed bed (with voidage equal to  $\varepsilon_{mf}$ ). The minimum fluidization velocity is determined graphically as point A in Figure 2-2.

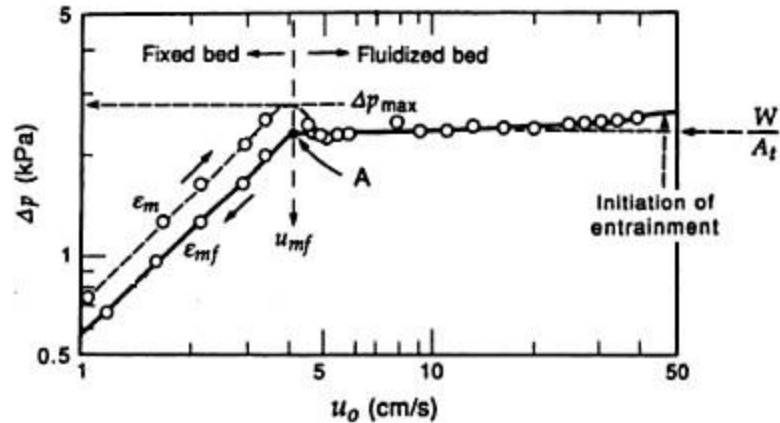


**Figure 2-2:  $\Delta p$  vs  $U_g$  for uniformly sized sharp sand (Kunii & Levenspiel, 1991)**

Conversion (combustion and gasification) of carbonaceous solid materials such as coal and biomass in a fluidized bed at a high temperature has proved to be promising for generating steam, electricity and syngas.

## 2.2 Biomass and ash chemistry

In order to produce bioenergy from biomass it is necessary to break-down the organic compounds that constitute the different types of biomass. These organic compounds have a wide range of complexity, containing numerous functional groups (alkanes, alkenes, alkynes, aromatics, etc) that ultimately determine the structure and chemistry of biomass (Cheng, 2009). Biomass organic materials are generally composed of cellulose, hemicellulose, lignin, lipids, proteins, simple sugars and starches; where cellulose, hemicellulose and lignin are its three major constituents (Zhang, et al., 2010). Biomass typical elemental composition (dry-and-ash-free basis) is 42 to 71 wt% C, 3 to 11 wt% H and 16 to 49 wt% O (Vassilev, et al., 2010).

Biomass also contain in its structure inorganic elements including alkali metals, Si, Al, Ti, Ca, Fe, Mg, P, S and chlorine. Many of these elements are involved in different ways in problems related with combustion/gasification systems as they are involved in chemical reactions that lead to ash fouling and slagging, corrosion and agglomeration of bed materials.

The biomass composition and especially ash components vary a lot depending on the plant types, growth condition, weather and so on. Biomass ashes are normally dominated by silicon, calcium and potassium (Vassilev, et al., 2010).

Ash could be defined as the inorganic uncombustible part of the biomass, left after complete combustion of the organic matters. During biomass conversion a large part of the ash leaves the facility as fly ash while a smaller part remains in the bed, this fraction is known as bottom ash.

The inorganic material in biomass includes two types:

- Inherent inorganic material, which are generally within the organic structure of the biomass in combination with oxygen-containing functional groups.
- External inorganic materials, which are added to the fuel through processing steps, for example, additives (e.g. crystalline silicates, alumina) incorporated as common soil, sands, clays and other contaminants, during harvesting, processing and handling of the biofuels (Khan, et al., 2009).

The inherent inorganic material are homogeneously dispersed in the fuel structure and are characterized to be much more mobile than the external inorganic material, making them very volatile in burning char (Obernberger, et al., 1999). Therefore, inherent inorganic materials are mainly responsible for ash deposition in biomass conversion (combustion/gasification).

### 2.2.1 Biomass classification

Biomass energy resources are diverse and a comprehensive classification system is needed in order to be able to predict properties and behaviors.

Vassilev et al (2010) performed an extended overview of the chemical composition of different kind of biomass, where 86 varieties of biomass were included in their study. They used a classification of biomass varieties according to their biological diversity, source and origin. 1) Wood and woody biomass, 2) Herbaceous and agricultural biomass,



3) Aquatic biomass, 4) Animal and human biomass wastes, 5) Contaminated biomass and industrial biomass wastes, 6) Biomass mixtures (blend from the other varieties)

In the case of combustion/gasification for thermal power generation a major interest is focused in the first two biomass groups:

1) Wood and woody biomass: Coniferous or deciduous, angiospermous or gymnospermous; soft or hard; stems, branches, foliage, bark, chips, pellets, briquettes, sawdust, sawmill and others from various wood species (e.g. poplar, pine bark, pine chips, sawdust, willow, wood residue, etc).

2) Herbaceous and agricultural biomass: Annual or perennial and field-based or processed based biomass such as: Grasses and flowers (e.g. bamboo, cane, switchgrass, etc), Straws (e.g. corn, oat, rice, sunflower, wheat, etc), other residues (e.g. fruits, shells, hulls, seeds, stalks, pulps, etc).

Herbaceous and Agricultural residues have high contents of alkali oxides and salts (Werther, et al., 2000) which can promote agglomeration of the bed material. For an overview of the different biomass varieties, see (Vassilev, et al., 2010).

In Chapter 5, Table 5-2 the Wood/woody biomass ash composition is presented.

### 2.2.2 Biomass as a Fuel

In comparison with fossil fuels, biomass has lower heating values on similar weight basis, mainly due to its carbohydrate structure. One useful mean to compare and ranking fuels is through their chemical constituents, for example, atomic ratios. Figure 2-3 (van Krevelen diagram) plots hydrogen to carbon ratio (H/C) and oxygen to carbon (O/C) ratio.

Two important conclusions can be obtained from Figure 2-3:

- Biomass have much higher ratios of (O/C) and (H/C) than fossil fuels
- The lower the respective ratios the greater the energy content of the material.

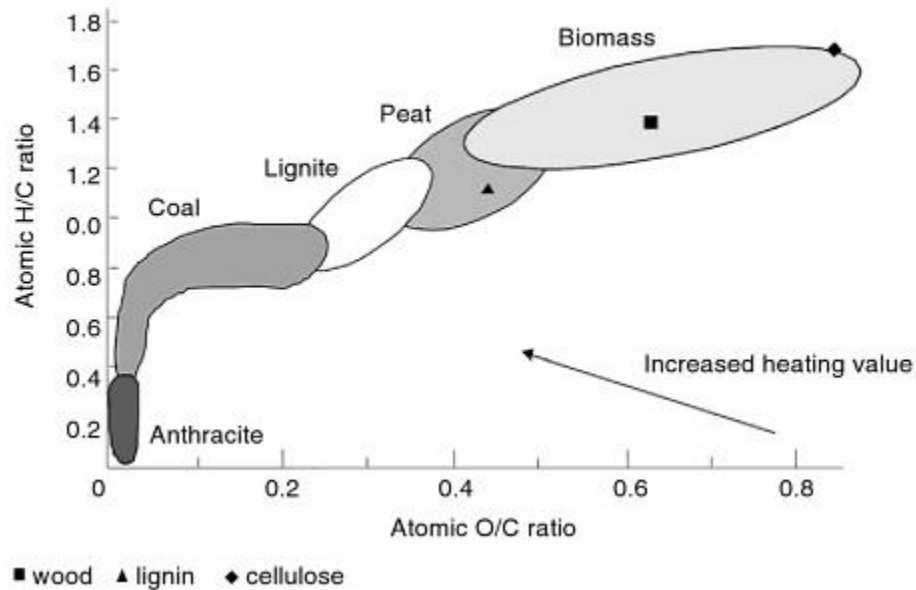


**Figure 2-3: Classification solids fuels by their H/C and O/C ratios (Basu, 2010)**

Despite lower heating values, the high oxygen and hydrogen content of biomass results in high volatile (biomass can lose up to 90% of their masses in the first stage of combustion) and liquid yields respectively (Basu, 2010).

The high volatile matter (light hydrocarbons, carbon monoxide, carbon dioxide, hydrogen, moisture and tar) confers to biomass's high ignition stability (Zhang, et al., 2010).

## 2.3 Agglomeration

Since the first particulate solids were formed on Earth, agglomeration has existed, participating in the stability of wet and dry soil and in the development of rock formations, for example, sandstone is one of the most easily recognized “agglomerates” where bending mechanisms between solid particles play a key role.

Humans and higher developed organisms have been using agglomeration since prehistoric times, for example, ancient doctors used agglomeration as a tool to improve

powder characteristics, they produced pills, binding medicinal powder with honey to form small agglomerates, birds and other animals built nests, etc.

Despite that agglomeration has existed since earth formation, as a technology it started only about 150 years ago. As a unit operation, it started around the middle of the nineteenth century as a method to recover and use coal fines (Pietsch, 2002).

Agglomeration process plays a very important role in many industries and their performance is essential for the efficiency and success of many processes. For example in the pharmaceutical and fertilizer industries, agglomeration is desired to reduce dustiness, stabilize mixtures and facilitate dosing. On the other hand, in processes such as fluidized bed combustion/gasification, and fluid coking process, agglomeration is not desired as it affects product yield, produces fouling, and in the worst case can lead to de-fluidization of the reactor which results in a lengthy and expensive unscheduled shutdown (Weber, et al., 2008).

### 2.3.1 Basics of agglomeration in BFB biomass boilers

In a gas-solid fluidization system, the particles interact with the neighboring particles through physical contact or by attractive forces between the interaction points.

There is a common agreement between many researchers that the agglomeration process in BFB boilers is the result of stickiness or adhesiveness of bed material produced by alkali compounds, mainly potassium and sodium. “Stickiness” of bed particles can refer to van der Waals and electrostatic forces and/or the presence of a liquid (melt) phase.

The alkali compounds mainly potassium (K) and sodium (Na) can be problematic as they form low-melting alkali compounds and may also react with the bed material, usually silica sand, forming low-melting alkali silicates, leading to agglomeration during combustion. Visser et al. (2008) proposed two different types of agglomeration mechanisms: 1) “melt-induced” agglomeration and 2) “coating-induced” agglomeration.

In the melt induced mechanism, the bed particles adhesion is produced by molten ash (alkali compounds) that acts as a “glue”, and liquid bridges are formed between the bed

particles. On the other hand, in the coating-induced mechanism a sticky uniform coating layer is formed on the surface of the bed material. The coating layer is generated for the contact of ash melts, condensation and/or reaction of gas phase fuel derived alkali compounds on the bed material particle surface. This mechanism is dominated by viscous flow sintering.

It has been reported that the coating layer in the coating-induced mechanism is mainly composed by silicon (dominating element), potassium, and sometimes with small amounts of calcium (Ohman & Nordin, 2000).

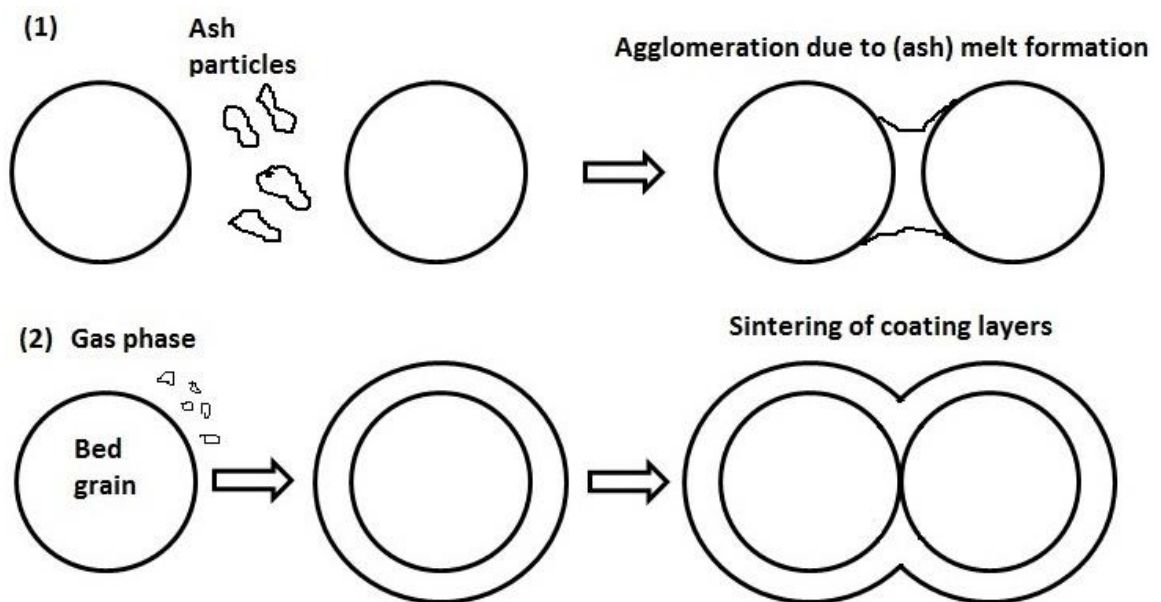


**Figure 2-4: Coating- induce mechanism (1) and melt induce mechanism (2)**

Seville and Cliff (1984) showed in their study how the fluidization conditions changed when a liquid (melt) phase is present in the system. They reported that when a small amount of involatile liquid was added to a fluidized bed, a change in the ratio between the particle gravity and inter particle forces is produced, as the inter-particle cohesive forces are increased by increasing the amount of liquid the fluidization behavior of group B particles can move towards group A to C. At high temperatures, which is the case of BFB biomass boilers, Gluckman et al (1976) showed that there is a temperature above which the minimum fluidization velocity increased sharply and it will not follow the

theoretical value calculated by Ergun equation. They called this temperature initial sintering temperature  $T_s$ .

Sintering can be defined either as a migration of holes or lattice vacancies, or as a motion of atoms to a less dense area of material. If two particles come in contact in a fluidized bed operating at a high temperature but below the melting point, they will tend to bond together because the rate of sintering is enough to allow material to migrate to the point of contact to form a bond, however this will never happen at room temperature as the sintering rate is not enough to form a bond (at higher temperatures the sintering rate is increased). Sintering can possibly take place by a number of mechanisms, in the case of single phase materials: flow of the material (viscous flow), surface diffusion, volume diffusion and vaporisation – condensation. In the case of fluidized beds, viscous or plastic flow of material is the most important mechanism as it is faster (Seville, et al., 1998). Viscous flow is sometimes mentioned as sintering in the presence of a liquid phase, and this mechanism tends to form agglomerates with stronger bonds than those caused by diffusion mechanisms (Siegelell, 1984). The initial sintering temperature depends on chemical composition and characteristics of the particles and can be used as a predictor for agglomeration tendency in BFB boilers.

### 2.3.2 Alkali metals

Potassium is a key element in biomass growth, and also is a key element during combustion as it contributes to ash related problems (agglomeration) and corrosion (produced by alkali metal sulfates and chlorides). It is highly mobile, and the plants absorbed it through the root system (Jones, et al., 2007). 90% of the alkali metals are found in water soluble or ion exchangeable forms and are available for release during combustion. It has been proven that the chemical composition of biomass influences the volatilization of alkalis, for example, it was shown that chlorine increases the alkali metal emission from the ash residue during thermal conversion of biomass (Olsson, et al., 1997).

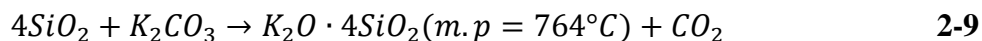
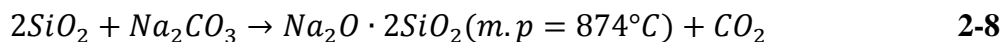
Some researchers (Kowalski, et al., 2007; Olsson, et al., 1997) have shown that in pyrolysis studies the emission of alkali metals apparently occurs in two temperature

intervals. The first interval goes up to 500°C and a small fraction of the alkali content is released, the researchers agree to attribute this to the decomposition of organic alkali salts. In samples with low organic content, alkali emission is restricted to the second interval. The second interval (>500°C) appears to be due to alkali metal evaporation from the ash component of the resulting ash. Very interesting, the chlorine content only enhances the alkali metal release in gasification or pyrolysis at high temperatures (>500°C). Combustion experiments performed using switchgrass, with a high content in alkali metal (potassium) and chlorine, showed that the most abundant alkali metal containing specie released during combustion was KCl. The researchers divided the combustion in 3 phases: (1) combustion where the volatile matter combusts, O<sub>2</sub> is consumed and mainly CO<sub>2</sub>, CO and H<sub>2</sub>O are formed; (2) the char burning phase during which much of the alkali metal is released; and (3) the “ash-cooking” stage where very small amounts of alkali metals are released (Dayton, et al., 1995).

As it was previously mentioned, potassium is dispersed in biomass in ionic and organometallic forms. During combustion, potassium is likely to be volatilized with organic species. If chlorine is presented in the fuel, it may be released as KCl, one of the most stable alkali-containing specie in the gas phase at high temperature (Khan, et al., 2009). If chlorine is not present hydroxides (most stable form in moist oxidizing environments), oxides, sulphates or carbonates may be formed (Jenkins, et al., 1994). Potassium species can react with sulfur dioxide present in the gas phase, forming sulphate particles (e.g K<sub>2</sub>SO<sub>4</sub> m.p. 1069°C). During ash formation, alkali and alkali earth metals ions are primarily associated with sulfate, carbonate and chloride ions (Olanders & Steenari, 1995). Some researchers indicate that most of the potassium remains in the bed as they are recaptured from the vapor by some mineral components in the ash under BFB conditions (Lin, et al., 2003; Zevenhoven-Onderwater, et al., 2001).

Agglomeration begins when the alkali compounds melt and cause adhesion of bed particles. As was previously mentioned, silica sand (SiO<sub>2</sub>) is normally used as a bed material, whose melting point is around 1450°C. Besides the adhesion effect of the melted ash, the alkali compounds can react with the silica sand, forming eutectic mixtures

with melting points lower than the individual components, mostly with the structure  $K_2O \cdot nSiO_2$  and  $Na_2O \cdot nSiO_2$ , for example (Werther, et al., 2000):



Other alkali silicates have relatively low melting points, such as  $K_2O \cdot 3SiO_2$  740°C,  $K_2O \cdot SiO_2$  976°C,  $3Na_2O \cdot 8SiO_2$  793°C, very similar to the operating temperatures of BFB biomass boilers (Olofsson, et al., 2002). A small addition of calcium will shift this value roughly to 1080°C (Ohman & Nordin, 2000). On the other hand, CaO can be problematic if is added to the  $Na_2O$ - $SiO_2$  system because it can form a eutectic composition of  $Na_2O$ -CaO- $5SiO_2$  and  $3Na_2O$ - $8SiO_2$ , with a low melting point of 755°C (Olofsson, et al., 2002), but it can also form other sodium calcium silicates with melting points above 1000°C. Thus, depending on the system which CaO is interacting with, it can promote or inhibit agglomeration. It has been reported that alkaline earth metals (Ca and Mg) may promote or inhibit the generation of agglomerates during incineration in a fluidized bed (Lin, et al., 2009).

The following images show the effects of alkali melt compounds (Potassium) in the agglomeration process with silica sand particles in a bubbling fluidized bed.

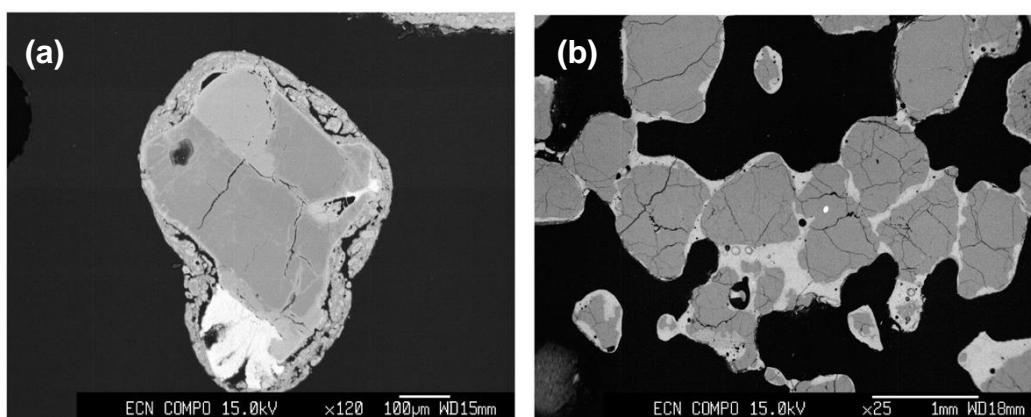


**Figure 2-5: (A) sand particle surrounded by a rich potassium layer, (B) agglomerates formatted by binding material rich in potassium SEM/EDX analysis (Khan, et al., 2009).**

It can be seen in Figure 2-5 (a) how the sand particles become coated with a sticky layer, this layer makes sand particles agglomerate upon collisions and grow larger with time (Figure 2-5 (b)).

Other interesting alkali melting points are presented in the following table:

**Table 2-2: Alkali melting points**

Compound	Melting point, °C
KCl	770
NaCl	801
K <sub>2</sub> SO <sub>4</sub>	1069
Na <sub>2</sub> SO <sub>4</sub>	884
K <sub>2</sub> CO <sub>3</sub>	891
Na <sub>2</sub> CO <sub>3</sub>	851

Mixtures of the compounds presented in Table 2-2 can form eutectics that can start melting at a temperature as low as 520°C depending on the K content.

It has been reported that elements such as Fe readily react with alkali metals present in the bed reducing the formation rate of agglomerates. Fe<sub>2</sub>O<sub>3</sub> react with alkali metals as follow:



Where X can be either K or Na. The eutectics formed have melting temperatures above 1135°C (Olofsson, et al., 2002).

Alumina rich compound can also reduce the formation rate of agglomerates as they form alkali-aluminum silicates (K<sub>2</sub>O-Al<sub>2</sub>O<sub>3</sub>-SiO<sub>2</sub>) which have much higher melting points (Bartels, et al., 2008).

If the biomass has a low content of K (e.g rice husk, pine chips) it can be burnt in a fluidized bed without agglomeration problems (Natarajan, et al., 1998; Preto, et al., 1987), showing the key role of potassium in the agglomeration process.



### 2.3.3 Effect of operating parameters

Although the presence of alkali melting compounds is a major factor in bed material agglomeration and de-fluidization, the operating parameters also play a very important role.

#### 2.3.3.1 Effect of temperature

Lin et al (2003) have shown in their research that the rate of agglomeration increases at higher combustion temperatures. They studied the agglomeration phenomena at different temperatures using a laboratory-scale fluidized bed combustor with an inner diameter of 68mm and total height of 1.2 m, equipped with pressure transducers and thermocouples to monitor the pressure drop over the bed and the temperature profile. Silica sand was used as a bed material while firing pellets of Danish wheat straw with a high content of  $K_2O$  in the ash (29 wt%). They performed their experiments until the de-fluidization of the bed occurred, representing the agglomeration tendency by the de-fluidization time (time between the start of the feeding to de-fluidization of the bed).

They showed that as the temperature increased the de-fluidization time decreased because the sintering effect became dominant. They concluded that as the temperature increases, the fraction of ash melt increases and the viscosity of the melt on the particle surface decreases, thus the melt on the particle surface moves easily to other particles improving agglomeration.

Lin et al (2006) showed the same tendency in their research. Instead of used real biomass their work was performed using a synthetic biomass mix with different concentrations of Na (from low to high). The experiments were carried out using silica sand as the bed material. They concluded that as the temperature increases the de-fluidization time decreases, mainly due to more eutectics liquid is formed and because the viscosity of the eutectics liquid decreases simplifying its flow toward other particles and hence increasing agglomeration.

Lin et al (2011) examined agglomeration in a lab-scale bubbling fluidized reactor using materials of different particle size distribution (PSDs) at various operating temperatures

and revealed that the de-fluidization time increased with decreasing operating temperature and this effect was independent of the PSD of the bed material. They also concluded that as the operating temperature increases, lower melting point eutectics are generated which melt easily forming a liquid phase that cover the surface of the particles via particle collision, and additionally the viscosity of the melt decreases as the temperature increases enabling the flow through other particles and decreasing the time to de-fluidization.

The same results have been reported by other researchers (Olofsson, et al., 2002; Shiyuan, et al., 2010).

### 2.3.3.2 Effect of particle size

Lin et al (2003) showed that an increase in particle size decreased the de-fluidization time, because larger particles have a lower specific outer superficial area and therefore a thicker coating layer is formed. Similar results were reported by other researchers.

### 2.3.3.3 Effect of gas velocity (Flow rate)

Lin et al (2003) showed that as the flow rate was increased, the de-fluidization time was increased, because higher gas velocities led to better mixing and increased the breaking forces produced by the bubbles. This same effect was reported by Lin et al (2011) who examined agglomeration in a lab-scale bubbling fluidized reactor using bed materials of different particle size distributions (PSDs) at various gas velocities. They concluded that increasing the gas velocity can delay agglomeration and de-fluidization.

Experiments by Shiyuan et al (2010) have shown that the de-fluidization time will be extended as the gas velocity increases. They concluded that a higher gas velocity will lead to two effects, a better mixing of the particles and increased quantity of fuel ash in the gas, slowing the de-fluidization.

### 2.3.4 Mitigation

Additives can mitigate ash related issues by 1) capturing problematic ash species via chemical adsorption and reactions, 2) physical adsorption and elutriating troublesome ash

species from combustion facilities, 3) increasing the biomass ash melting temperature, and 4) hindering the biomass ash sintering process by diluting the ash with additives (Wang, et al., 2012).

Other mitigation strategies include the use of alternative bed materials, and blending (co-fire) of biomass with other fuels, the second fuel must contain less alkalis (thus the overall alkali content is reduced) or be rich in elements such as Fe, Al, which will form eutectics with higher melting points (Werther, et al., 2000). Olofsson et al (2002) reported in a study that the use of alternative bed materials, such as magnesite (84.4% MgO, 4% SiO<sub>2</sub>) and mullite (75% Al<sub>2</sub>O<sub>3</sub>, 24.5% SiO<sub>2</sub>) mitigated the agglomeration in comparison when quartz sand was used (98%SiO<sub>2</sub>). The use of Mullite produced the formation of alkali aluminum silicates which have higher melting points than the alkali silicates. Mullite and magnesite keep the SiO<sub>2</sub> content in the bed low. However, some biomass have high contents of alkali and SiO<sub>2</sub> (e.g straw). In this case agglomeration is unavoidable.

Kuo, et al. (2011) reported in their study that adding Al<sub>2</sub>O<sub>3</sub> can significantly mitigate the de-fluidization process.

## 2.4 Summary

Fluidization in bubbling biomass boilers is a complex phenomenon that becomes even more complex at high temperatures and when agglomeration problems are present, due that it involves chemical reaction and transport phenomena. To understand the mechanisms and factors affecting the agglomeration process it is necessary to have knowledge about how agglomeration affects the hydrodynamics of the bed, the role of the operating parameters such as temperature, gas velocity and particle size, and how the chemical elements interact with each other.

In order to solve the problems associated with agglomeration in bubbling fluidized biomass boilers (BFB), a better understanding of the mechanisms and factors involved is very important and has received a great deal of attention in recent years. Various technical approaches for reducing ash deposition and bed agglomeration have been

studied. However, the mechanism of agglomeration and the temporal dynamics of particle agglomeration are not well understood.

One of the important factors that influence agglomeration is the formation of low-melting alkali compounds. These low melting alkali compounds, depending on the bed material temperature, could melt, forming a liquid phase which in turn coats the sand particles. This makes bed particles agglomerate upon collision and grow larger with time. To the best of the author's knowledge there is no answer yet for what is the minimum amount of liquid (molten alkali compounds) to agglomerate the bed material. Therefore, the aim of this thesis is to determine experimentally the critical amount of liquid (molten ash in real biomass boiler operations) that would result in bed agglomeration and defluidization.

## 2.5 References

- Bartels, M., Lin, W., Nijenhuis, J., Kapteijn, F., & Ommen, J. (2008). Agglomeration in fluidized beds at high temperatures: Mechanisms, detection and prevention. *Energy and Combustion Science*(34), 633-666.
- Bartels, M., Nijenhuis, J., Lensselink, J., Siedlecki, M., Jong, W., Kapteijn, F., et al. (2009). Detecting and counteracting agglomeration in fluidized bed biomass combustion. *Energy&Fuel*(23), 157-169.
- Basu, P. (2010). *Biomass Gasification and Pyrolysis: Practical design and Theory* (First ed.). Burlington: Academic Press.
- Chandler, A., & Group, I. A. (1997). *Municipal solid waste incinerator residues*. New York: Elsevier.
- Cheng, J. (2009). *Biomass to renewable energy processes* (First ed.). Florida: CRC Press.
- Dayton, D., French, R., & Milne, T. (1995). Direct Observation of Alkali Vapor Release during Biomass Combustion and Gasification. 1. Application of Molecular Beam Mass Spectrometry to Switchgrass combustion. *Energy & Fuels*(9), 855 - 865.

- Ergun, S. (1952). Fluid flow through packed columns. *Chemical Engineering Progress*(48), 89-94.
- Gluckman, M., Yerushalmi, J., & Squires, A. (1976). Defluidization characteristics of sticky materials on agglomeration bed. *Fluidization Technology*, 395-422.
- Jenkins, B., Baxter, L., Miles, T., Miles, J. T., Oden, L., Bryers, R., et al. (1994). Composition of ash deposits in biomass fuelled boilers: results of full-scale experiments and laboratory simulations. *Paper presented at the 1994 international ASAE summer meeting, Kansas City*.
- Jones, J., Darvell, L., Bridgeman, T., Pourkashanian, M., & Williams, A. (2007). An investigation of the thermal and catalytic behavior of potassium in biomass combustion. *Proceedings of the Combustion Institute*(31), 1955-1963.
- Khan, A., Jong, W., Jansens, P., & Spliethoff, H. (2009). Biomass combustion in fluidized bed boilers: Potential problems and remedies. *Fuel Processing Thecnology*(90), 21-50.
- Kowalski, T., Ludwig, C., & Wokaun, A. (2007). Qualitative Evaluation of Alkali release during the Pyrolysis of Biomass. *Energy & Fuels*(21), 3017-3022.
- Kunii, D., & Levenspiel, O. (1991). *Fluidization Engineering* (Second ed.). Stoneham: Butterworth-Heinemann.
- Kuo, J.-H., Lin, C.-L., & Wey, M.-Y. (2011). Effect of alkali concentrations and operating conditions on agglomeration/defluidization behavior during fluidized bed air gasification. *Powder Technology*(214), 443-446.
- Leva, M. (1959). *Fluidization*. New york: McGraw-Hill.
- Lin, C.-L., Kuo, J.-H., Ming-Yen, W., Chang, S.-H., & Kai-Sung, W. (2009). Inhibition and promotion: The effect of earth alkali metals and operating temperature on particle agglomeration/defluidization during incineration in fluidized bed. *Powder Technology*(189), 57-63.

- Lin, C.-L., Peng, T.-H., & Wang, W.-J. (2011). Effect of particle size distribution on agglomeration/defluidization during fluidized bed combustion. *Powder Technology*(207), 290-295.
- Lin, C.-L., Wey, M.-Y., & Lu, C.-Y. (2006). Prediction of defluidization time of alkali composition at various operating conditions during incineration. *Powder technology*(161), 150-157.
- Lin, W., Dam-Johansen, K., & Frandsen, F. (2003). Agglomeration in bio-fuel fired fluidized bed combustors. *Chemical Engineering Journal*(96), 171-185.
- Natarajan, E., Ohman, M., Gabra, M., Nordin, A., Liliedahl, T., & Rao, A. (1998). Experimental determination of bed agglomeration tendencies of some common agricultural residues in fluidized bed combustion and gasification. *Biomass and Bioenergy*(2), 163-169.
- Niessen, W. R. (2002). *Combustion and incineration processes* (3rd ed.). New York: Marcel Dekker.
- Obernberger, I., Dahl, J., & Brunner, T. (1999). Formation, composition and particle size distribution of fly ashes from biomass combustion plants. *The 4th Biomass Conference of the Americas*, 1377-1385.
- Ohman, M., & Nordin, A. (2000). Bed agglomeration characteristics during fluidized bed combustion of biomass fuels. *Energy&Fuel*(14), 169-178.
- Olanders, B., & Steenari, B.-M. (1995). Characterization of ashes from wood and straw. *Biomass Energy*(2), 105-115.
- Olofsson, G., Ye, Z., & Bjerle, I. (2002). Bed agglomeration problems in fluidized-bed biomass combustion. *Industrial and Engineering Chemistry Research*(41), 2888-2894.
- Olsson, J., Jaglid, U., & Petterson, J. (1997). Alkali Metal Emission during Pyrolysis of Biomass. *Energy & Fuels*(11), 779-784.

- Pietsch, W. (2002). *Agglomeration Process: Phenomena, Technologies, Equipment* (First ed.). Weinheim: Wiley-VCH.
- Preto, F., Anthony, E., & Friederich, F. (1987). Combustion trials of rice husks in a pilot scale combustor. *Proceedings of the 9th international Conference on Fluidized Bed Combustion*, 1123-7.
- Richardson, J., & St Jeronimo, M. (1979). Velocity-voidage relations for sedimentation and fluidization. *Chemical Engineering Science*(34), 1419-1422.
- Seville, J., & Clift, R. (1984). The effect of thin liquid layers on fluidization characteristics. *Powder technology*(37), 117-129.
- Seville, J., Silomon-Pflug, H., & Knight, P. (1998). Modelling of sintering in high temperature gas fluidisation. *Powder Technology*(97), 160-169.
- Shiyuan, L., Qinggang, L., & Haipeng, T. (2010). Agglomeration during fluidized-bed combustion of biomass. *The 13th International Conference on Fluidization-New Pradigm in Fluidization Engineering*.
- Siegell, J. (1984). High-Temperature defluidization. *Power Technology*(38), 13-22.
- Thonglimp, V., Hiquily, N., & Lagueira, C. (1984). *Powder Tech*, 233-253.
- Vassilev, S., Baxter, D., Andersen, L., & Vassileva, C. (2010). An overview of the chemical composition of biomass. *Fuel*(89), 913-933.
- Visser, H., van Lith, S., & Kiel, J. (2008). Biomass Ash-Bed Material Interactions Leading to Agglomeration in FBC. *Journal of Energy Resources Technology*.
- Wang, L., Hustad, J., Skreiberg, O., & Gronli, M. (2012). A critical review on additives to reduce ash related operation problems in biomass combustion applications. *Energy Procedia*(20), 20-29.

- Weber, S., Briens, C., Berruti, F., Chan, E., & Gray, M. (2008). Effect of agglomerate properties on agglomerate stability in fluidized beds. *Chemical Engineering Science*(63), 4245-4256.
- Wen, C., & Yu, Y. (1966). A generalized method for predicting the minimum fluidization velocity. *AIChE Journal*(12), 610-612.
- Werther, J., Saenger, M., Hartge, E.-U., Ogada, T., & Siagi, Z. (2000). Combustion of agricultural residues. *Progress in Energy and Combustion Science*(26), 1-27.
- Yang, W.-C. (2005). *Handbook of Fluidization and Fluid-Particle Systems*. Marcel Dekker.
- Zevenhoven-Onderwater, M., Backman, R., Skrifvars, B., & Hupa, M. (2001). The ash chemistry in fluidized bed gasification of biomass fuels. Part I: predicting the chemistry of melting ashes and ash-bed material interaction. *Fuel*(80), 1489-1502.
- Zhang, L., Xu, C., & Champagne, P. (2010). Overview of recent advances in thermo-chemical conversion of biomass. *Energy Conversion and Management*(51), 969-982.



## Chapter 3

### 3 Study on the critical amount of liquid for bed materials agglomeration in a bubbling fluidized bed.

Agglomeration of bed materials at a high temperature is one of the most important and challenging problems for fluidized-bed biomass boilers for thermal/power generation.

In the present study, the critical amount of liquid (molten ash in real biomass boiler operations) that would result in severe bed agglomeration and defluidization was studied in a small pilot-scale cold bubbling fluidized bed (BFB) test rig filled with silica sand particles as bed materials equipped with non-invasive capacitance sensors and differential pressure transducers.

In the cold BFB test rig, a solution of glycerol-water (30% v/v), employed to simulate molten ash in real biomass boiler operations, was injected to the bed in different quantities during the tests.

#### 3.1 Introduction

The declining resources and soaring prices of fossil fuels have intensified the interest and efforts in searching for alternative energy resources (particularly the carbon-neutral energy sources) to substitute for fossil fuels (Shao, et al., 2012). As a carbon-neutral energy source, biomass has received a great deal of attention (Liu, et al., 2009). Among the technologies that can be used to burn biomass for thermal/power generation, fluidized beds are emerging as the most commonly used due to their fuel flexibility and high efficiency (Khan, et al., 2009). Conversion of carbonaceous solid material such as coal and biomass in fluidized bed (FB) has proved to be promising for generating steam, electricity and hydrogen (Bartels, et al., 2008).

High pressure steam and electric power are needed in pulp and paper mills, for many processes including drying pulp and paper products, heating water and process liquors, concentrating spent cooking liquor (e.g., black liquor). Burning concentrated black liquor in recovery boilers contributes about 60 to 70% of the energy requirement in a modern

pulp/paper mill, while the remaining 30 to 40% is generated by biomass combustion in biomass boilers. There are about 300 large biomass boilers in pulp and paper mills in North America; along with a large number smaller units operated in lumber mills, tissue mills, and plywood mills, etc.

Despite its broad application, biomass combustion/gasification in fluidized bed processes still has some technical difficulties. Bed material agglomeration is a major operational problem. Usually, a fluidized bed biomass boiler involves silica sand as bed material in the presence of ash. Inorganic alkali components from the fuel, mainly potassium (K) and sodium (Na), can be problematic as they form low-melting alkali compounds and may also react with the bed material forming low-melting alkali silicates. The alkali content can vary much between fuels; it is especially high in the case of agricultural crop residues. When both alkalis and silica are present in the bed, they can form compounds with low melting temperatures, forming a “viscous” layer to coat the sand particles and form agglomerates. The sand particles agglomerates with a sticky layer would grow larger with time upon collisions. This eventually leads to partial or complete defluidization of the reactor, which in turn results in a lengthy and expensive unscheduled shutdown (Bartels, et al., 2008).

In terms of agglomeration mechanisms, when two particles adhere to agglomerate, material at the point of contact migrates forming a neck with adhesion forces that are stronger than the disruptive forces in the fluidized bed (Seville, et al., 1998). Two types of adhesion were proposed: 1) visco-plastic sintering of glassy material, 2) liquid phase (leading to capillary force) produced by melting or by chemical reactions (Skirfvars, et al., 1992; Skirfvars, et al., 1994). It is obvious that exist a minimum or critical amount of visco-plastic or liquid phase to form the bed materials agglomerates. However, to the best of the authors’ knowledge, such minimum or critical amount of visco-plastic or liquid phase for bed materials agglomeration is yet to be reported.

There is a common agreement between many researchers that the bed materials agglomeration process in a bubbling fluidized bed (BFB) boiler is the result of stickiness or adhesiveness of bed material caused by alkali compounds. “Stickiness” of bed

particles can result mainly from the presence of a liquid (melt) phase or glassy phase by visco-plastic sintering.

Bed materials agglomeration dramatically changes the fluidization behavior of a BFB, thus the fluidization characteristics of the bed such as minimum fluidization velocity, bubble size and bubble frequency, among others are highly affected (Tardos & Pfeffer, 1995). Therefore changes in bubble properties can be used as a method for agglomeration detection in BFBs.

The main objective of this work is to investigate and determine the critical amount of liquid phase required to form agglomeration in BFB boilers. The results of this research would help develop new strategies to prevent bed agglomeration in biomass BFB boilers. In this study, a small pilot-scale cold BFB test rig was used, and a solution of glycerol-water (30% v/v) was employed to simulate molten ash in real biomass boiler operations and was injected to the bed at different quantities during the tests. Two techniques used for agglomeration detection were planar capacitance sensors and differential pressure drop signals.

## 3.2 Experimental apparatus and methods

### 3.2.1 Facility description

The research was completed at room temperature in a small pilot-scale cold BFB test rig at ICFAR in Western University. A schematic of the cold BFB test rig is shown in Figure 3-1. The rig is 1.97 m total high, has stainless steel walls with a trapezoidal cross sectional area, and is equipped with planar capacitance sensors located on the outside of the bed wall over a rectangular wood window embedded in the reactor wall. The rig is also equipped with a differential pressure transducer to monitor the total bed pressure drop. A porous steel plate distributor is located at the bottom of the bed.

Cold BFB tests were chosen and a mixture of glycerol-water solution was used to simulate the molten ash in real biomass boiler operations, because at room temperature the simulated molten ash can be injected into the reactor in a well-controlled way.

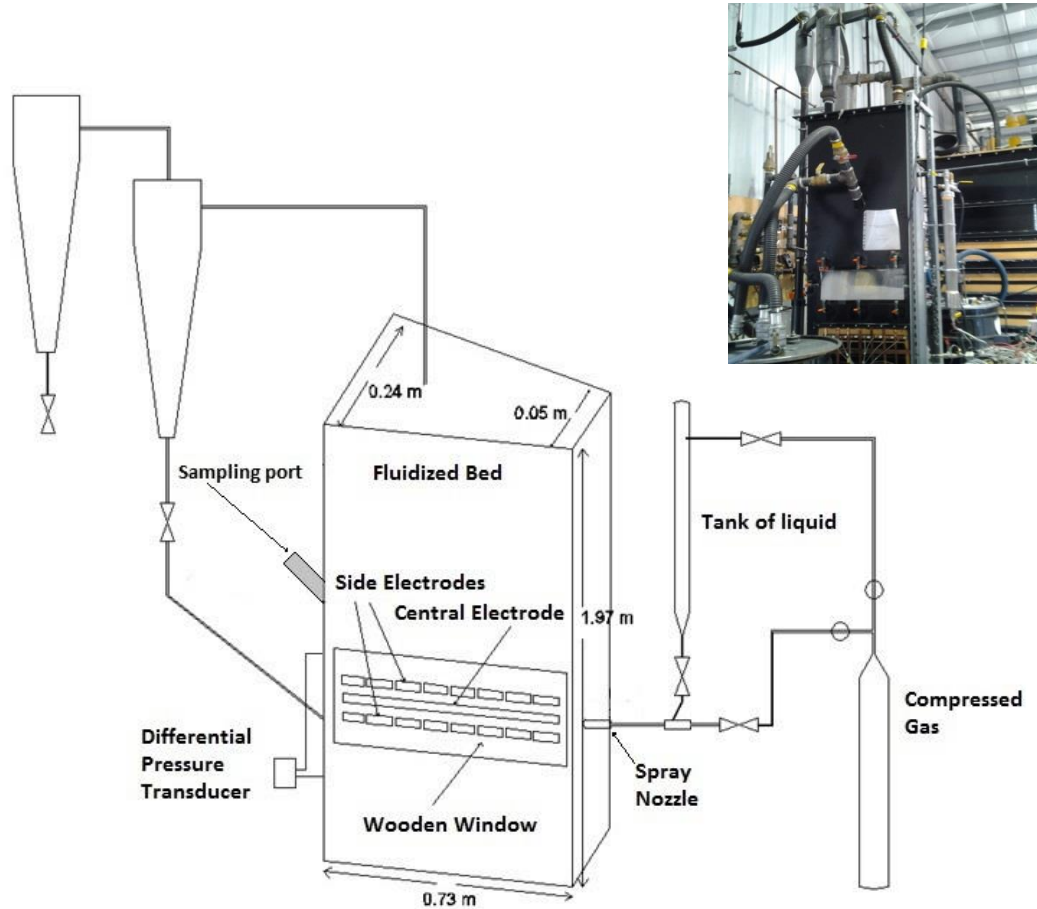


**Figure 3-1: Schematic diagram of the small pilot-scale cold BFB test rig used**

### 3.2.2 Methods

To determine the critical amount of liquid (molten ash in real biomass boiler operations) that would result in severe bed agglomeration and defluidization, the cold BFB test rig (Figure 3-1) was used. In each test, the bed was filled with approx. 68 kg quartz sand (silica) as bed material (with a Sauter mean diameter of 204  $\mu\text{m}$  and particle density of 2600  $\text{kg/m}^3$ ). The bed materials were fluidized with air at various superficial gas velocities at ambient temperature and pressure.

Different quantities of a glycerol-water (30% v/v) solution were injected to the bed with a spray nozzle using compressed air, i.e., 0.0, 0.1, 0.2, 0.3, 0.4, 0.5, 0.6, 0.7, 0.8, 1.0 and

1.4 wt% in relation to the weight of silica sand loaded to the BFB test rig. The glycerol-water (30% v/v) mix was chosen as simulated liquid for molten ash in real biomass boiler operations because it has a viscosity of around 3-4 cP at room temperature, as shown in Table 3-1, similar to the viscosity of the liquid (alkali compounds melts) phase at a high temperature (Tran, et al., 2006; Janz, et al., 1968). Table 3-1 shows the glycerol-water (30% v/v) viscosity.

**Table 3-1: Viscosities of glycerol-water mix (30% v/v) at various temperatures measured following the ASTM D445 Standard**

Temperature (°C)	Viscosity (cp)
22	3.6
25	3.4
31.5	2.9

The bed was fluidized with air and three superficial gas velocities were used in order to examine the effects of gas velocity on the bed agglomeration phenomena. The superficial air velocities tested were: 0.14 m/s, 0.2 m/s, 0.27 m/s, corresponding to 4, 6 and 8 times of  $U_{mf}$ , respectively.

The bubble properties were measured through planar capacitance sensors and its signal was measured with an acquisition frequency of 100 kHz for 55 sec. The bed pressure drop was measured with a differential pressure transducer with acquired frequency of 1 kHz for 10 min. After each glycerol-water (30% v/v) injection, the bed was fluidized for 15 min in order to reach steady state conditions then the capacitance and pressure signals were collected in the manner described above.

In each test, bed material samples were carefully collected using a custom-designed particle sampling device from the sampling port above the freeboard zone of the BFB test rig (as shown in Figure 3-1). The obtained samples were however too fragile to be measured in particle size by sieving or other analytical methods, except that photos were taken for image analysis. For some typical samples, SEM images were taken using a Hitachi 3400-N Variable Pressure Scanning Electron Microscope (VP-SEM).

As was previously mentioned, variations in bubble behaviors can be used as a detection method for bed materials agglomeration. While viscous liquid is injected into the bed, agglomerates would form, resulting in changes in the bubble behaviors within the bed, e.g., forming channeling and defluidized zones in some locations of the BFB bed which could lead to different bubble frequencies at different locations in the bed.

Bubble frequency can be defined as the number of bubbles passing through a specific area of the bed in a certain period of time. Under normal fluidized conditions, it is expected that the bubble frequency through different sections along the bed are similar. However, when the bed materials undergo agglomeration it causes changes in the bubbling fluidization behavior, e.g., the bubble frequency through different locations within the bed is expected to be different, as conceptually illustrated in Figure 3-2.

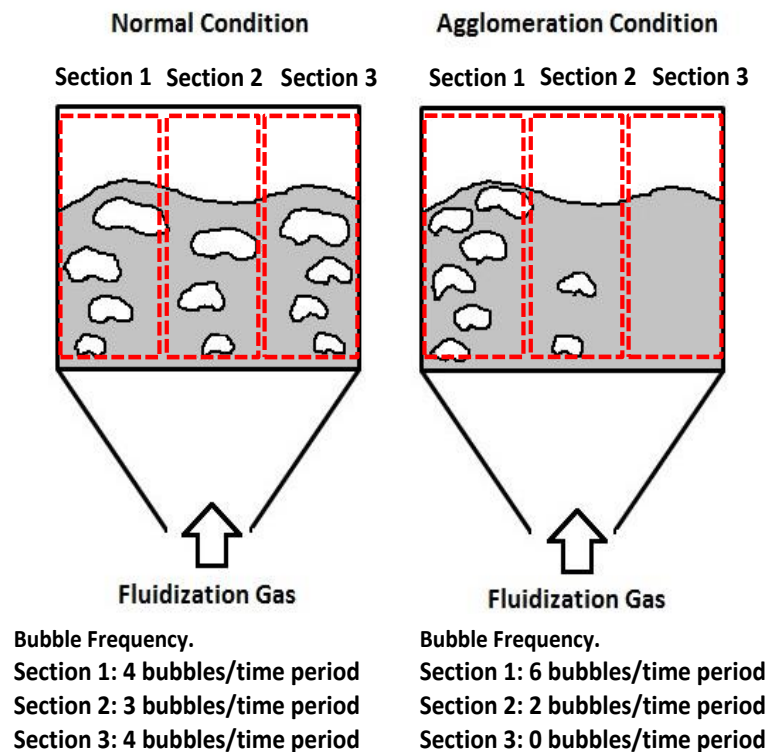


**Figure 3-2: Bubble frequency in a fluidized bed divided into three different sections under different fluidizing conditions**

Standard deviation of bubble frequency (STDBF) for various electrodes located along the BFB (Figure 3-1) has been considered as an important tool for evaluating the bubbling fluidization status (Hamidi, et al., s.f.). A uniformly bubbling bed can be characterized by lower STDBF and a bed with agglomeration or channelling problems can be characterized by higher STDBF. In this work, in order to study the critical amount of viscous liquid for bed agglomeration, the STDBF for 7 electrodes located along the bed was recorded vs. the amount of injected liquid.

Differential pressure drop is another commonly used indicator for the status of a bubbling fluidized bed; in uniformly bubbling fluidization, the pressure drop through the bed shall be equal to the total hydrostatic pressure drop of the bed, that is:

$$\Delta P = \rho_b L_B g \quad \mathbf{3-1}$$

Where  $\Delta P$  is the pressure drop across the bed,  $\rho_b$  is the bulk density of the bed,  $L_B$  is the height of the bed, and  $g$  is the gravity.

A normal fluidized bed can be characterized by a higher pressure drop and an agglomerate fluidized bed can be characterized by a lower pressure drop due the channeling and agglomerated zones.

### 3.3 Results and Discussion

#### 3.3.1 Capacitance and pressure analysis

Figure 3-3 shows the variation of standard deviation of bubble frequency (STDBF) in the BFB with the injected amount of glycerol-water (30% v/v) at different fluidization velocities ( $U_g$ ).

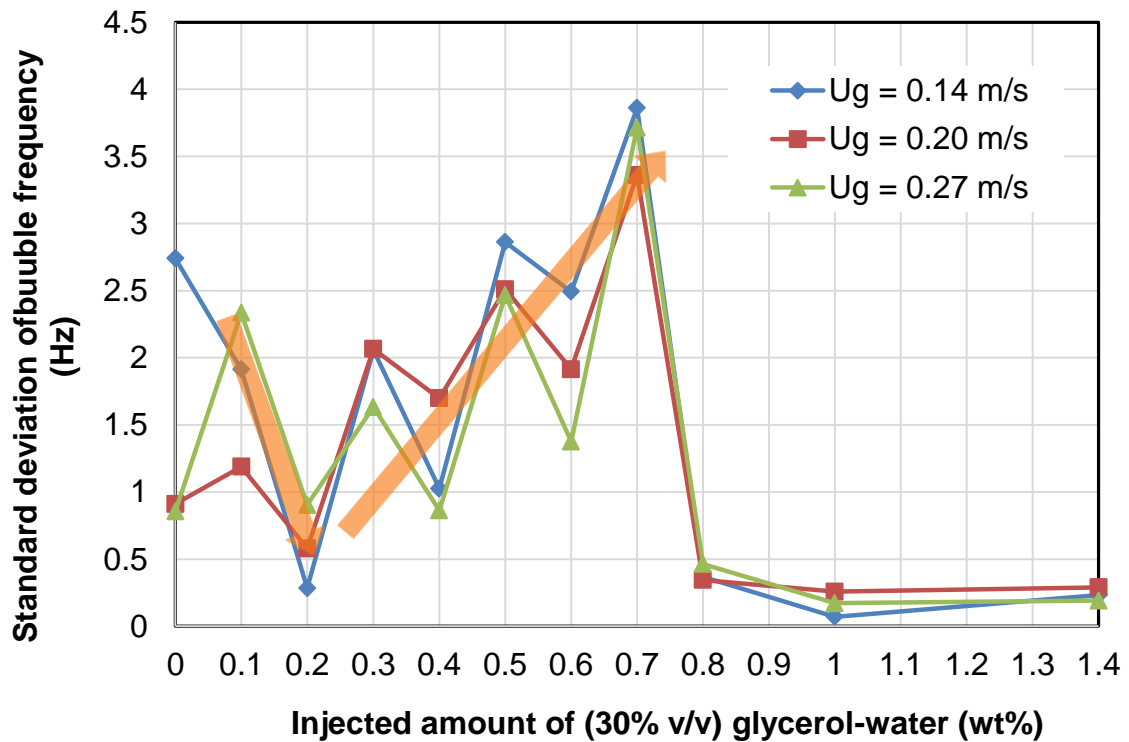


**Figure 3-3: Standard deviation of bubble frequency vs. injected amount of glycerol-water (30% v/v) (wt% in relation to the bed material loaded into the bed)**

From Figure 3-3 it can be seen that the STDBF is relatively high for the operation at lower velocity ( $U_g = 0.14$  m/s, corresponding to  $4U_{mf}$ ) when the bed is dry (at 0 wt% liquid injection of glycerol-water (30% v/v)), but the STDBF decreases with increasing the liquid injection amount up to 0.2 wt%. Fluidization of dry sand materials at lower gas



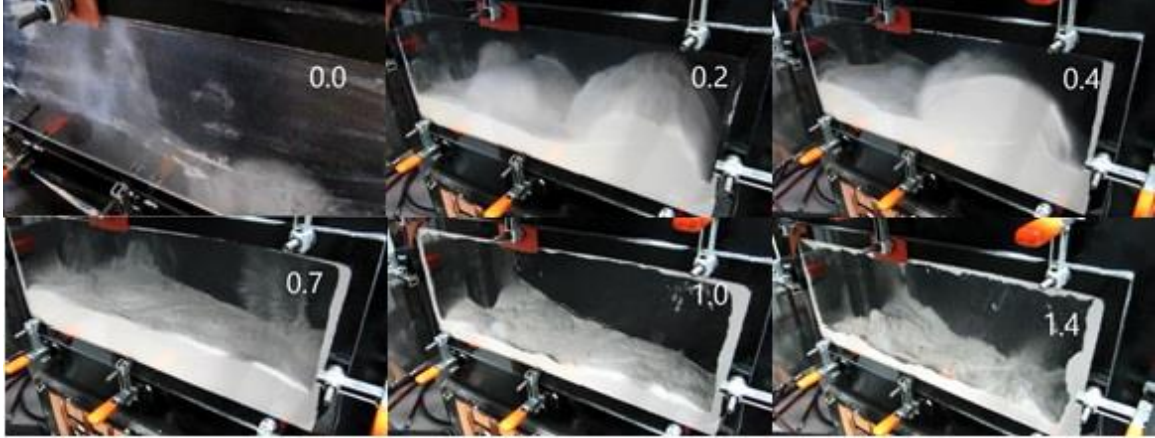
velocities could not be homogeneous enough due to the existence of interparticle cohesive forces (e.g., electrostatic force) (Hassani, et al., 2013; Ciborowski & Wlodarski, 1962), which may explain the larger STDBF at 0 wt% liquid injection (Figure 3-3). In addition, while the gas velocity is low, the number of bubbles is less or the size of bubbles is small which increases the difficulty of measuring bubbles using capacitance electrodes, which hence could result in a larger STDBF value. As the gas velocity  $U_g$  is increased, more bubbles of a larger size are formed throughout the bed, and more importantly an increased  $U_g$  would lead to an increased drag force that overcomes the cohesive electrostatic force. As a result, the STDBF values at a higher  $U_g$  are generally lower and more uniform when comparing with those at a lower  $U_g$ , as evidenced in Figure 3-3. Very interestingly, when injecting a small amount ( $\leq 0.2$  wt%) of glycerol-water liquid into the bed materials, the electrostatic cohesive force seemed to be reduced, which hence improves the bubbling fluidization uniformity, as evidenced by the drastically decreased STDBF at 0.2 wt% liquid injection (Figure 3-3).

As liquid injection amount increased further to above 0.2 wt%, for all gas velocities, the STDBF started to increase gradually, while the bed was observed to begin channeling (agglomeration) in some locations due to the increased cohesion of the bed materials caused by the increased injection amount of the glycerol-water liquid.

As clearly shown in Figure 3-3, the values of STDBF sharply decrease while increasing the liquid injection amount to  $> 0.7$  wt%, which is likely due to the severe agglomeration and channeling and even de-fluidization of the bed due to the poor fluidization conditions.

The variation of the fluidization state inside the BFB at  $U_g$  of 0.14m/s (or  $4U_{mf}$ ) with the glycerol-water liquid injection amount increasing from 0 to 1.4 wt% is depicted in Figure 3-4. It is clearly shown that the bed materials were fluidized uniformly up to 0.2 wt% liquid injection. After that, increasing liquid injection amount led to more non-uniformly distributed bubbles and lumps of the sands caused by increased viscous properties of the bed materials. Severe bed materials agglomeration and channeling were observed while the liquid injection amount was above 0.7 wt%. Thus, the bed materials started to

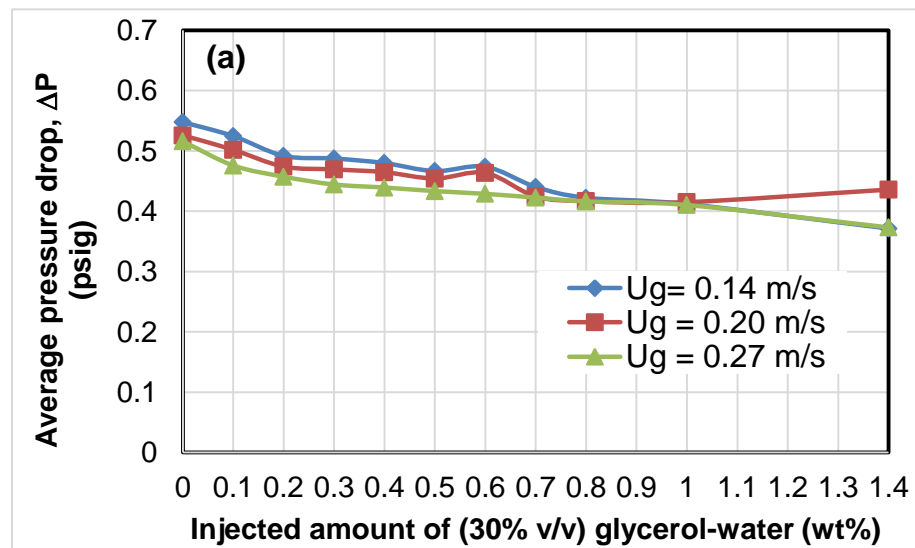
agglomerate from 0.2 wt% liquid injection, and the bed materials agglomeration/channeling became severe after 0.7wt% liquid injection, resulting in a very poor fluidization state.



**Figure 3-4: Variation of the fluidized state inside the BFB at  $U_g$  of 0.14m/s (or  $4U_{mf}$ ) with the glycerol-water liquid injection amount increasing from 0 to 1.4 wt%**

Also it can be seen from Figure 3-3, that the fluidization gas velocities do not affect the bed agglomeration behaviors.

Figure 3-5a and Figure 3-5b show the effect of the glycerol-water (30% v/v) injection and superficial gas velocities on the average pressure drop of the bed, and the slope of the bed pressure drop versus the liquid injection amount, respectively.



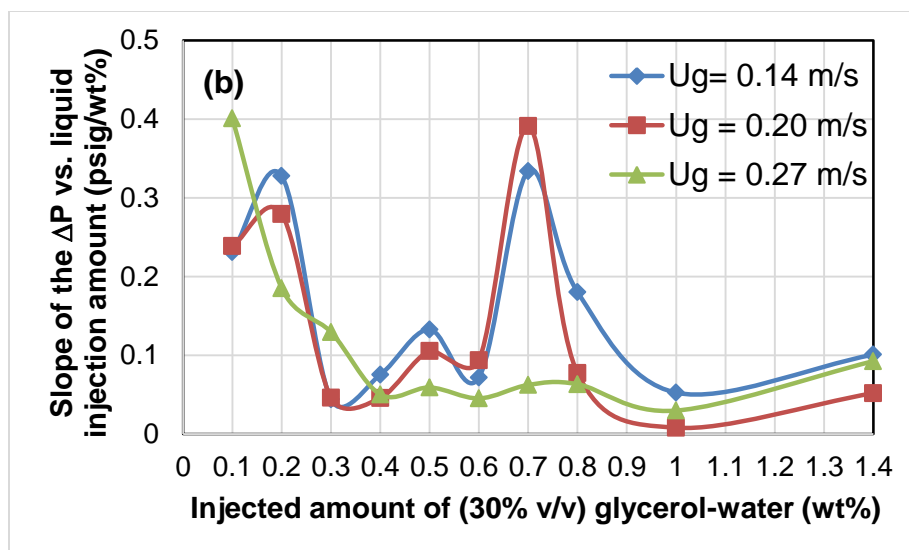


**Figure 3-5: Effect of the glycerol-water (30% v/v) (wt% in relation to the bed material loaded into the bed), injection and superficial gas velocities on the average pressure drop of the bed (a), and the slope of the bed pressure drop versus the liquid injection amount (b)**

As a common observation clearly shown in Figure 3-5, the fluidizing gas velocity has negligible effects on the bed pressure drop, which is expected as the fluidized bed is in its bubbling fluidization regime at all the superficial air velocities tested: 0.14 m/s, 0.2 m/s, 0.27 m/s, corresponding to 4, 6 and 8 times of  $U_{mf}$ , respectively. On the other hand, the average bed pressure drop decreases continuously with increasing the liquid injection amount. The continuously decreasing behavior for all the velocities while the glycerol-water (30%v/v) was injected implies the increased formation of channeling and agglomeration phenomena inside the BFB.

In order to examine the magnitude of the average pressure drop decreases against the injection amount of the liquid mix, we made first derivative (or calculate the slope) of the pressure drop plots (Figure 3-5a), to produce the slope of the pressure drop vs. wt% of liquid injection amount, as displayed in Figure 3-5b. Interestingly, it can be seen from Figure 3-5b that there are 2 peak positions at 0.1-0.2 wt%, 0.7-0.8 wt% of the injected liquid, respectively, that coincidentally match with the critical/severe bed channeling/agglomeration points as determined previously from Figure 3-3. This is also

expected, since the formation of channels/agglomerates would cause bypassing of the fluidizing gas through the channels or vicinities of the agglomerates, hence decreasing the overall bed pressure drop across the fluidized bed.

### 3.3.2 Analysis of bed material samples

For further analysis on the bed materials, samples were collected from the BFB during the fluidization experiments at various liquid injection amounts at various fluidizing gas velocities.

It was found that it is extremely difficult to measure the particle size distribution for the agglomerates as the agglomerates formed in the fluidization operations are very weak in mechanical strength, and they broke during the sampling and discharging operations. Figure 3-6 shows the photos taken for four samples of bed materials after injection of glycerol-water (30% v/v) liquid at different concentrations (0.0 wt%, 0.2wt%, 0.5 wt%, 1.4 wt%). It can be seen from the photos, that the bed materials appear to be more cohesive with more agglomerates at a higher injection amount of the liquid.



**Figure 3-6: Samples of bed materials after fluidization at different glycerol-water (30% v/v) injection amounts**

Figure 3-7a and Figure 3-7b show the SEM images for samples of the bed materials at 0 wt% (pure silica sand) and 1.4wt% glycerol-water (30%v/v) liquid injection, respectively. Comparing with dry sand particles of relatively smooth surface as illustrated in Figure 3-7a, the surfaces of the sand particles from the bed at 1.4wt% liquid injection are rougher and covered with a thin coating layer likely of glycerol (Figure 3-7b), which would form liquid bridge between particles during fluidization, responsible for the formation of channeling/agglomeration of the bed materials.

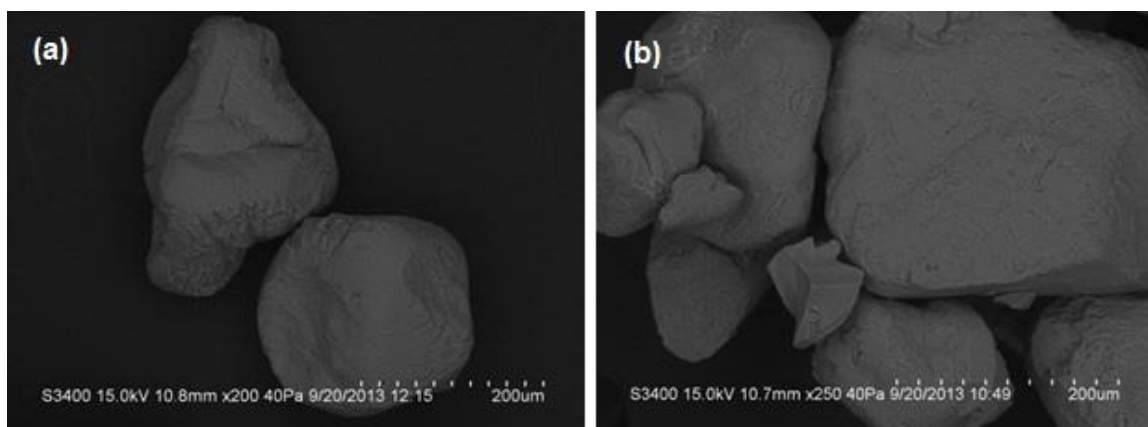


**Figure 3-7: SEM image of sand particles from the BFB at 0.0wt% (a) and 1.4wt% (b) liquid injection, respectively**

### 3.4 Conclusions

A systematic study was conducted to investigate and determine the critical amount of liquid required to form bed materials agglomeration in biomass BFB boilers, employing a cold BFB test rig by injection of a liquid solution of glycerol-water (30% v/v) to simulate molten ash in real biomass boiler operations. From this study, it was determined that in the BFB fluidization system tested the critical liquid amount that could cause the bed materials start to form agglomeration/channeling, and form severe agglomeration/channeling (poor fluidization) is approx. 0.2 wt% and 0.7wt%, respectively. In the present fluidization system, the fluidization gas velocity did not appear to affect the bubbling and pressure drop behaviors, nor the minimum amount of liquid required for bed materials agglomeration.

### 3.5 References

- Bartels, M., Lin, W., Nijenhuis, J., Kapteijn, F., & Ommen, J. (2008). Agglomeration in fluidized beds at high temperatures: Mechanisms, detection and prevention. *Energy and Combustion Science*(34), 633-666.
- Ciborowski, J., & Wlodarski, A. (1962). On electrostatic effects in fluidized beds. *Chemical Engineering Science*(17), 23-32.
- Hamidi, M., Berruti, F., Briens, C., & McMillan, J. (s.f.). Bogging detection in a fluidized bed using planar capacitance sensors.
- Hassani, M., Zarghami, R., Norouzi, H., & Mostoufi, N. (2013). Numerical investigation of effect of electrostatic forces on the hydrodynamics of gas-solid fluidized beds. *Powder Technology*(246), 16-25.
- Janz, G., Dampier, F., Lakshmi-Narayanan, G., & Lorenz, P. (1968). *Molten salts: Volume 1*. National standard Reference Data Series.
- Khan, A., Jong, W., Jansens, P., & Spliethoff, H. (2009). Biomass combustion in fluidized bed boilers: Potential problems and remedies. *Fuel Processing Thecnology*(90), 21-50.
- Liu, H., Feng, Y., Wu, S., & Liu, D. (2009). The role of ash particles in the bed agglomeration during the fluidized bed combustion of rice straw. *Bioresource Technology*(100), 6505-6513.
- Seville, J., Silomon-Pflug, H., & Knight, P. (1998). Modelling of sintering in high temperature gas fluidisation. *Powder Technology*(97), 160-169.
- Shao, Y., Xu, C., Zhu, J., Preto, F., Wang, J., Tourigny, G., y otros. (2012). Ash and chlorine deposition during co combustion of lignite and chlorine-rich Canadian peat in a fluidized bed - Effects of blending ratio, moisture content and sulfur addition. *Fuel*(95), 25-34.

- Skirfvars, B., Hupa, M., & Hiltunen, M. (1992). Sintering of ash during fluidized bed combustion. *Ind Eng Chem*(31), 1026-1030.
- Skirfvars, B., Hupa, M., Backman, R., & Hiltunen, M. (1994). Sintering mechanisms of FBC ashes. *Fuel*(73), 171-176.
- Tardos, G., & Pfeffer, R. (1995). Chemical reaction induced agglomeration and defluidization of fluidized beds. *Powder Technology*(85), 28-35.
- Tran, H., Sunil, A., & Jones, A. (2006). The fluidity of Recovery Boiler Smelt. *Pulp and Paper Science*(3), 182-187.

## Chapter 4

### 4 Study of bed materials agglomeration in a heated bubbling fluidized bed (BFB) using silica sand as the bed material and KOH to simulate molten ash

#### 4.1 Introduction

The continuously increasing prices and consumption of fossil fuels, as well as concerns about their availability in the near future, have resulted in an increasing interest for alternative energy resources (Cheng, 2009).

The production of bioenergy from biomass has received a great deal of attention, due to its renewability and carbon neutrality (Gustavsson, et al., 1995). In the last decades, many biomass thermal/power plants with different technologies have been built. Among these technologies, fluidized beds (FB) are emerging as the most commonly used technology (Khan, et al., 2009).

Fluidized bed conversion (combustion and gasification) is an industrial practice for thermal/power generation, mainly due to its high combustion efficiency, low emission level and good fuel flexibility. However, biomass ash normally has high alkali content (it is especially high in the case of agricultural crop residues), which can form compounds with low melting temperature, eventually leading to agglomeration of the bed materials, corrosion and deposition problems (Khan, et al., 2009).

Typically, conversion of solid fuels is carried out in fluidized bed reactors with silica sand as bed material in the presence of ash derived from the solid fuels. Inorganic alkali components from the fuel, mainly potassium (K) and sodium (Na), can be problematic as they form low-melting temperature alkali compounds and may also react with the bed material forming low-melting alkali silicates. These low-melting temperature alkali compounds would coat the sand particles with a sticky layer. This makes sand particles agglomerate upon collisions and grow larger with time, eventually leading to partial or complete de-fluidization of the reactor.



Formation of agglomerates makes particle size distribution of the bed material wider, which can result in segregation inside the bed and uneven temperature distribution (Ekinci, et al., 1990; Atakul & Ekinci, 1990). The following figure shows the progress of agglomeration, segregation and de-fluidization based on visual observations in a straw (with a high alkali content, approx. 26.37 wt%) fluidized bed boiler (Lin & Dam-Johansen, 1997).

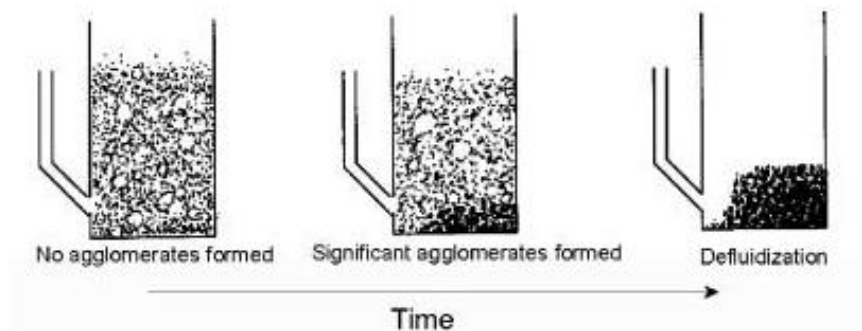


**Figure 4-1: Agglomeration, segregation and de-fluidization in a BFB (Lin & Dam-Johansen, 1997)**

When severe agglomeration occurs, the bed could lose fluidization, and several large channels are formed through the bed by the fluidization air. The interparticle forces which caused the particles to agglomerate are relatively weak, thus the channels are rather easily formed. Pressure drop measurements can be used as a method for agglomeration detection in BFBs (Siegell, 1984). Large fluctuations of the bed pressure can be detected in the beginning of agglomeration in a BFB (Werther, et al., 2000). At the point of de-fluidization, there is a rapid decrease in pressure drop, mainly because most of the fluidization gas goes through channels rather through the slumped bed.

In addition, temperature measurements may be used as a detection method for agglomeration, in a well fluidized bed the bed temperature is very uniform, but when agglomerations occurs the difference between the bottom of the bed and other points above becomes larger due to poor mixing and/or severe segregation conditions (Siegell, 1984; Ekinci, et al., 1990).

Bed agglomeration is one of the major operational challenges in BFB boiler operation, particularly when agricultural residues with high KCl contents are burned. Various technical approaches for reducing ash deposition and bed agglomeration have been studied, including addition of additives such as aluminum sulphate and kaoline to convert KCl to  $K_2SO_4$  and potassium aluminum silicates (Jensen, et al., 2000; Westberg, et al., 2003); co-firing biomass with low fouling-tendency fuels (Theis, et al., 2006), lowering the dense phase fluidized-bed temperature, and using alternative bed materials (Olofsson, et al., 2002).

Visser et al. (2008) proposed two types of agglomeration mechanisms: 1) “melt induced” where a liquid phase is produced by molten ash or by chemical reactions 2) visco-plastic sintering of glassy material “coating-induced”.

The particles that form the agglomerate structure are held together by short range physical or chemical forces between the particles, or through substances that act as binders by adhering physically or chemically to form material bridges between particles, for example, liquid bridges (Pietsch, 2002). In biomass conversion in BFB at a high temperature the low melting alkali compounds act as a free liquid forming liquid bridges, and their forces arise from liquid surface tension and capillary forces. The alkali compounds can also act as, solid bridge forces, a type of strong bonding force produced by chemical reactions, sintering, melting or recrystallization (Zhou, et al., 2013).

This study concerns the liquid-solid agglomeration formed by the low-melting alkali compounds by the “melt induced” mechanism. The amount of liquid (molten ash) within an agglomerate determine the state of liquid saturation of the agglomerate. In the pendular state, particles are held together by liquid bridges at their contact points. As the pore space is filled with liquid the agglomerate saturation becomes funicular (transition between pendular and capillary state). When the agglomerate is saturated and reaches the capillary state, all the voids are filled with liquid and the surface liquid is drawn back into the pores under capillary action (Pietsch, 2002).

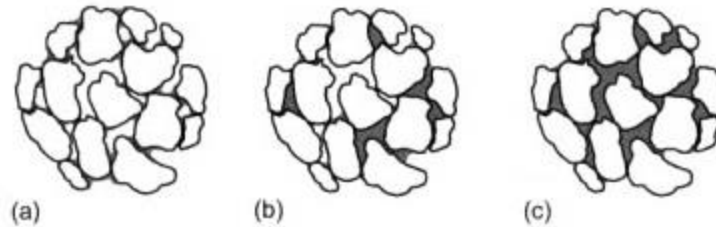


**Figure 4-2: Saturation states in liquid-solid agglomerates. (a) Pendular state, (b) Funicular state, and (C) Capillary state (adapted from Pietsch, 2002)**

However, the mechanism of agglomeration and the temporal dynamics of particle agglomeration are not well understood. It is not clear if bed agglomeration is caused simply by molten alkali salts that bind ash and bed particles together as they collide in-flight, or by chemical reactions between alkalis, other ash components and bed materials at high temperatures. The objective of this research project was therefore to investigate the bed agglomeration mechanisms and factors affecting bed agglomeration in BFB boilers burning mixtures of biomass. The research was and will be carried out in four stages:

- Stage I involving experiments in a cold BFB test rig using glycerol-water as the model system to simulate molten ash (the results were reported previously in Chapter 3);
- Stage II using a hot BFB (electrically heated to  $\sim 400^{\circ}\text{C}$ ) and a low melting point salt to simulate molten ash (the results are reported in the present Chapter);
- Stage III involving a hot BFB (heated to  $800^{\circ}\text{C}$  electrically) with addition of different amounts of a mixture of  $\text{KCl}$ ,  $\text{K}_2\text{SO}_4$ ,  $\text{NaCl}$  and  $\text{Na}_2\text{SO}_4$  to simulate molten ash, and
- Stages IV involving a hot BFB (heated to  $\sim 800^{\circ}\text{C}$  by wood pellet combustion) with addition of different amount of agricultural residues (corn stalk) with high  $\text{KCl}$  contents (the results of Stages III and IV will be reported in the future).

The main objective of this study (Stage II) was to investigate and determine the critical amount of liquid phase for agglomerating the bed material (silica sand particles) in a bubbling fluidized bed operated at elevated temperatures using low melting-point salt (KOH, melting point  $\sim 400^{\circ}\text{C}$ ) to simulate molten ash. The results of this research would help develop new strategies to prevent bed agglomeration in biomass BFB boilers.

## 4.2 Experimental Materials and methods

### 4.2.1 Facility description

The experiments were conducted in a small pilot-scale hot BFB test rig located at Western Research Park (Sarnia). A schematic of the hot BFB is shown in Figure 4-3. The test rig was made of stainless steel 316L, is 1.75m total height and its column has an inner diameter of 76 mm.

As is illustrated in Figure 4-3, the facility is equipped with two electric furnaces to heat the column and to preheat the fluidization air, a screw feeding system combined with a rotary airlock valve, a deposit collecting port (top of the bed), a cyclone for removal and collection of small particles in the effluent gas, a bag filter, a primary air inlet (fluidization gas) and a secondary air inlet (to assist volatile combustion when the reactor is used as a combustor for biomass), a water-cooled condenser for tar removal, and a flue gas sampling port. The non-condensable gases are vented to the outside of the building and into the environment.

The reactor's instrumentation consists of 7 thermocouples, 2 pressure transducers and 2 pressure gauge located at different positions in the system (Figure 4-3). The signals from the thermocouples and the pressure transducers are collected with an Omega data acquisition system which is connected by an USB port to a personal computer equipped with a custom-designed software.

The reactor has a firing capacity of 1-2 kg/hr dry biomass. For more details about the facility, please see Appendix A.

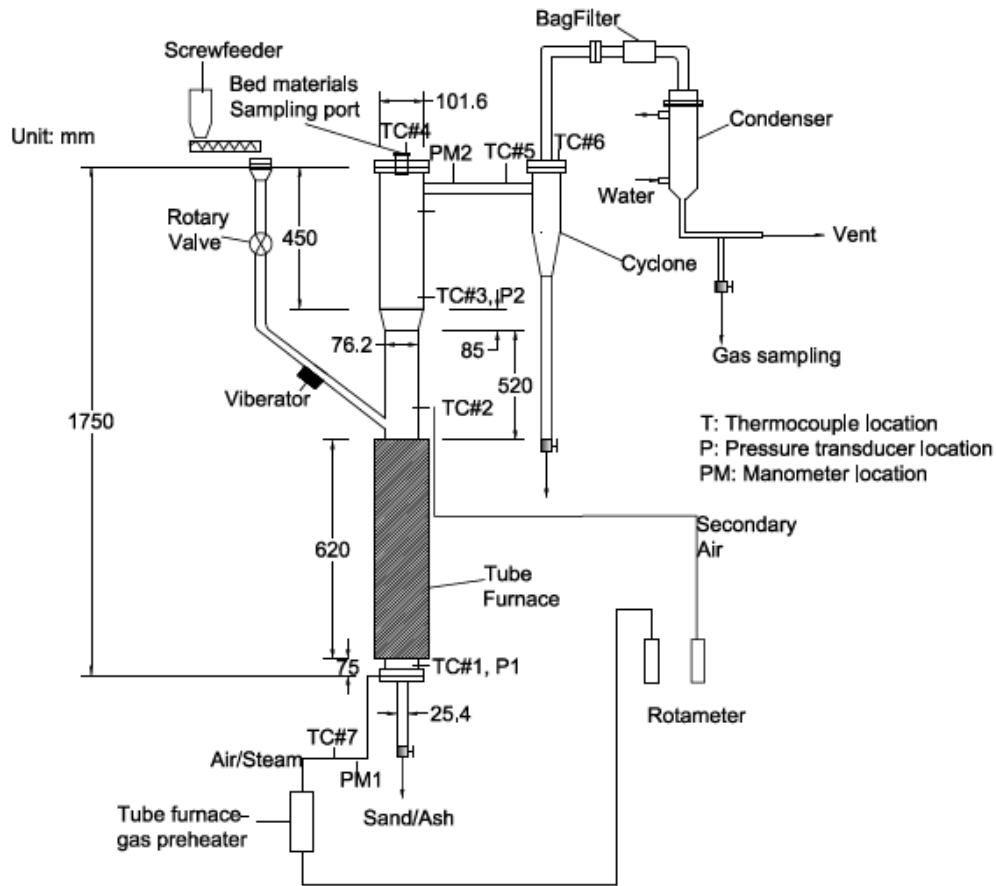


**Figure 4-3: Schematic diagram of the bubbling fluidized-bed system at Western Research Park, Sarnia.**

#### 4.2.2 Methods

To determine the critical amount of liquid (molten ash) that would result in severe bed agglomeration and de-fluidization, the bed was filled with silica sand (99.88%  $\text{SiO}_2$ , melting temperature  $1450^\circ\text{C}$ ) mixed with different quantities of a low melting-point salt (KOH) to simulate molten ash, at 0.2%, 0.5% or 0.8% wt% in relation to the weight of silica sand loaded to the BFB test rig.

In all the experiments the same amount of sand particles (approx. 6.19 kg with a Sauter mean diameter of  $204\ \mu\text{m}$  and particle density of  $2600\ \text{kg/m}^3$ ) were used with a static bed height of approximately 0.5 m.

Due to the operational challenges caused by the low melting point salt (KOH) (becoming cohesive while absorbing moisture) and the very small quantities required it for the tests, KOH in each test was pre-mixed with 2.5 kg of the bed material and were fed into the reactor directly from the ash sampling port at the top of the freeboard zone. The remaining 3.69 kg of silica sand were fed using the screw feeder feeding system. Before starting the experiments the bed material and the KOH were fluidized for a few minutes to enhance the homogeneous mixing. The superficial air velocities tested were: 0.14 m/s, and 0.21 m/s, corresponding to 3.9 and 5.9 times of  $U_{mf}$ , respectively.

The temperature and pressure in the bed were continuously measured using the Omega data acquisition system. At the end of each experiment the bed material was discharged from the bottom of the BFB test rig and analyzed for the particle size distribution by sieving.

A summary of the experimental tests and conditions are presented in Table 4-1

**Table 4-1: Summary of the tests**

Fluidization velocity	Test N°	KOH wt% of total bed material loaded <sup>1</sup>
3.9 $U_{mf}$	Test # 1	0.0
	Test # 2	0.2
	Test # 3	0.5
	Test # 4	0.8
5.9 $U_{mf}$	Test # 5	0.0
	Test # 6	0.2
	Test # 7	0.5
	Test # 8	0.8

<sup>1</sup>In relation to the weight (6.19kg) of silica sand loaded to the BFB test rig

The KOH used for the tests was reagent grade, flakes, purchased from Sigma-Aldrich. Due to the large and irregular particles (flakes) for the KOH, it was crushed using a mortar and sieved it between 300 $\mu$ m - 850  $\mu$ m.

Once the mix (silica sand – KOH) was filled in to the BFB, the reactor was heated up to around 415-420°C (this temperature was determined by the melting point of KOH ~

400°C) using the electric furnace, and it was kept in that temperature for approx. one hour in order to reach steady state conditions. Then both electric furnaces (for bed material heating and fluidizing air preheating) were set at room temperature and the reactor was cooled down to approx. 80°C, before discharging the bed-materials from the BFB column into a container, followed by sieving and weighing to evaluate the particle size distribution for the resulted agglomerates.

## 4.3 Results and Discussion

The following sections present the results obtained for the BFB tests operating at two superficial gas velocities (0.14 m/s, and 0.21 m/s, corresponding to 3.9 and 5.9 times of  $U_{mf}$ , respectively) when different amounts of KOH were mixed with the bed material and heated up to approx. 415-420°C.

### 4.3.1 Temperature and pressure measurements

#### 4.3.1.1 Blank tests without KOH

Figure 4-4 shows the variation of the temperature and pressure in the BFB against time during the blank test at  $3.9U_{mf}$  (A) and  $5.9 U_{mf}$  (B), respectively, where the concentration of KOH in the bed material was 0.0 wt %, including 3 stages of operation: 1) warming up, 2) steady-state operation and 3) cooling down.

From Figure 4-4 A and B, it can be seen that as the temperature increases the pressure fluctuation increases. The pressure fluctuation can be related to the motion of bubbles escaping at the surface of the bed. Fan et al (1981) have reported that one of the most important causes for pressure fluctuations is the gas bubbles bursting at the bed surface. The increase in the pressure fluctuation is believed to be related to the altered gas viscosity at various temperatures. As is well known, gas viscosity increases with increasing temperature. For instance, viscosity of air increases from 0.019 cP at room temperature to 0.033 cP at 400°C. Due to the increase in gas viscosity and hence the drag force of the fluidizing gas at a higher temperature, as the temperature is increased the minimum fluidization velocity ( $U_{mf}$ ) would decrease (Lin, et al. 2002; Pattipati & Wen, 1981). Thus, the minimum bubbling velocity would decrease, and larger bubbles are expected to form, which are faster moving due to a bigger size. The faster rising velocity and larger bubble sizes would produce a larger pressure fluctuation when they burst at the surface of the fluidized bed.



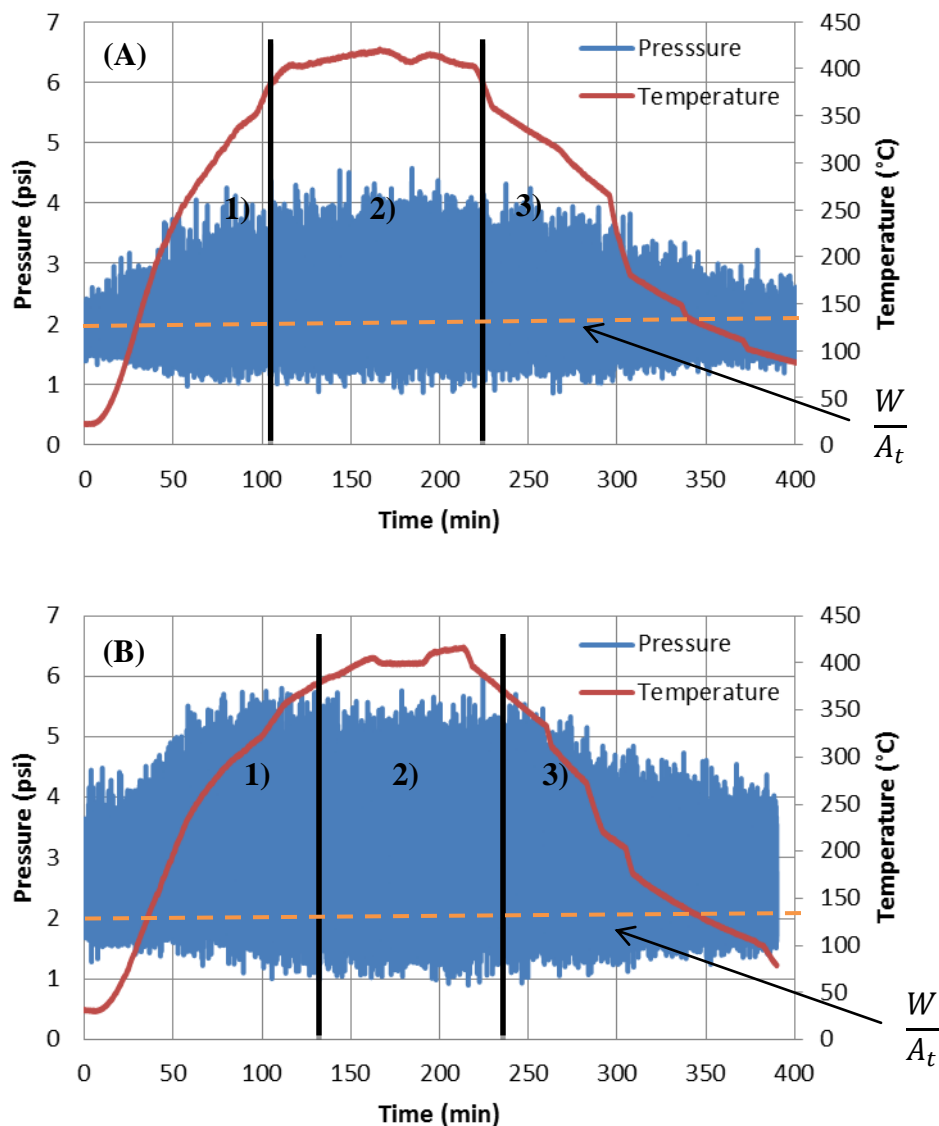


**Figure 4-4: Temperature and pressure measurements in the blank test with 0.0 wt% KOH in the bed material at  $3.9U_{mf}$  (A) and  $5.9 U_{mf}$  (B)**

In comparison with that shown in Figure 4-4A with 0 wt% KOH at  $3.9 U_{mf}$ , the pressure fluctuation as shown in Figure 4-4B at  $5.9 U_{mf}$  are greater. The pressure signals varied from 1 to 5.5 psi at the  $5.9 U_{mf}$  steady state operation, in comparison with from 1 to 4 psi at the  $3.9 U_{mf}$  steady state operation. This difference was expected, as when the fluidizing gas flow rate was increased, the bubble size would become larger and therefore the pressure fluctuation increased. Also from Figure 4-4A and B, it can be seen that the average pressure drop increases when the superficial gas velocity is increased from

3.9 $U_{mf}$  (A) to 5.9  $U_{mf}$  (B). For a normal fluidized bed operating a low velocity the pressure drop through the bed can be defined as:

$$\Delta P_{bed} = \frac{W_{bed\ particles}}{A_t} \quad \mathbf{4-1}$$

Where  $\Delta P$  is the pressure drop of the bed,  $W_{bed\ particles}$  is the net bed weight of the particles,  $A_t$  is the bed cross sectional area. The theoretical pressure drop calculated with Equation 4-1 for the experiment at 3.9  $U_{mf}$  (Figure 4-4 A) is equal to 1.96 psi (represented by the segmented line) similar to the average pressure drop calculated from the data that is equal to 2.04 psi. On the other hand the average pressure drop calculated from the data for the experiment at 5.9  $U_{mf}$  (Figure 4-4 B) is equal to 2.72 psi higher than the theoretical pressure drop calculated with Equation 4-1 (1.96 psi, represented by the segmented line). An increase in gas velocity will eventually lead to a higher  $\Delta P$  due to the entrainment of particles. After the test at 5.9  $U_{mf}$ , 250 g of bed material particles were recovered in the cyclone, showing that at this velocity some entrainment had occurred. In contrast no particles were recovered in the cyclone at 3.9  $U_{mf}$ .

#### 4.3.1.2 Effects of KOH addition

Figure 4-5 and Figure 4-6 show the variation of the temperature and pressure against time during the BFB tests at 3.9  $U_{mf}$  and 5.9  $U_{mf}$ , respectively, when different amounts of KOH were added in the bed material (0.0 wt % (A), 0.2wt% (B), 0.5wt% (C), 0.8wt% (D)). Similar as was shown previously in the blank tests (Figure 4-4), the operation in each test included 3 stages of operation: 1) warming up, 2) steady-state operation and 3) cooling down.

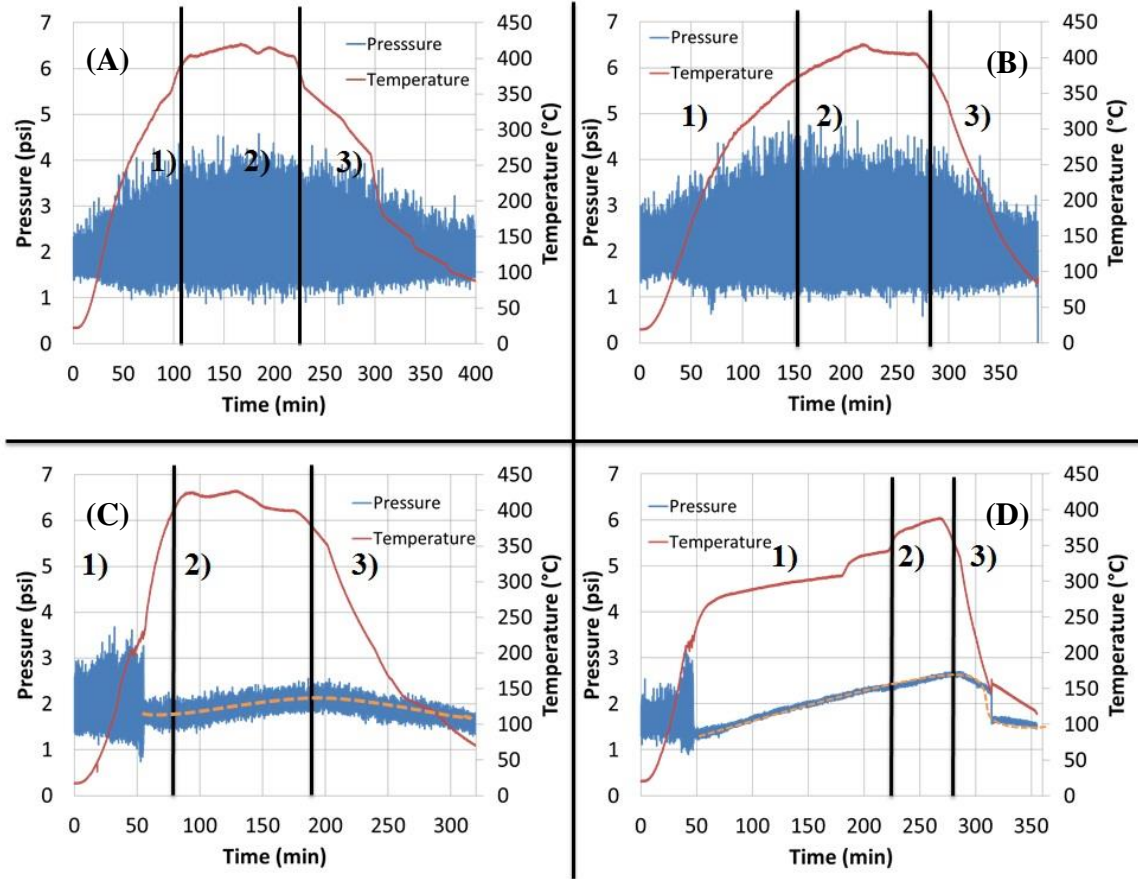


**Figure 4-5: Temperature and pressure measurements in the BFB tests at  $3.9U_{mf}$  with different amounts of KOH in the bed material, 0.0wt% (A), 0.2wt% (B), 0.5wt% (C) and 0.8wt% (D)**

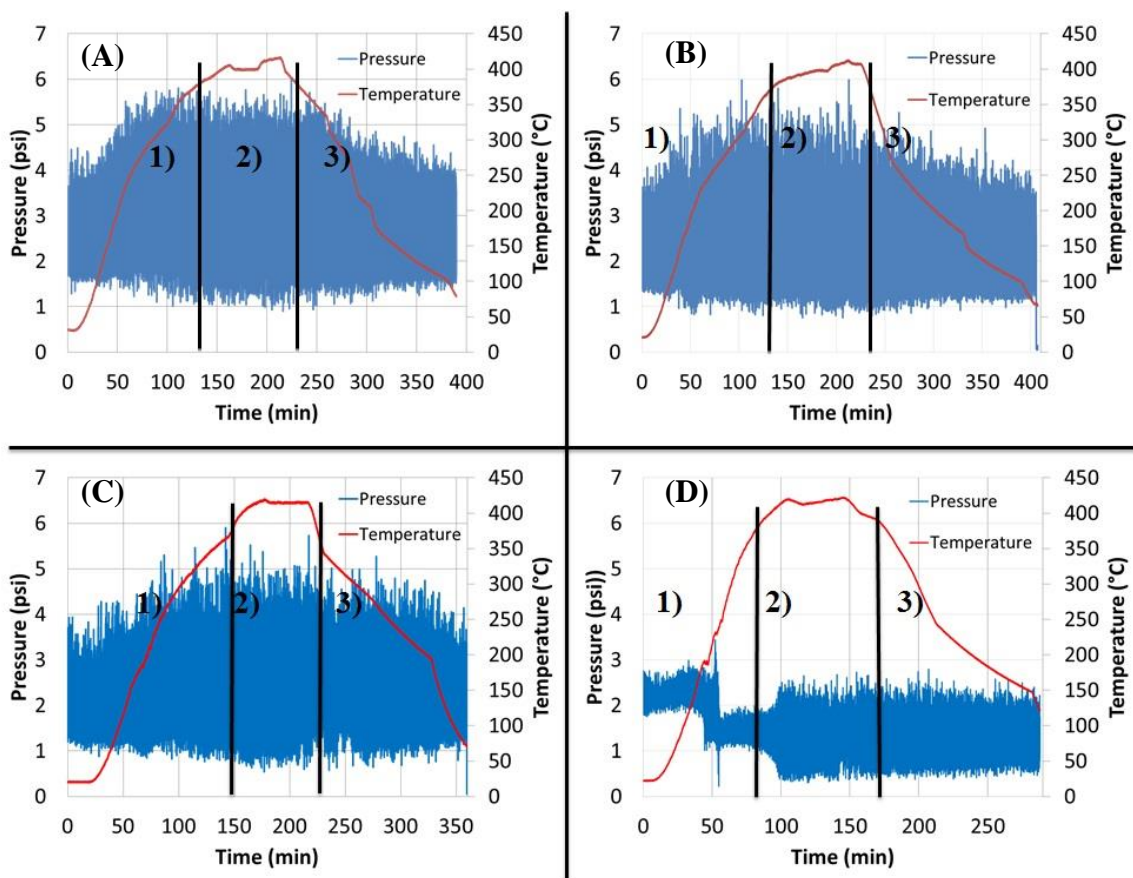


**Figure 4-6: Temperature and pressure measurements in the BFB tests at  $5.9U_{mf}$  with different amounts of KOH in the bed material, 0.0wt% (A), 0.2wt% (B), 0.5wt% (C) and 0.8wt% (D)**

From Figure 4-5 B and Figure 4-6 B, with 0.2wt% KOH addition, four different fluidization zones can be identified:

**a) Normal fluidization zone:** 0 - 50 min for the test at  $3.9 U_{mf}$  or 0 - 40 min at  $5.9 U_{mf}$ , at the temperature from room temperature to  $\sim 150^{\circ}\text{C}$ . In this zone, a normal fluidization can be observed, where the pressure fluctuation of the bed is climbing with increasing temperature, typical for bubbling fluidization at an increasing temperature.

**b) Agglomerates formation zone:** 50 - 150 min at  $150^{\circ}\text{C} \sim 370^{\circ}\text{C}$  for the test at  $3.9 U_{mf}$  (Figure 4-5B) or 40- 130 min at  $150^{\circ}\text{C} \sim 370^{\circ}\text{C}$  at  $5.9 U_{mf}$  (Figure 4-6B). In this zone, slightly increased fluctuation of the bed pressure can be detected, compared with the blank tests. Beginning of agglomeration in a fluidized bed is often indicated by the

presence of larger fluctuation of the bed pressure (Werther, et al., 2000). In this zone, the KOH added could start melting causing adhesion (liquid bridges are formed between the bed particles) of some of the bed particles. The interparticle cohesive forces are believed to increase by increasing the amount of liquid phase (addition of KOH) in the system, as will be evidenced later. It shall be noted that the pressure signals measured in the tests with 0.2 wt% KOH at both gas velocities are similar to those in the blank test (Figure 4-4), suggesting that the formation of agglomerates in these tests might not be significant.

As is explained in Chapter 5 (where fusion tests were carried out on a custom-designed microscope) KOH has a low melting point  $\sim 400^{\circ}\text{C}$  (Janz, et al., 1968). From Figure 4-5B and Figure 4-6B, the large fluctuation appears to start around  $200\sim 300^{\circ}\text{C}$  implying that the KOH started melting at that temperature. This discrepancy may be due to the hygroscopicity of KOH. KOH typically contains varying amounts of water and forms crystalline hydrates, for instance: monohydrate, dehydrate and tetrahydrate. These hydrate compounds have melting points lower than the pure KOH, for example, the monohydrate structure has a melting point as low as  $150^{\circ}\text{C}$ .

**c) Agglomerates fluidization zone:** 150 - 270 min for the test at  $3.9 U_{mf}$  (Figure 4-5B) or 130 - 230 min at  $5.9 U_{mf}$  (Figure 4-6B) at the temperature  $\sim 400^{\circ}\text{C}$  for both tests. In this steady-state operation zone, the BFB system was stable. Large but stable fluctuation of the pressure drop was detected due to the high bed temperature and the stable agglomerates formed due to the melted KOH.

**d) Agglomerates solidification zone:** 270 min - the end of the experiment for the test at  $3.9 U_{mf}$  (Figure 4-5B) or 230 min - the end of the experiment for the test at  $5.9 U_{mf}$  (Figure 4-6B). From Figure 4-5B and Figure 4-6B, it can be seen that the pressure fluctuation in this zone decreases with decreasing the bed temperature, similar to that discussed in the **a) normal fluidization zone**. As the reactor is in the cooling-down stage, the melted KOH tended to solidify; as a result, strong agglomerates formed, slightly changing the particle size distribution of the bed materials.

When the bed materials were discharged the particle size distribution was evaluated and the results will be presented and discussed in section 4.3.2.

From Figure 4-5 C and Figure 4-6 C, with 0.5wt% KOH addition, three distinct fluidization zones may be identified:

**a) Normal fluidization zone:** 0 - 36 min for the test at  $3.9 U_{mf}$  or 0 - 55 min at  $5.9 U_{mf}$ , at the temperature from room temperature to  $\sim 150^{\circ}\text{C}$ . In this zone, a normal fluidization can be observed, where the pressure fluctuation of the bed is climbing with increasing temperature, typical for bubbling fluidization at an increasing temperature.

**b) Agglomerates formation zone:** 36 - 50 min at  $150^{\circ}\text{C} \sim 210^{\circ}\text{C}$  for the tests at  $3.9 U_{mf}$  (Figure 4-5C) or 55- 125 min at  $150^{\circ}\text{C} \sim 340^{\circ}\text{C}$  at  $5.9 U_{mf}$  (Figure 4-6C). In this zone, greatly increased fluctuation of the bed pressure can be observed, in particular in the tests at  $3.9 U_{mf}$ , compared with the blank tests. In this zone, the KOH could start to melt causing adhesion (liquid bridges are formed between the bed particles) of bed particles and form agglomerates. In comparison with the tests with 0.2 wt% of KOH (Figure 4-5B) this zone was much shorter (only approx. 14 min for the tests at  $3.9 U_{mf}$  and 70 min for the tests at  $5.9 U_{mf}$ ) likely due to the larger amount of liquid phase formed while the KOH was melting. It was observed that increasing the amount of liquid can shift the fluidization behavior of group B powder (quartz silica) towards groups A and C particles, i.e., making the fluidization more difficult (Seville & Clift, 1984; Wright & Raper, 1998) due to the the agglomeration process and channeling. It shall be noted that the pressure signals measured (Figure 4-6C) in the tests with 0.5 wt% KOH at a high velocity  $5.9 U_{mf}$  are similar to those in the blank test (Figure 4-4B), implying that the formation of agglomerates at a high velocity might not be severe.

**c) Agglomerates fluidization zone:** from 50 min to the end of the test for the tests at  $3.9 U_{mf}$  (Figure 4-5C) or from 125 min to the end of the test at  $5.9 U_{mf}$  (Figure 4-6C). At  $3.9 U_{mf}$  (Figure 4-5C), the pressure amplitude sharply decreased likely due to the severe agglomeration and channeling. Also the segregation of large agglomerates to the bottom of the bed produced a decrease on the pressure drop. It can be seen that in this zone the average pressure drop (represented by the orange segmented line) kept increasing as the temperature increased until the reactor was cooled down, this is due to an increase in gas viscosity will lead to a higher  $\Delta P$ , according to the Ergun Equation (Eq. 4-1). At  $5.9 U_{mf}$

(Figure 4-6C), large fluctuations on the pressure drop were detected mainly due to the bubbling behavior at a higher temperature, and less likely due to the agglomeration of the bed materials, simply because the pressure signals measured (Figure 4-6C) in the tests with 0.5 wt% KOH at  $5.9 U_{mf}$  gas velocity are similar to those in the blank test (Figure 4-4B). Again, this result implies that the formation of agglomerates at a high gas velocity was not severe.

When the reactor was cooled down and discharged and the particle size distribution of the bed materials was evaluated (section 4.3.2). It was obtained that 0.09 wt% of the total bed materials has a particle size  $> 0.6$  mm for the test at  $5.9 U_{mf}$ , compared with 3.69 wt% for the test at  $3.9 U_{mf}$ . This confirms that formation of agglomerates at a high gas velocity was not severe, compared with that in the tests at a lower fluidizing velocity.

From Figure 4-5 D and Figure 4-6 D, with 0.8wt% KOH addition, three distinct fluidization zones may be identified:

**a) Normal fluidization zone.** 0 - 35 min at a temperature from room temperature to  $\sim 150^{\circ}\text{C}$  at both  $3.9 U_{mf}$  and or  $5.9 U_{mf}$ , where a normal fluidization can be observed. The pressure fluctuation of the bed is stable with relatively small amplitudes.

**b) Agglomerates formation zone.** 35 ~ 46 min at  $150^{\circ}\text{C} \sim 220^{\circ}\text{C}$  for the tests at  $3.9 U_{mf}$  (Figure 4-5D) or 35 ~ 50 min at  $150^{\circ}\text{C} \sim 220^{\circ}\text{C}$ , for the tests at  $5.9 U_{mf}$  (Figure 4-6D). A drastically large fluctuations of the bed pressure was recorded at the beginning of this zone, accompanied with a sudden drop in absolute pressure drop at the end of this zone, suggesting melting of the KOH causing severe agglomeration of the bed material. In comparison with the experiments with 0.2 wt% of KOH and 0.5% of KOH, the agglomerates formation zone with 0.8 wt% of KOH was shorter (only approx. 11-15 min) due to the more severe agglomeration of the bed forming channeling which explains the sudden drop in absolute pressure drop at the end of this zone.

**c) Agglomerates fluidization zone:** from 46 min to the end of the test for the tests at  $3.9 U_{mf}$  (Figure 4-5D) or from 50 min to the end of the test at  $5.9 U_{mf}$  (Figure 4-6D). At  $3.9 U_{mf}$  (Figure 4-5D), the pressure fluctuations remain constant and with a smaller

amplitude in comparison with the first two zones. It can be seen that in this zone the average pressure drop (represented by the orange segmented line) kept increasing as the temperature increased until the reactor was cooled down. Coincidentally, the temperature was kept increasing for a long time of operation even after 3 h under heating. The kept increasing temperature might be a reason to account for the continuously increased pressure drop of the bed. On the other hand, the increased cohesiveness of the bed materials with a high KOH addition could result in reduce voidage of the bed materials, which would increase the pressure drop according to the Ergun Equation (Eq. 4-1).

When the reactor was discharged and the particle size distribution was evaluated (section 4.3.2), it was obtained that 7.51wt% of the total bed materials were agglomerates with a particle size above 0.6 mm. Formation of agglomerates makes the particle size distribution wider, which can result in segregation inside the bed. The segregation could cause a decrease in pressure drop and uneven temperature distribution (Bartels, et al., 2008). As it can be seen from Figure 4-5D, it took a much longer time to heat up the bed material to 400°C (more than 3.0 hours). The bed temperature was measured around 5.5 inch above the distributor (see Appendix A for more details). When large agglomerates segregate to the bottom of the bed, the mixing and heat transfer in this area was very poor, therefore a longer time was needed to heat up the bed material. The bed temperature was unable to reach its set-point (~400°C) in 3 h. Such difficulty in bed material heating might also due to the melting of a large amount of KOH, an endothermic process that retarded rising of the bed temperature.

In contrast at  $5.9 U_{mf}$  (Figure 4-6D), in the beginning of this zone the pressure drop and pressure drop amplitude sharply decreased, likely due to the agglomeration and channeling. Pressure drop declined due segregation of large agglomerates to the bottom of the bed. It was found that due to the high fluidizing velocity, very poor fluidization conditions and high cohesive forces, the bed began to behave somewhat between a bubbling bed and a spouting bed which causing large pressure fluctuations again from 90 min until the reactor was cooled down to ~100°C (Kunii & Levenspiel, 1991). After the test, a larger amount of particles (1680 g) were recovered in the cyclone, compared with 500 g and 170 g particles recovered from the cyclone after the experiments with 0.2 wt%



KOH and 0.5wt% KOH. The above results may suggest that the fluidized bed at  $5.9 U_{mf}$  could be converted into a spouted bed.

As a general observation from figure Figure 4-5 ( $3.9 U_{mf}$ ), it can be seen that for 0.2 wt% KOH the pressure drop fluctuations are similar to those in the blank test, suggesting that the formation of agglomerates in these tests might not be significant. On the other hand for 0.5 and 0.8 the pressure drop sharply decrease due the agglomeration and channeling. It can be seen that large fluctuation appears to start around  $200\sim 300^{\circ}\text{C}$  implying that the KOH started melting at that temperature. From Figure 4-6( $5.9 U_{mf}$ ), It can be seen that the pressure fluctuations for 0.2 wt% and 0.5 wt% of KOH are similar to those in the blank test suggesting that the formation of agglomerates in these tests might not be significant but for 0.8wt% of KOH the pressure drop sharply decrease due to agglomeration and channeling. These results are in agreement with the results that are presented in the following section.

### 4.3.2 Particle size distribution analysis of the bed materials after the BFB tests

Figure 4-7 shows the cumulative distribution wt% of particles with a particle diameter  $\geq 0.04$  mm for the silica sand particles used as the bed material in all BFB tests in this study. It is clearly shown that the silica sand particles has a particle size  $< 0.5$  mm.

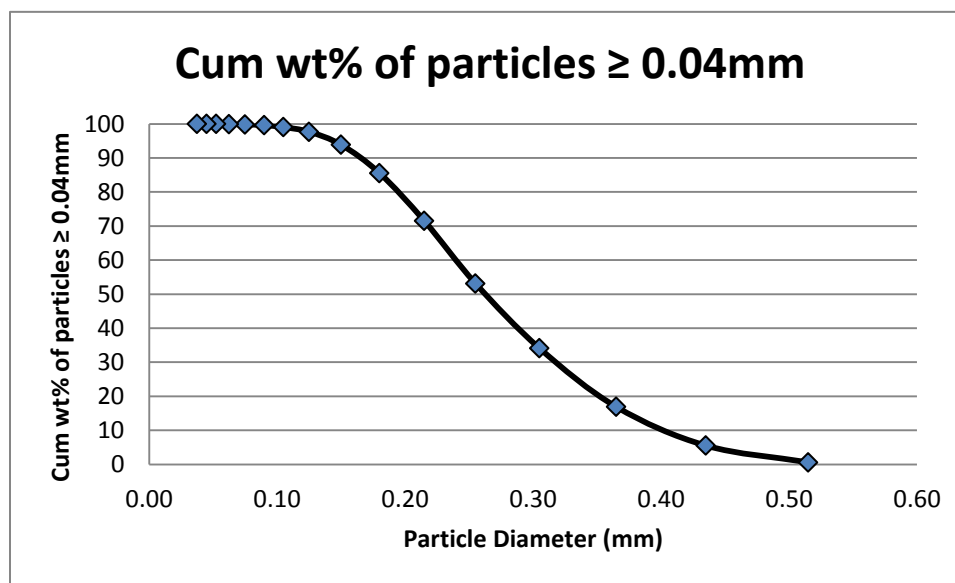


**Figure 4-7: Cumulative of particle size distribution for the silica sand particles used as the bed material in this study**

Figure 4-8 displays the cumulative distribution wt% of agglomerates with a particle size  $\geq 0.6$  mm obtained from the BFB tests at  $3.9U_{mf}$  with different KOH loading (0.2, 0.5 and 0.8 wt% of the bed material).

Figure 4-8 clearly shows that increasing KOH loading produced more agglomerates, which was expected because of more liquid phase from the melted KOH. In comparison with silica sand (Figure 4-10) the particle size distribution did not change significantly in the tests with 0.2wt% KOH loading as only 0.5 wt% of the total bed material was bigger than 0.6 mm. However, 0.5wt% and 0.8wt% KOH loading produced significant amount of agglomerates  $> 0.6$  mm, being 3.69 wt% and 7.51 wt% of the total bed material, respectively.

The above results suggest that in BFB tests at  $3.9 U_{mf}$ , the minimum amount of liquid to form significant agglomeration of bed materials appears to be 0.5 wt% of the bed material.

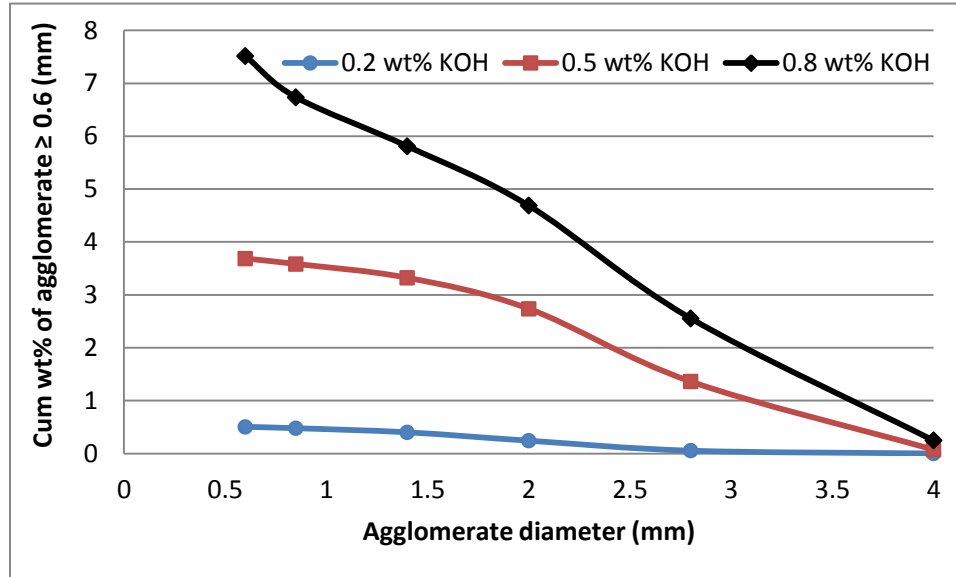


**Figure 4-8: Cumulative distribution wt% of agglomerates with a particle size  $\geq 0.6$  mm obtained from the BFB tests at  $3.9U_{mf}$  with different KOH loading (0.2, 0.5 and 0.8 wt% of the bed material)**

Figure 4-9 shows the cumulative distribution wt% of agglomerates with a particle diameter  $\geq 0.6$  mm from the fluidization tests at  $5.9 U_{mf}$  with different KOH loading (0.2, 0.5 and 0.8wt%).

From Figure 4-9, it is clear that bed material after the BFB tests at a higher gas velocity ( $5.9 U_{mf}$ ) with 0.2wt% and 0.5wt% KOH loading produced negligible amount of agglomerates bigger than 0.6 mm: cumulative wt% being 0.04 wt% and 0.09 wt% of the bed material, respectively. Whereas, when the KOH loading increased to 0.8 wt% of the bed material, the cumulative wt% of agglomerates bigger than 0.6 mm was more significant, attaining 2.28 wt% of the bed material.

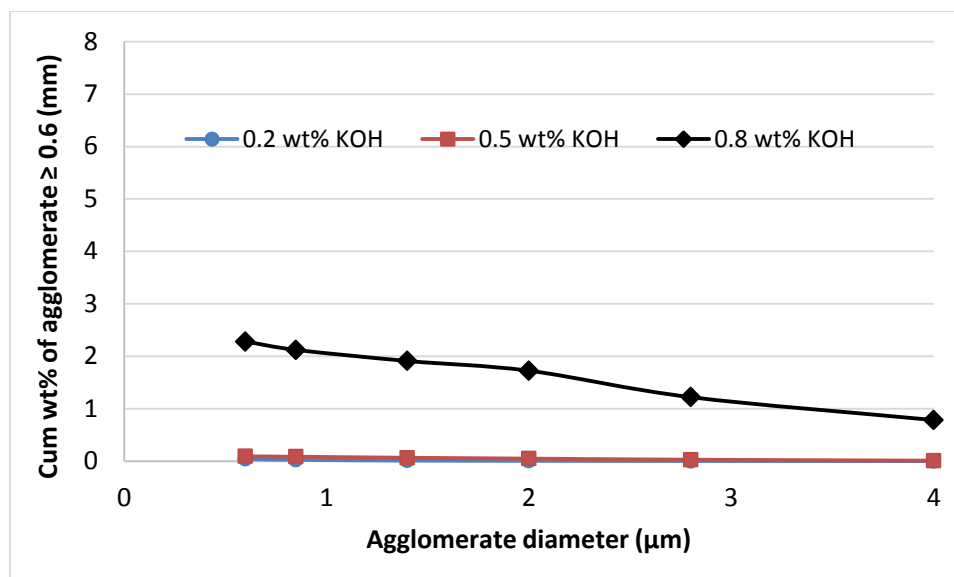


**Figure 4-9: Cumulative distribution of agglomerates with a particle diameter  $\geq 0.6$  mm from the fluidization tests at  $5.9 U_{mf}$  with different KOH loading (0.2, 0.5 and 0.8 wt%)**

In comparison with those from the tests at  $3.9 U_{mf}$ , much less amount of agglomerates were obtained from the experiments operating at  $5.9 U_{mf}$  (after the bed material was discharged from the BFB reactor), this might be due to that the higher disruptive forces present in the bed at a higher fluidizing gas velocity.

The above results also suggest that in BFB tests at  $5.9 U_{mf}$ , the minimum amount of liquid to form significant agglomeration of bed materials appears to be 0.8 wt% of the bed material.

#### 4.3.2.1 Photos of the bed materials after the BFB tests

Figure 4-10 shows the photos taken to the agglomerates obtained in the BFB test with 0.8 wt% KOH in the bed material at  $3.9U_{mf}$ . As was explained before after the reactor was discharged the bed material was sieved ( $4000 \mu\text{m}$ ,  $2800 \mu\text{m}$ ,  $2000 \mu\text{m}$ ,  $1400 \mu\text{m}$ ,  $1000 \mu\text{m}$ ,  $850 \mu\text{m}$ , and  $600 \mu\text{m}$ ) to evaluate the particle size distribution, Figure 4-10 shows the agglomerates obtained and also shows pure silica sand for comparison.



**Figure 4-10: Agglomerates obtained in the BFB tests with 0.8 wt% KOH in the bed material at  $3.9U_{mf}$**

## 4.4 Conclusions

A study was conducted to determine the critical amount of liquid phase for bed material agglomeration in a bubbling fluidized bed operated at elevated temperatures using low melting-point salt (KOH) to simulate molten ash. From this study some conclusions were drawn:

- In the BFB fluidization system tested, the critical liquid amount of simulate molten ash that could cause the bed materials start to form agglomeration/channeling, and form severe agglomeration/channeling (poor fluidization) is approx. 0.5 wt% and 0.8wt% at a lower fluidizing gas velocity ( $3.9 U_{mf}$ ) and a higher fluidizing gas velocity ( $5.9 U_{mf}$ ), respectively.
- With more low-melting-point compound (KOH) present in the BFB, more agglomerates of bed material are formed. Increasing the amount of liquid could change the fluidization behavior of group B (silica silica) particles towards group A and even C, depending on the amount of the low-melting-point compound in the bed material.
- In comparison with those from the tests at a lower gas velocity, much less amount of agglomerates were obtained from the experiments operating at a higher gas velocity, due to the higher disruptive forces present in the bed at a higher fluidizing gas velocity.

### **Acknowledgements:**

This investigation is a part of the NSERC CRD project titled “FUNDAMENTAL STUDIES OF DRYING, COMBUSTION AND ASH PROPERTIES OF BIOMASS, AND IMPACTS ON BOILER AND PULP AND PAPER MILL OPERATIONS”, led by one of the authors (H. Tran) at The University of Toronto. The authors (C. Xu and H. Tran) would also like to acknowledge the financial support provided by NSERC via the Discovery Grants, as well as the industrial support from various pulp and paper companies.

## 4.5 References

- Atakul, H., & Ekinici, E. (1990). Agglomeration in lignite ash flotsam-rich and jetsam-rich systems. *Powder technology*(60), 77-82.
- Bartels, M., Lin, W., Nijenhuis, J., Kapteijn, F., & Ommen, J. (2008). Agglomeration in fluidized beds at high temperatures: Mechanisms, detection and prevention. *Energy and Combustion Science*, 633-666.
- Cheng, J. (2009). *Biomass to renewable energy processes*. CRC Press.
- Ekinici, E., Atakul, H., & Tolay, M. (1990). Detection of segregation tendencies in a fluidized-bed using temperature profiles. *Powder Technology*(61), 185-192.
- Fan, L., Ho, T.-C., Hiraoka, S., & Walawender, W. (1981). Pressure fluctuations in a fluidized bed. *AIChE Journal*(3), 388-396.
- Geldart, D. (1973). Types of gas fluidization. *Powder Technology*(7), 285-292.
- Gustavsson, L., Borjesson, B., Johansson, B., & Svenningsson, P. (1995). Reducing CO<sub>2</sub> emission by substituting biomass for fossil fuels. *Energy*(20), 1097-1113.
- Janz, G., Dampier, F., Lakshmi-Narayanan, G., & Lorenz, P. (1968). *Molten salts: Volume I*. National standard Reference Data Series.
- Jensen, P., Frandsen, F., & Dam-Johansen, K. S. (2000). Experimental investigation of the transformation and release to gas phase of potassium and chlorine during straw pyrolysis. *Energy&Fuels*(14), 1280-1285.
- Khan, A., Jong, W., Jansens, P., & Spliethoff, H. (2009). Biomass combustion in fluidized bed boilers: Potential problems and remedies. *Fuel Processing Technology*(90), 21-50.
- Kunii, D., & Levenspiel, O. (1991). *Fluidization Engineering*. Butterworth-Heinemann.

- Lin, C.-L., Wey, M.-Y., & You, S.-D. (2002). The effect of particle size distribution on minimum fluidization velocity at high temperature. *Powder Technology*(126), 297-301.
- Lin, W., & Dam-Johansen, K. (1997). *Sintering in biofuel and coal-biofuel fired FBC*. Department of Chemical Engineering: Technical University of Denmark.
- Olofsson, G., Ye, Z., & Bjerle, I. (2002). Bed agglomeration problems in fluidized-bed biomass combustion. *Industrial and Engineering Chemistry Research*(41), 2888-2894.
- Pattipati, R., & Wen, C. (1981). Minimum fluidization velocity at high temperatures. *Ind. Eng. Chem. Process Des. Dev.*(20), 705-707.
- Pietsch, W. (2002). *Agglomeration Process: Phenomena, Technologies, Equipment* (First ed.). Weinheim: Wiley-VCH.
- Seville, J., & Clift, R. (1984). The effect of thin liquid layers on fluidization characteristics. *Powder technology*, 117-129.
- Siegell, J. (1984). High-Temperature defluidization. *Power Technology*, 13-22.
- Theis, M., Skrifvars, B.-J., Zevenhoven, M., Hupa, M., & Tran, H. (2006). Fouling tendency of ash resulting from burning mixtures of biofuels. Part 3: Influence of probe surface temperature. *Fuel*(85), 2002-2011.
- Visser, H., van Lith, S., & Kiel, J. (2008). Biomass Ash-Bed Material Interactions Leading to Agglomeration in FBC. *Journal of Energy Resources Technology*.
- Werther, J., Saenger, M., Hartge, E.-U., Ogada, T., & Siagi, Z. (2000). Combustion of agricultural residues. *Progress in Energy and Combustion Science*(26), 1-27.
- Westberg, H., Bystrom, M., & Leckner, B. (2003). Distribution of K, Cl, and S between solid and vapor phases during combustion of wood chips and coal. *Energy&Fuels*(17), 18-28.



Wright, P., & Raper, J. (1998). Examination of dispersed liquid-phase three-phase fluidized beds Part 1. Non-porous, uniform particle systems. *Powder Technology*(97), 208-226.

Zhou, Y., Shi, Q., Huang, Z., Wang, J., Yang, Y., Liao, Z., y otros. (2013). Effects of interparticle forces on fluidization characteristics in liquid containing and hight temperature fluidized beds. *Ind. Eng. Chem.*(52), 16666–16674.

## Chapter 5

### 5 Fusion behavior of synthetic and real biomass ashes – Effects of potassium

#### 5.1 Introduction

Biomass conversion for thermal/power generation in fluidized bed processes still has some technical difficulties. As discussed in previous Chapters, agglomeration of bed materials at high temperature is one of the most important and challenging problems. Typically, the fluidized bed conversion (combustion or gasification) of the solid fuel is carried out with silica sand as bed material in the presence of ash. Inorganic alkali components from the fuel, mainly potassium (K) and sodium (Na) can be problematic as they form low-melting alkali compounds and may also react with the bed material forming low-melting alkali silicates (Bartels, et al., 2008; Werther, et al., 2000; Lin, et al., 2003; Liu, et al., 2009). These low-melting alkali compounds, characterized by low melting temperatures, coated the sand (or other bed materials) particles with a sticky layer. This causes sand particles agglomerate upon collisions and grow larger with time, eventually leading to partial or complete defluidization of the fluidized bed reactor (Bartels, et al., 2008; Lin, et al., 2003; Natarajan, et al., 1998).

##### 5.1.1 Biomass ash composition

The biomass composition and especially ash components vary a lot depending on the plant types, growth condition, weather and so on. Biomass ashes are commonly dominated by calcium, silicon, and potassium (Vassilev, et al., 2010). Silicon is found in biomass primarily as hydrated silica grains while potassium is distributed mainly in ionic and organometallics forms (Jenkins, et al., 1994). During combustion, potassium is probably to be volatilized with organic species. If chlorine is presented in the fuel it may be released as KCl, if not, hydroxides, oxides, sulphates or carbonates may form. Some researchers indicates that most of the potassium would remain in the bed as they could be recaptured from the vapours by some mineral components in the ash under bubbling fluidized bed (BFB) conditions (Lin, et al., 2003; Zevenhoven-Onderwater, et al., 2001).

Based on experimental investigation, Ohman and Nordin (2000) proposed a three-step agglomeration mechanism.

Step 1: Ash deposition on the bed material via 3 mechanisms, a) Attachment of small particles to the bed material b) Condensation of gaseous alkali species (KCl, KOH,  $K_2SO_4$ , K) on the bed particles c) Chemical reactions of the alkali compounds on the bed particles surface.

Step 2: The inner layer of the coating is probably homogenized and strengthened via sintering while is growing during time.

Step 3: Agglomeration of the coated particles, controlled by adhesive inter-particle forces (such as the capillary force or adhesion force caused by the liquid bridge of melted ashes). The following image shows the 3 steps proposed by Ohman and Nordin (2000).

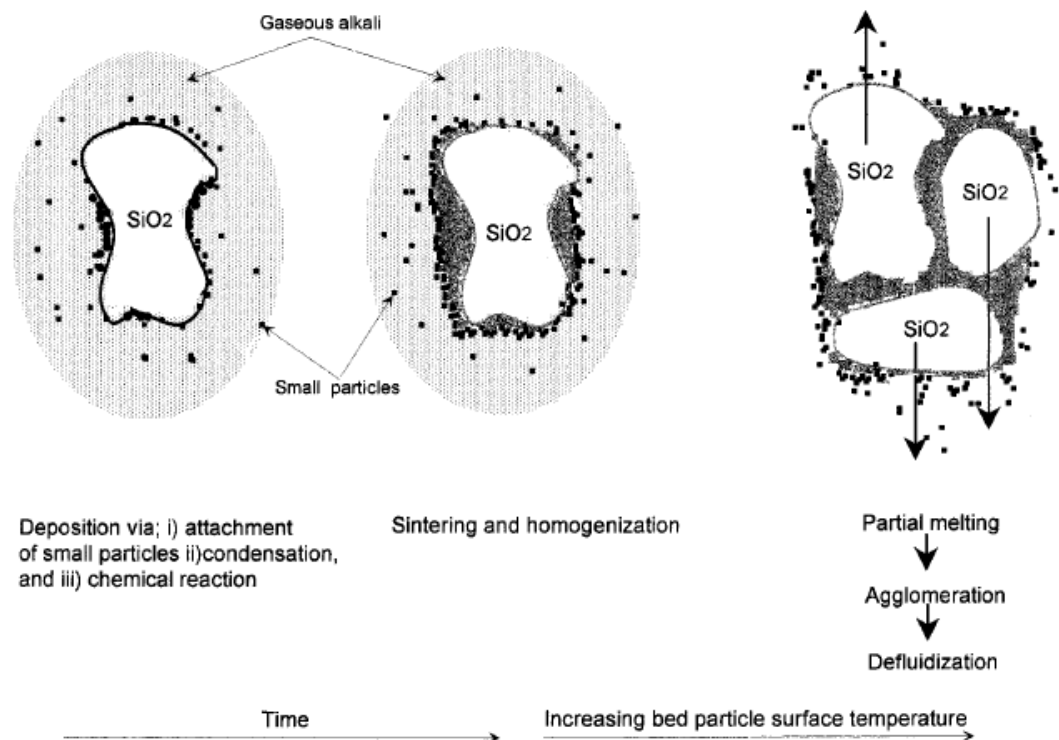


**Figure 5-1: Three-step agglomeration mechanism (Ohman & Nordin, 2000)**

It has been reported that K, Ca, and Si play a key role in bed agglomeration (Li, et al., 2010). Olofsson et al (2002) have suggested that potassium, sodium and silicon are the

most important elements in the interaction between the fuel ash and the bed material during the agglomeration process, they also proposed that the presence of calcium enhances the agglomeration tendency. On the other hand, magnesium (Mg), iron (Fe) and aluminum (Al) are elements that can suppress agglomeration at temperatures not higher than 1000°C. Also it has been reported that S, and Cl may reduce the ash melting point, hence increasing the bed materials agglomeration tendency (Ohman & Nordin, 1998; Bakker, et al., 2002).

### 5.1.2 Agglomeration detection methods

Several methods have been proposed for study the agglomeration phenomena in fluidized beds. These methods can be classified into on-line measurement methods and off-line measurement methods. The online methods include X-ray computed tomography (CT) **measurements** methods and are based on the measurement of process parameters during fluidized bed operation, for example, pressure (reflects the hydrodynamics of the fluidized bed), temperature (delivery information on the degree of mixing of the fluidized bed), acoustic emission (refers to a broad range of frequencies emitted from a fluidized bed). In contrast, the off-line methods include measurements of fuel ash and bed materials samples, carried out outside of the fluidized bed operation. Different on-line and off-line methods are described in details in the work of Bartel et al. (2008).

Some off-line methods for fuel ash measurements are briefly introduced below:

- Simultaneous dilatometry-electrical conductance, measures the electrical conductance of an ash sample while the temperature in the furnace is linearly increase. A plot of electrical resistance v/s inverse of temperature is used to get the sintering point (the sintering point is indicated by a change in the slope of the curve). The problem is that sometimes the sintering point is very difficult to determine because the change in slope can be rather small. In addition, the electrical resistance are affect by particle size and bulk density of the ash samples (Raask, 1979).
- The American Society for Testing and Materials (ASTM) fusion tests (ASTM, 1987) are carried out by heating ash samples to determine the initial deformation

temperature, softening temperature, hemispherical temperature and fluid temperature. This method has been extensively criticized as it has been shown that agglomerates could form several hundred degrees below the initial deformation temperature of the ash, determined by the ASTM fusion test (Stallman & Neavel, 1980). Pang et al (2013), proposed a test that combines the conventional ash fusion test, dilatometry and sinter strength by means of image analysis, where they claimed that the error is approximately 15°C and 50% lower than that determined by the conventional ash fusion test.

- Thermal mechanical analysis, measures the thermal contraction/expansion of an ash sample. The sample is heated while a defined force is applied in the sample with a piston, the thermal expansion curve is measured (change in length vs temperature) (He, 1999).

From Ohman and Nordin (2000) and as depicted in Figure 5-1, the agglomeration of coated particles is controlled by adhesive inter-particle forces (such as the capillary force or adhesion force caused by the liquid bridge of melted ashes). On the other hand, as discussed previously potassium (K) can be problematic as it forms low-melting alkali compounds (Bartels et al., 2008). This study aimed to investigate on the effects of K on the formation of liquid bridge/fusion between fluidized bed materials (silica sand particles) upon heating using synthetic biomass ash (of composition that of typical fly ash from biomass boilers), pure K compound (KOH), and a real biomass fly ash obtained from a biomass boiler in a Canadian pulp mill. The fusion tests were carried out on a custom-designed microscope equipped with a heating stage of a heating capacity up to 1100°C. The softening of the synthetic/real ash and the formation of liquid bridge between sand particles were photographed during heating of the mixture from room temperature up to 1100°C.

## 5.2 Materials and methods

### 5.2.1 Materials

The bed materials used in this work were silica sand particles, with a Sauter mean diameter of 204  $\mu\text{m}$  and particle density of 2600  $\text{kg/m}^3$ . The compounds used in this work for preparation of synthetic ash samples, i.e.,  $\text{SiO}_2$ ,  $\text{CaO}$ ,  $\text{KOH}$  (for  $\text{K}_2\text{O}$ ),  $\text{P}_2\text{O}_5$ ,  $\text{Al}_2\text{O}_3$ ,  $\text{MgO}$ ,  $\text{Fe}_2\text{O}_3$ ,  $\text{S}$  (for  $\text{SO}_3$ ),  $\text{NaOH}$  (for  $\text{Na}_2\text{O}$ ) and  $\text{TiO}_2$ , were all ACS grade pure chemicals purchased from Sigma-Aldrich. A real fly ash was sampled from a biomass boiler in a Canadian pulp mill and its composition is shown in Table 5-1.

**Table 5-1: Composition of a real fly ash sampled from a biomass boiler in a Canadian pulp mill**

Ash component	Composition (wt%)
$\text{SiO}_2$	18.48
$\text{TiO}_2$	0.42
$\text{Al}_2\text{O}_3$	6.68
$\text{Fe}_2\text{O}_3$	3.45
$\text{MnO}$	3.27
$\text{MgO}$	4.92
$\text{CaO}$	26.31
$\text{K}_2\text{O}$	19.93
$\text{Na}_2\text{O}$	12.32
$\text{P}_2\text{O}_5$	3.45
$\text{Cr}_2\text{O}_3$	0.08
$\text{BaO}$	0.36
$\text{SrO}$	0.09
Total	99.91

### 5.2.2 Apparatus

The experiments were carried out in a custom-designed microscope (Transmitted light petrographic scope with three long working distance objectives (4x, 32x and 50x)), equipped with a heating stage of a heating capacity of up to 1100°C, located at the University of Windsor. A picture of the experimental apparatus is shown in Figure 5-2.

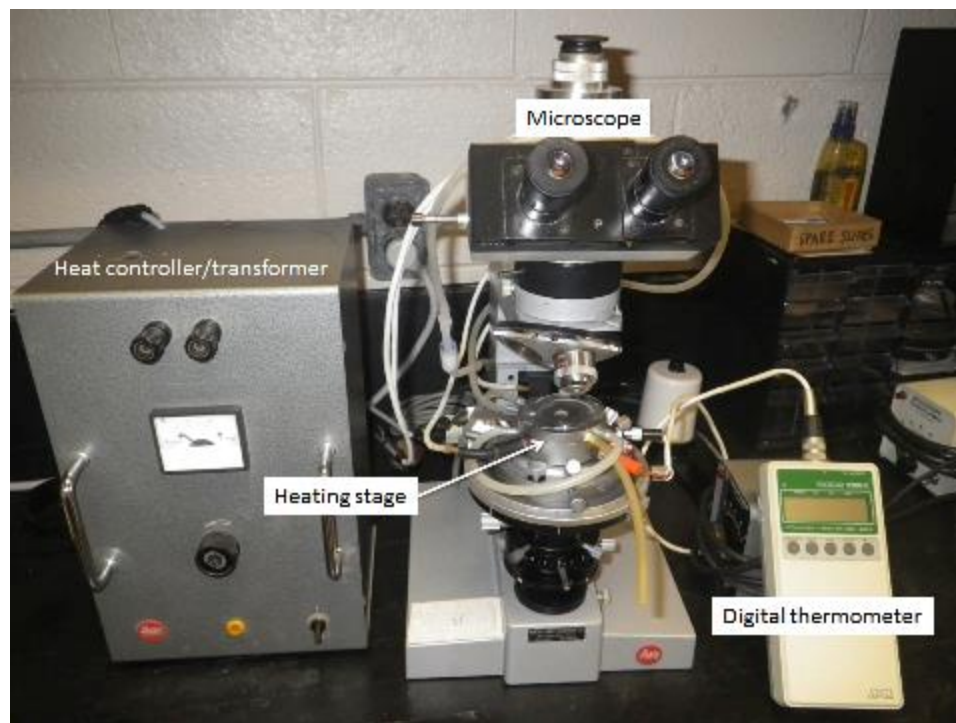


**Figure 5-2: Picture of Wild Leitz Microscope Heating Stage 1350 and Microscope.**

The heating stage (Wild Leitz Microscope Heating Stage 1350) is attached to the object stage with two knurled screws. It is heated with low-voltage via a heat controller transformer to achieve fine temperature control; the temperature is monitored with an Ahlborn THERM 2280-2 digital thermometer attached to the stage. The heating stage is also equipped with a water flow cooling system.

To monitor online the fusion behavior of the ash compounds and the liquid bridge formation between sand particles while heating, the optical microscope is equipped with a digital camera (QImaging Retiga 2000-R Colour Cooled). The camera is connected to a personal computer equipped with QCapture Suite software for pictures/videos acquisition.

### 5.2.3 Preparation of test samples

Synthetic ashes of typical ash compounds of wood/woody biomass were prepared following the mean composition presented in Table 5-2. The quantities for all ash components are shown in Appendix 5.1 (calculations on the basis of 5 g sample per test).

**Table 5-2: Wood/woody biomass ash composition wt% (Vassilev et al. 2010).**

Biomass group, sub-group and variety	SiO <sub>2</sub>	CaO	K <sub>2</sub> O	P <sub>2</sub> O <sub>5</sub>	Al <sub>2</sub> O <sub>3</sub>	MgO	Fe <sub>2</sub> O <sub>3</sub>	SO <sub>3</sub>	Na <sub>2</sub> O	TiO <sub>2</sub>	Sum	Mn (ppm)	n <sup>a</sup>
<i>1. Wood and woody biomass (WWB)</i>													
1. Alder-fir sawdust	37.49	26.41	6.10	2.02	12.23	4.04	8.09	0.83	1.81	0.98	100.00		1
2. Balsam bark	26.06	45.76	10.70	4.87	1.91	2.33	2.65	2.86	2.65	0.21	100.00	20160	1
3. Beech bark	12.40	68.20	2.60	2.30	0.12	11.50	1.10	0.80	0.90	0.10	100.00	3100	1
4. Birch bark	4.38	69.06	8.99	4.13	0.55	5.92	2.24	2.75	1.85	0.13	100.00	22870	2
5. Christmas trees	39.91	9.75	8.06	2.46	15.12	2.59	9.54	11.66	0.54	0.37	100.00		1
6. Elm bark	4.48	83.46	5.47	1.62	0.12	2.49	0.37	1.00	0.87	0.12	100.00	775	1
7. Eucalyptus bark	10.04	57.74	9.29	2.35	3.10	10.91	1.12	3.47	1.86	0.12	100.00	10850	1
8. Fir mill residue	19.26	15.10	8.89	3.65	5.02	5.83	8.36	3.72	29.82	0.35	100.00	13640	2
9. Forest residue	20.65	47.55	10.23	5.05	2.99	7.20	1.42	2.91	1.60	0.40	100.00	13180	3
10. Hemlock bark	11.12	59.62	5.12	2.34	2.34	14.57	1.45	2.11	1.22	0.11	100.00	9300	1
11. Land clearing wood	65.82	5.79	2.19	0.66	14.85	1.81	5.27	0.36	2.70	0.55	100.00		1
12. Maple bark	8.95	67.36	7.03	0.79	3.98	6.59	1.43	1.99	1.76	0.12	100.00	5430	2
13. Oak sawdust	29.93	15.56	31.99	1.90	4.27	5.92	4.20	3.84	2.00	0.39	100.00		1
14. Oak wood	48.95	17.48	9.49	1.80	9.49	1.10	8.49	2.60	0.50	0.10	100.00	14900	2
15. Olive wood	10.24	41.47	25.16	10.75	2.02	3.03	0.88	2.65	3.67	0.13	100.00		1
16. Pine bark	9.20	56.83	7.78	5.02	7.20	6.19	2.79	2.83	1.97	0.19	100.00	12400	2
17. Pine chips	68.18	7.89	4.51	1.56	7.04	2.43	5.45	1.19	1.20	0.55	100.00	2090	1
18. Pine pruning	7.76	44.10	22.32	5.73	2.75	11.33	1.25	4.18	0.42	0.17	100.00		1
19. Pine sawdust	9.71	48.88	14.38	6.08	2.34	13.80	2.10	2.22	0.35	0.14	100.00	10550	2
20. Poplar	3.87	57.33	18.73	0.85	0.68	13.11	1.16	3.77	0.22	0.28	100.00	4500	3
21. Poplar bark	1.86	77.31	8.93	2.48	0.62	2.36	0.74	0.74	4.84	0.12	100.00	2330	1
22. Sawdust	26.17	44.11	10.83	2.27	4.53	5.34	1.82	2.05	2.48	0.40	100.00	27910	2
23. Spruce bark	6.13	72.39	7.22	2.69	0.68	4.97	1.90	1.88	2.02	0.12	100.00	13950	3
24. Spruce wood	49.30	17.20	9.60	1.90	9.40	1.10	8.30	2.60	0.50	0.10	100.00		1
25. Tamarack bark	7.77	53.50	5.64	5.00	8.94	9.04	3.83	2.77	3.40	0.11	100.00	26360	1
26. Willow	6.10	46.09	23.40	13.01	1.96	4.03	0.74	3.00	1.61	0.06	100.00		11
27. Wood	23.15	37.35	11.59	2.90	5.75	7.26	3.27	4.95	2.57	1.20	100.00	35740	1
28. Wood residue	53.15	11.66	4.85	1.37	12.64	3.06	6.24	1.99	4.47	0.57	100.00		2
Mean	22.22	43.03	10.75	3.48	5.09	6.07	3.44	2.78	2.85	0.29	100.00	13160	28
Minimum	1.86	5.79	2.19	0.66	0.12	1.10	0.37	0.36	0.22	0.06		775	28
Maximum	68.18	83.46	31.99	13.01	15.12	14.57	9.54	11.66	29.82	1.20		35740	28

The synthetic ashes were prepared by mixing the compounds (i.e., SiO<sub>2</sub>, CaO, KOH (for K<sub>2</sub>O), P<sub>2</sub>O<sub>5</sub>, Al<sub>2</sub>O<sub>3</sub>, MgO, Fe<sub>2</sub>O<sub>3</sub>, S (for SO<sub>3</sub>), NaOH (for Na<sub>2</sub>O) and TiO<sub>2</sub>) at the mean concentration (from Table 5-2). Then, the test samples were prepared by mixing the synthetic ashes with the bed materials (silica sand particles) at the composition of 10% synthetic ash compounds and 90% silica sand particles.

In total, 5 test samples containing 3 different levels of K<sub>2</sub>O in synthetic ash mixtures, pure K<sub>2</sub>O and a real fly ash, respectively, were prepared in this study, in order to examine their influence on the fusion behavior of the ash (or synthetic ash) and the liquid bridge formation between sand particles upon heating. The tests and the test samples



composition are detailed in Table 5-3. As given in the Table 5-3, test samples were prepared with synthetic ash mixtures containing 3 different levels (wt.%) of  $K_2O$  (K-1, K-2 and K-3, with 0-29 wt%  $K_2O$  out of the total ash amount), 1 sample with pure  $K_2O$  (PURE-1), and 1 sample prepared with the real biomass fly ash (REAL-1).

In designing the test samples composition, a reference sample (K-1 in Table 5-3) was prepared based on the mean ash composition presented in Table 5-2, a blank test (K-3 in Table 5-3) was prepared with key ash compound ( $K_2O$ ) fixed at 0 wt%. A sample (K-2 in Table 5-3) with other composition of the key ash compound ( $K_2O$ ) was prepared: K-2 contains  $K_2O$  at 29 wt% out of the total ash, higher than that of the reference sample (10.75 wt%  $K_2O$ ).

**Table 5-3: Summary of the tests and the test samples composition<sup>1</sup>.**

$K_2O$ tests <sup>2</sup>	Test #	K-1	K-2	K-3
	$K_2O$ wt% out of the total ash	10.75	29	0
Pure $K_2O$ test <sup>2</sup>	Test #	PURE-1		
	$K_2O$ wt% out of the total ash	100		
Real fly ash test	Test #	REAL-1		
	Real ash wt% out of the total ash	100		

<sup>1</sup> Each test sample contains 90 wt% silica Sand and 10 wt.% total ash components

<sup>2</sup>  $K_2O$  was obtained from KOH

#### 5.2.4 Experimental procedure

Before all the tests, the heating stage as depicted in Figure 5-3 was calibrated using pure chemical standards of  $K_2Cr_2O_7$ , NaCl and  $Na_2SO_4$  (crystals) with fixed melting temperatures. The calibration results are provided in 5.3.1.

In the experiments, the specific test sample was heated up in a sampler chamber (Figure 5-3) from room temperature to 900°C. Pictures were taken every 89°C from room temperature to 590°C and then every 44°C at > 590°C. After a target temperature was reached, the heating stage was heated gradually to a higher temperature and kept constant

for a few seconds at the temperature for photo-taking. After each test was finished, the heating stage was cooled down to room temperature using the cooling system.

Some typical tests were performed in duplicate or triplicate, in order to ensure the reproducibility of the experiments.

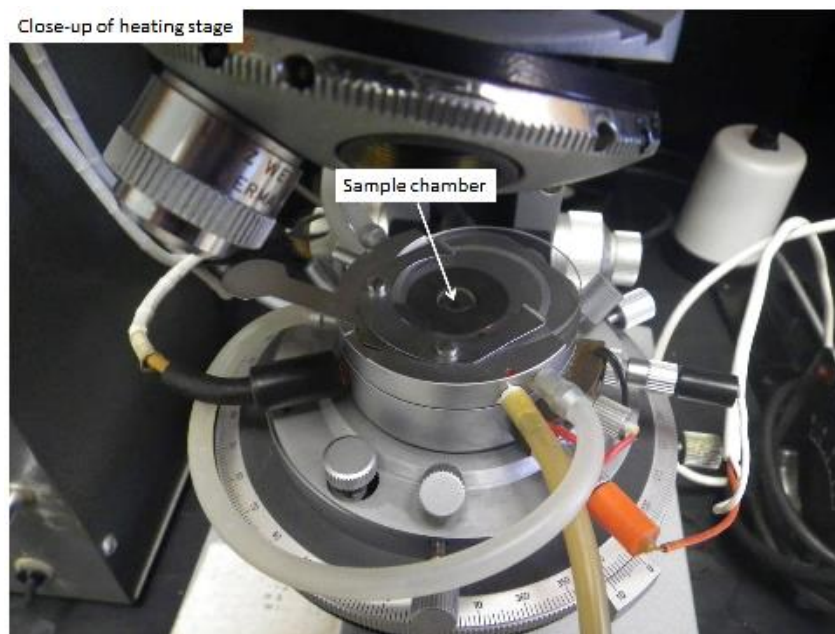


**Figure 5-3: Close-up of the heating stage**

## 5.3 Results and Discussion

### 5.3.1 Heating stage calibration

Pure standards of  $K_2Cr_2O_7$ , NaCl and  $Na_2SO_4$  (crystals) with fixed melting points were used to calibrate the heating stage. Their standard melting temperatures and the melting points measured on the heating stage are presented in the following Table:

**Table 5-4: Heating stage calibration**

Chemical	Standard melting temperature (°C)	Measured melting Temperature (°C)
$K_2Cr_2O_7$	398	383
$Na_2SO_4$	884	932
NaCl	801	843

A calibration curve was obtained using the above results by linear data fitting, and it is presented in the following Figure 5-4:

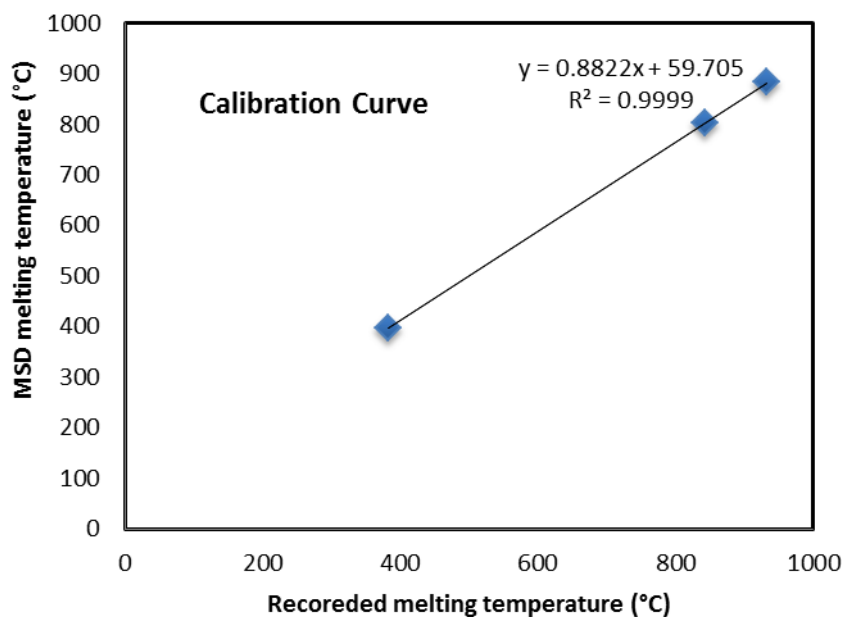


**Figure 5-4: Heating stage calibration curve.**

### 5.3.2 Fusion tests of mixtures of synthetic ash compounds and silica sand particles

Figure 5-5 displays microscopic photos of the mixture of synthetic ash compounds and silica sand particles in which  $K_2O$  accounts for 10.75 wt% of the total ash (Test#: K-1) at various temperatures.

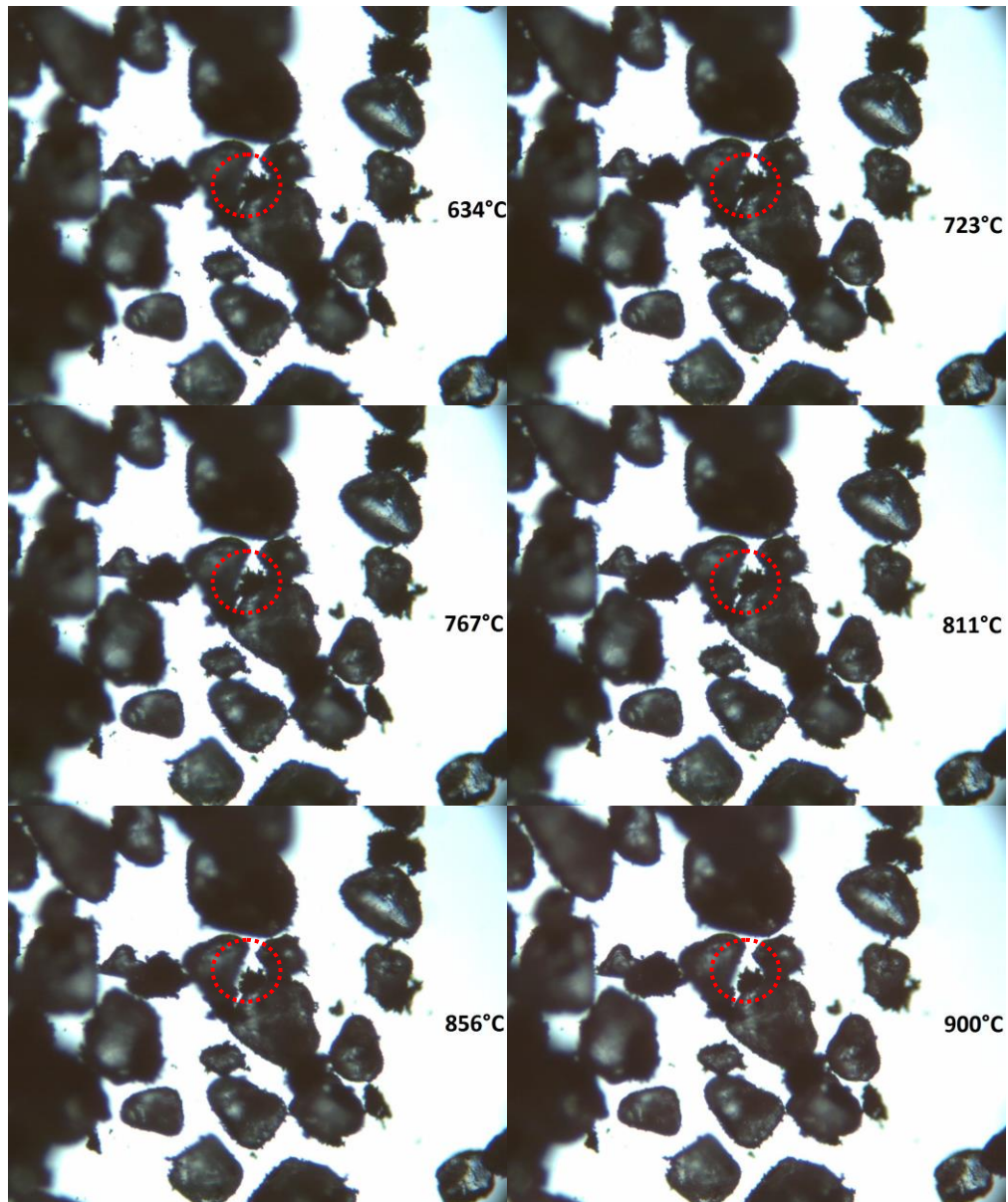


**Figure 5-5: Microscopic photos of the mixture of synthetic ash compounds and silica sand particles in which  $K_2O$  accounts for 10.75 wt% of the total ash (Test# K-1) at various temperatures**

If focused on the images of a small lump of alkali salts as highlighted in the photos, it can be seen from Figure 5-5 that the small lump of the synthetic ash reduces in size gradually when temperature is higher than 767°C, likely caused by melting of the synthetic ash compounds or volatilization of some of alkali salts. Thus, the fusion of synthetic ash appeared to occur noticeably at >767°C.

Figure 5-6 shows the microscopic photos taken from a repeated experiment with the same test sample (K-1) in order to check the reproducibility of the experimental result as shown previously in Figure 5-5.

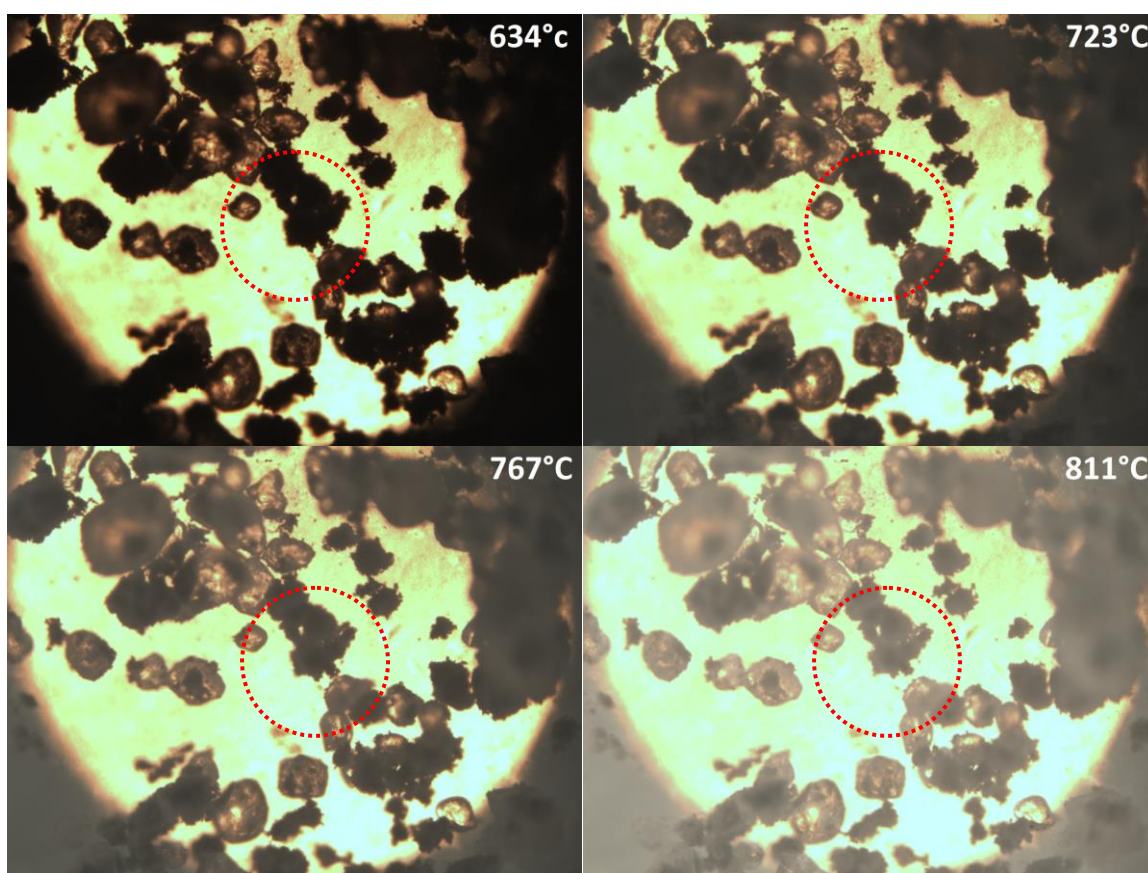
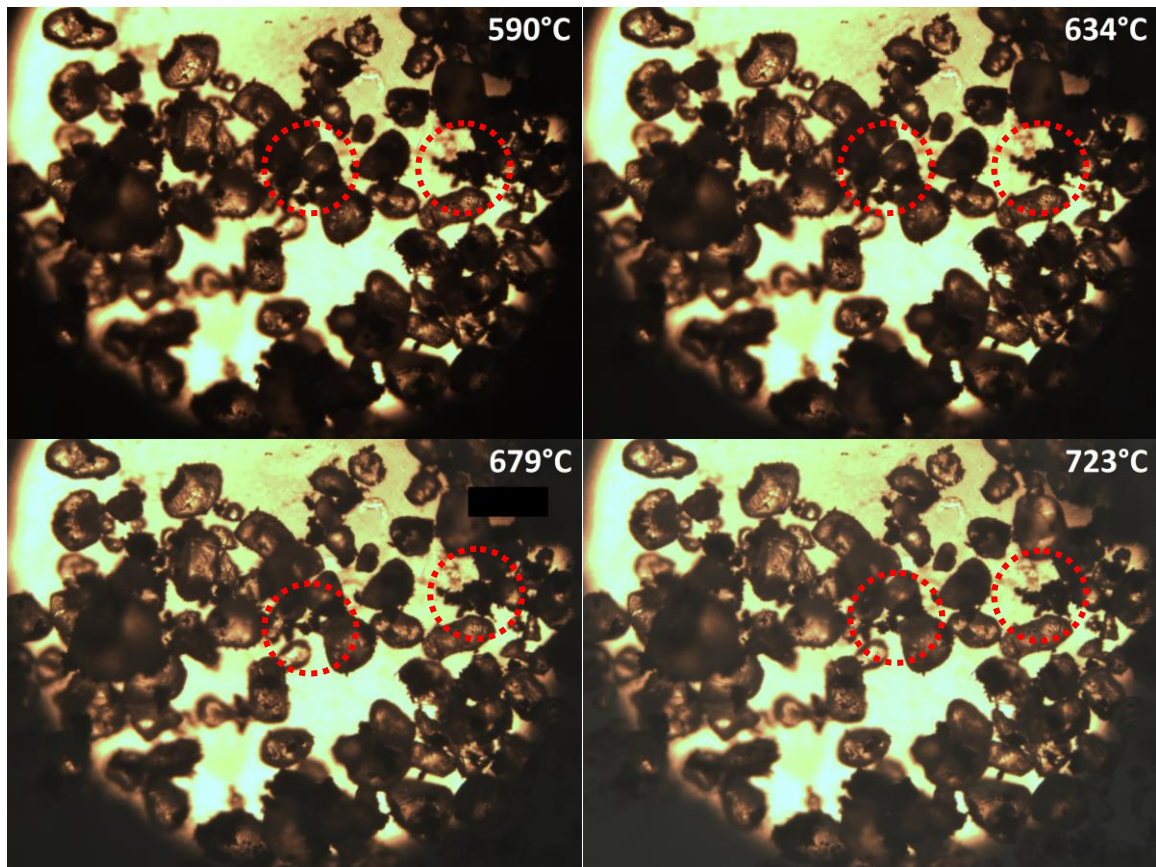


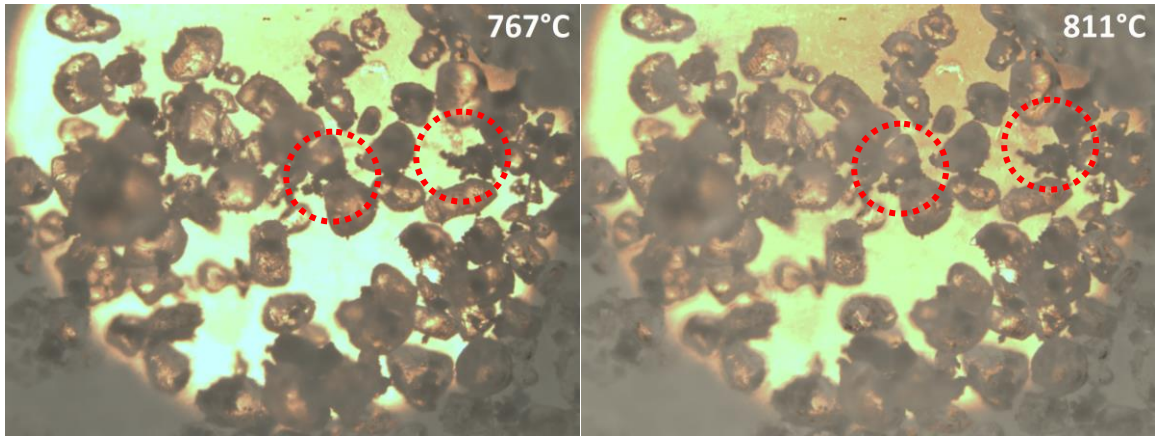
**Figure 5-6: Microscopic photos taken at various temperatures during the repeated experiment with the same test sample (Test # K-1)**

It can be seen from Figure 5-6 that the small lump of synthetic ash in the photos starts to reduce in size at above 767°C (being obviously at 811°C), showing that the fusion of these alkali salts appeared to occur noticeably at >767°C, as concluded from Figure 5-5.

As both experiments were performed on different days with the same test sample (K-1), the results shows that there is good reproducibility and the synthetic ash containing 10.75 wt%  $K_2O$  appears to have a fusion temperature at  $>767^\circ C$ .

Figure 5-7 displays microscopic photos of the mixture of silica sand particles with synthetic ash compounds containing a larger amount of  $K_2O$  (29 wt% of the total ash) (Test#: K-2) at various temperatures. It can be seen from Figure 5-7 that the small lumps of the synthetic ash highlighted in the photos starts to reduce in size at around  $679^\circ C$ , implying that the fusion of the synthetic ash appeared to start noticeably at  $>679^\circ C$ . Thus, for a synthetic ash sample, when increasing the  $K_2O$  content from 10.75 wt% to 29 wt% of the total ash, its fusion temperature decreases from  $\sim 767^\circ C$  to  $\sim 679^\circ C$ , which is as expected as alkali components, mainly potassium (K) and sodium (Na) form low-melting alkali compounds and may also react with the bed material forming low-melting alkali silicates (Bartels et al. 2008; Ohman and Nordin, 2000).

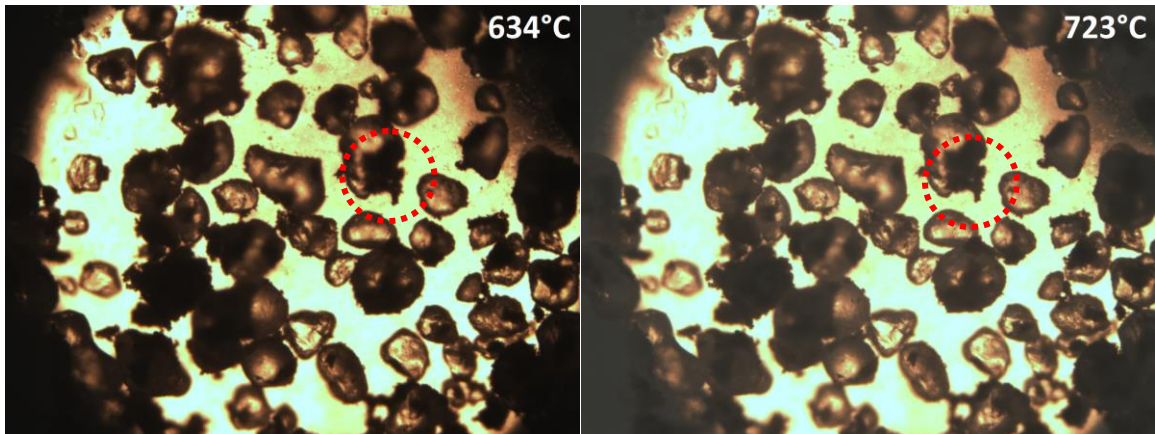




**Figure 5-7: Microscopic photos of the mixture of silica sand particles with synthetic ash compounds containing a larger amount of  $K_2O$  (29 wt% of the total ash) (Test# K-2) at various temperatures.**

As shown in Figure 5-7, some minor changes were also noticed starting around  $634^\circ C$ . The difference in the fusion behavior as compared with Figure 5-6 (Test# K-1) is likely due to the higher percentage of potassium present in the K-2 sample.

Figure 5-8 displays microscopic photos of mixture of silica sand particles with synthetic ash compounds containing 0 wt%  $K_2O$  (Test# K-3) at various temperatures.



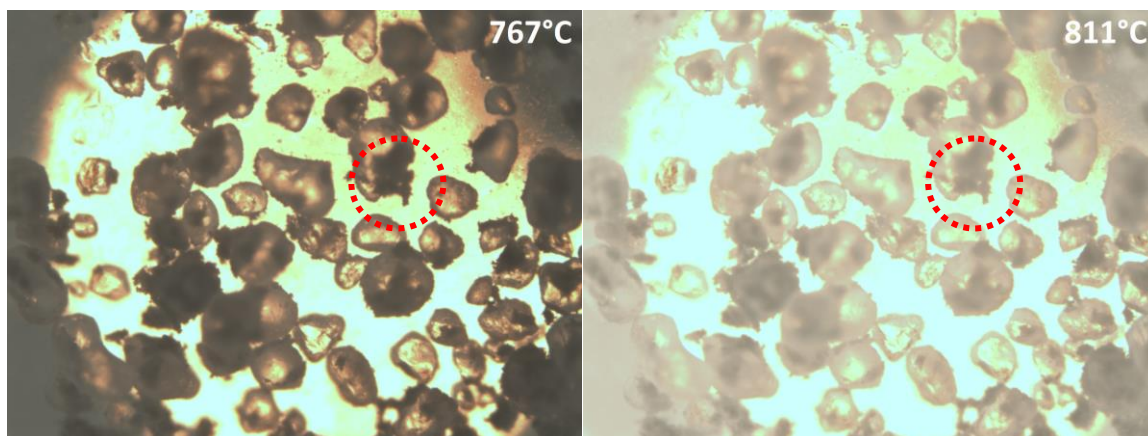
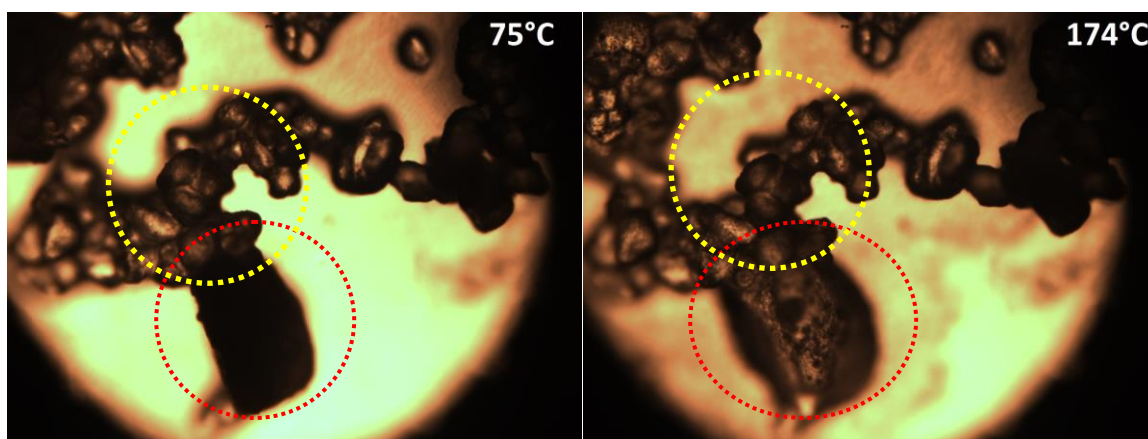


**Figure 5-8: Microscopic photos of a mixture of silica sand particles with synthetic ash compounds containing a 0 wt%  $K_2O$  (Test# K-3) at various temperatures.**

From Figure 5-8, no noticeable change can be observed for the highlighted lump of the synthetic ash. This suggests that the synthetic ash without K is thermally stable even at  $>800^\circ\text{C}$ . No fusion phenomena were observed up to  $900^\circ\text{C}$ .

### 5.3.3 Fusion tests of the mixture of pure KOH and silica sand particles

Figure 5-9 displays microscopic photos of a mixture of pure KOH (10 wt%) and silica sand particles (90 wt%) (Test #: PURE-1) at various temperatures.





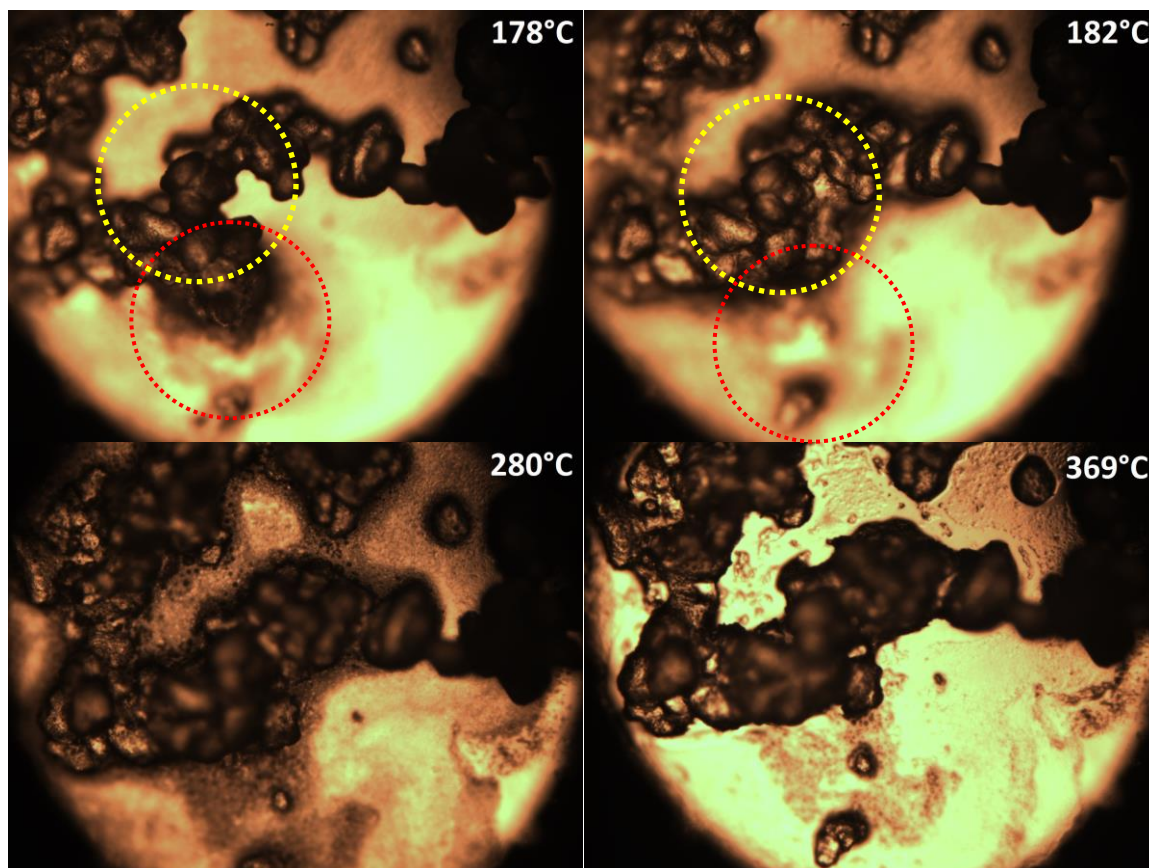


**Figure 5-9: Microscopic photos of a mixture of pure KOH (10 wt%) and silica sand particles (90 wt%) at various temperatures**

It can be seen from the pictures that the red highlighted lump of particles of KOH starts melting at around 170°C. It should be noted that pure KOH has a melting point of 360°C (Janz, et al., 1968). This discrepancy is because the KOH used in this study absorbed moisture (hygroscopic). KOH when contain varying amounts of water forms hydrates, e.g., monohydrate, dehydrate and tetrahydrate. These compounds have melting points lower than the pure KOH. For example, the monohydrate structure has a melting point of 150°C.

Interestingly, as shown in Figure 5-9, the melted KOH moves through the sand particles forming liquid bridges between them, causing agglomeration of the sand particles at ~180°C, as highlighted by yellow circles on the microscopic photos.

### 5.3.4 Fusion tests of the mixture of the real biomass fly ash and silica sand particles

Figure 5-10 shows microscopic photos of a mixture of the biomass real fly ash sampled from a biomass boiler in a pulp mill and silica sand particles (Test #: REAL-1) at various temperatures.

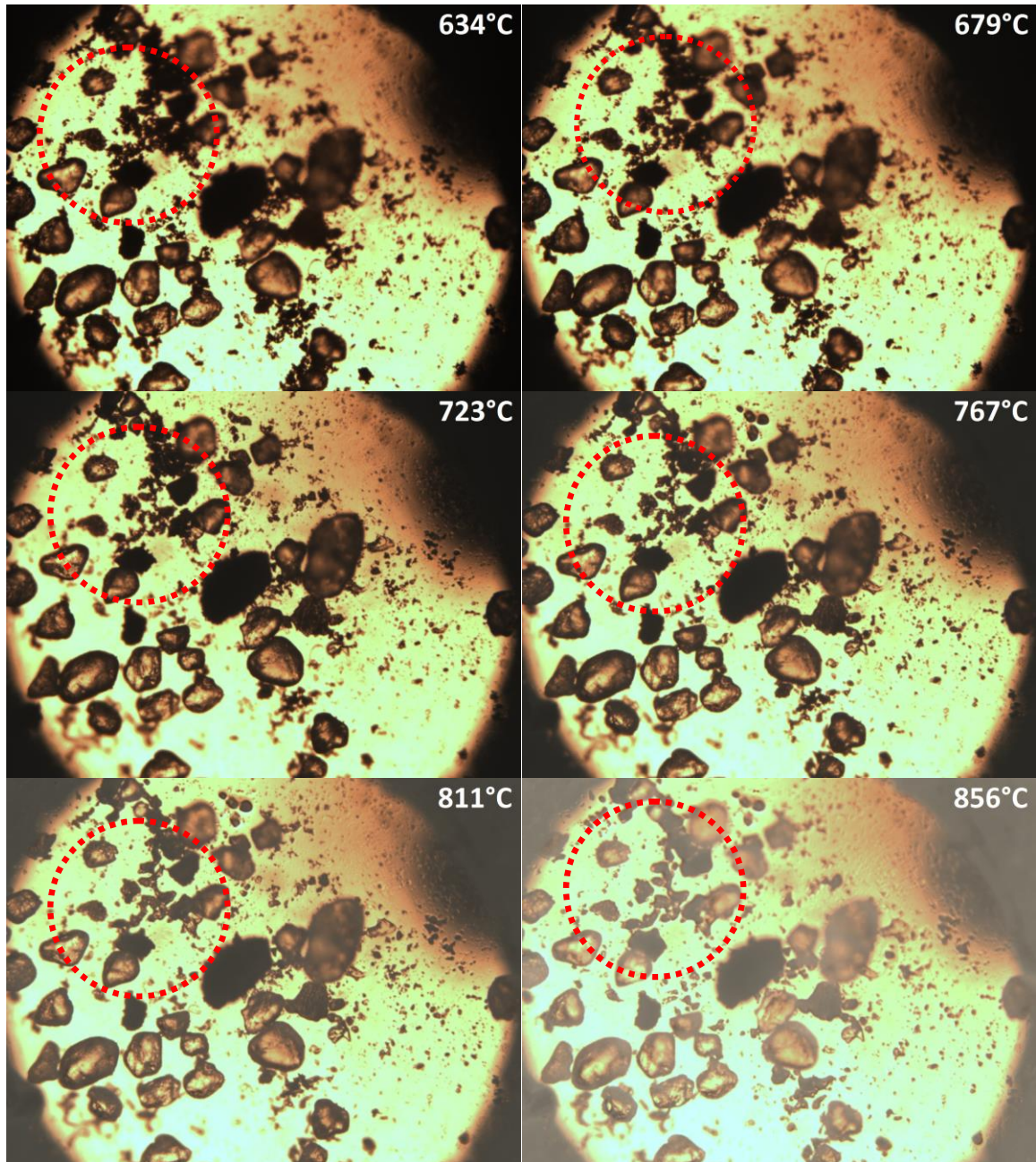


**Figure 5-10: Microscopic photos of a mixture of the real biomass fly ash (10 wt%) and silica sand particles (90 wt%) at various temperatures**

It can be seen from Figure 5-10 that the particle density of the highlighted area decreases between 634-679°C, suggesting the fusion of these alkali salts-containing fly ash, whose composition was given previously in Table 5-1. The difference in melting/fusion behavior between the synthetic ash samples (Tests # K-1, K-2 and K-3) and the real biomass fly ash (Test # REAL-1) is likely due to the much higher concentration of potassium and sodium in the latter (K<sub>2</sub>O 19.93 wt%; Na<sub>2</sub>O 12.32 wt%).

Admittedly, there are some limitations associated with the reported microscope-heating stage method for fusion studies of biomass fly ash, of which the main challenge is that at temperatures above 811°C the image quality decreased significantly, making it difficult to observe changes in the heated test sample.

## 5.4 Conclusions

This study aimed to investigate the effects of K on the formation of liquid bridge/fusion between fluidized bed materials (silica sand particles) upon heating using synthetic biomass ash (of composition that of typical ash from biomass boilers), pure K compound (KOH), and a real biomass fly ash obtained from a biomass boiler in a Canadian pulp mill. The fusion tests were carried out on a custom-designed microscope equipped with a heating stage of a heating capacity up to 1100°C. The softening of the synthetic/real ash and the formation of liquid bridge between sand particles were photographed during heating of the mixture from room temperature up to 1100°C. Some conclusions were drawn from this work:

- For a synthetic ash sample, when increasing the  $K_2O$  content from 10.75 wt% to 29 wt% of the total ash, its fusion temperature decreases from ~767°C to ~679°C, which is as expected as alkali components, mainly potassium (K) and sodium (Na) form low-melting alkali compounds and may also react with the bed material forming low-melting alkali silicates.
- Pure KOH added to the silica sand particles started to melt at around 170°C, much lower than the standard melting point (360°C) of pure KOH, because the KOH used in this study absorbed moisture in air, resulting in great reduction in melting points. The melted KOH moves through the sand particles forming liquid bridges between them, causing agglomeration of the sand particles at ~180°C.
- The fusion of the high alkali salts-containing fly ash started to melt at as low as 634-679°C likely due to the much higher concentration of potassium and sodium in the real fly ash ( $K_2O$  19.93 wt%;  $Na_2O$  12.32 wt%).

### **Acknowledgements:**

This investigation is a part of the NSERC CRD project titled “FUNDAMENTAL STUDIES OF DRYING, COMBUSTION AND ASH PROPERTIES OF BIOMASS, AND IMPACTS ON BOILER AND PULP AND PAPER MILL OPERATIONS”, led by one of the authors (H. Tran) at The University of Toronto. The authors (C. Xu and H.

Tran) would also like to acknowledge the financial support provided by NSERC via the Discovery Grants, as well as the industrial support from various pulp and paper companies.

## 5.5 References

ASTM. (1987). *Annual book of ASTM Standards Pt 26*. Philadelphia: American Society for Testing and Materials.

Bakker, R., Jenkins, B., & Williams, R. (2002). Fluidized bed combustion of leached rice straw. *Energy&Fuels*(16), 356-365.

Bartels, M., Lin, W., Nijenhuis, J., Kapteijn, F., & Ommen, J. (2008). Agglomeration in fluidized beds at high temperatures: Mechanisms, detection and prevention. *Energy and Combustion Science*(34), 633-666.

He, Y. (1999). Characterisation of spouting behaviour of coal ash with thermo-mechanical analysis. *Fuel Processing Technology*(1), 69-79.

Janz, G., Dampier, F., Lakshmi-Narayanan, G., & Lorenz, P. (1968). *Molten salts: Volume 1*. National standard Reference Data Series.

Jenkins, B., Baxter, L., Miles, T., Miles, J. T., Oden, L., Bryers, R., et al. (1994). Composition of ash deposits in biomass fuelled boilers: results of full-scale experiments and laboratory simulations. *Paper presented at the 1994 international ASAE summer meeting, Kansas City*.

Li, S., Lu, Q., & Teng, H. (2010). Agglomeration during fluidized-bed combustion of biomass. *The 13th International Conference on Fluidization-New Paradigm in Fluidization Engineering*(36).

Lin, W., Dam-Johansen, K., & Frandsen, F. (2003). Agglomeration in bio-fuel fired fluidized bed combustors. *Chemical Engineering Journal*(96), 171-185.

- Liu, H., Feng, Y., Wu, S., & Liu, D. (2009). The role of ash particles in the bed agglomeration during the fluidized bed combustion of rice straw. *Bioresource Technology*(100), 6505-6513.
- Natarajan, E., Ohman, M., Gabra, M., Nordin, A., Liliedahl, T., & Rao, A. (1998). Experimental determination of bed agglomeration tendencies of some common agricultural residues in fluidized bed combustion and gasification. *Biomass and Bioenergy*(2), 163-169.
- Ohman, M., & Nordin, A. (1998). A New Method for Quantification of Fluidized Bed Agglomeration Tendencies: A Sensitive Analysis. *Energy & Fuels*(12), 90-94.
- Ohman, M., & Nordin, A. (2000). Bed Agglomeration Characteristics during Fluidized Bed Combustion of Biomass Fuels. *Energy&Fuel*(14), 169-178.
- Olofsson, G., Ye, Z., & Bjerle, I. (2002). Bed agglomeration problems in fluidized-bed biomass combustion. *Industrial and Engineering Chemistry Research*, 2888-2894.
- Pang Heng, C., Hewakandamby, B., Wu, T., & Lester, E. (2013). An automated ash fusion test for characterisation of the behavior of ashes from biomass and coal at elevated temperatures. *Fuel*(103), 454-466.
- Raask, E. (1979). Sintering characteristics of coal ashes by simultaneous dilatometry-electrical conductance measurements. *Journal of Thermal Analysis and Calorimetry*(16), 91-102.
- Stallman, J., & Neavel, R. (1980). Techniques to Measure the Temperature of Agglomeration of Coal Ash. *Fuel*(59), 584-586.
- Vassilev, S., Baxter, D., Andersen, L., & Vassileva, C. (2010). An overview of the chemical composition of biomass. *Fuel*(89), 913-933.
- Werther, J., Saenger, M., Hartge, E.-U., Ogada, T., & Siagi, Z. (2000). Combustion of agricultural residues. *Progress in Energy and Combustion Science*(26), 1-27.

Zevenhoven-Onderwater, M., Backman, R., Skrifvars, B., & Hupa, M. (2001). The ash chemistry in fluidized bed gasification of biomass fuels. Part I: predicting the chemistry of melting ashes and ash-bed material interaction. *Fuel*(80), 1489-1502.

## 5.6 Appendix 5-1

**K2O**

	%	gram
Silica sand	90	4.5
Ash	10	0.5

Test 1 K2O 10.75%											
	SiO2	CaO	K2O	P2O5	Al2O3	MgO	Fe2O3	SO3	Na2O	TiO2	Total
Ash composition gram	0.1111	0.2152	0.0538	0.0174	0.0255	0.0304	0.0172	0.0139	0.0143	0.0015	0.50
Ash composition %	22.22	43.03	10.75	3.48	5.09	6.07	3.44	2.78	2.85	0.29	100
Ash composition (gram) corrected	0.1122	0.2152	0.0711	0.0174	0.0255	0.0310	0.0172	0.0056	0.0190	0.0015	

Test 2 K2O 29%											
	SiO2	CaO	K2O	P2O5	Al2O3	MgO	Fe2O3	SO3	Na2O	TiO2	Total
Ash composition gram	0.1111	0.2152	0.1450	0.0174	0.0255	0.0304	0.0172	0.0139	0.0143	0.0015	0.6174
Ash composition %	22.22	43.03	29	3.48	5.09	6.07	3.44	2.78	2.85	0.29	118.25
Ash composition (gram) corrected	0.1122	0.2152	0.1919	0.0174	0.0255	0.0310	0.0172	0.0056	0.0190	0.0015	

Test 3 K2O 0%											
	SiO2	CaO	K2O	P2O5	Al2O3	MgO	Fe2O3	SO3	Na2O	TiO2	Total
Ash composition gram	0.1111	0.2152	0.0000	0.0174	0.0255	0.0304	0.0172	0.0139	0.0143	0.0015	0.4255
Ash composition %	22.22	43.03	0	3.48	5.09	6.07	3.44	2.78	2.85	0.29	89.25
Ash composition (gram) corrected	0.1122	0.2152	0	0.0174	0.0255	0.0310	0.0172	0.0056	0.0190	0.0015	



## Chapter 6

# 6 CONCLUSIONS AND RECOMMENDATIONS

## 6.1 Conclusions

A study was conducted to determine the critical amount of liquid required to form bed materials agglomeration in biomass BFB boilers, employing a cold BFB test rig by injection of a liquid solution of glycerol-water (30% v/v) to simulate molten ash in real biomass boiler operations. From this study, it was obtained that in the BFB fluidization system tested the critical liquid amount that could cause the bed materials start to form agglomeration/channeling, and form severe agglomeration/channeling (poor fluidization) is approx. 0.2 wt% and 0.7wt%, respectively. In the present fluidization system, the fluidization gas velocity did not appear to affect the bubbling and pressure drop behaviors, nor the minimum amount of liquid required for bed materials agglomeration.

Also a study was conducted to investigate and determine the critical amount of liquid phase for bed material agglomeration in a bubbling fluidized bed operated at elevated temperatures using low melting-point salt (KOH) to simulate molten ash. From this study some conclusions were drawn:

- In the BFB fluidization system tested, the critical liquid amount of simulate molten ash that could cause the bed materials start to form agglomeration/channeling, and form severe agglomeration/channeling (poor fluidization) is approx. 0.5 wt% and 0.8wt% at a lower fluidizing gas velocity ( $3.9 U_{mf}$ ) and a higher fluidizing gas velocity ( $5.9 U_{mf}$ ), respectively.
- With more low-melting-point compound (KOH) present in the BFB, more agglomerates of bed material are formed. Increasing the amount of liquid could change the fluidization behavior of group B (silica silica) particles towards group A and even C, depending on the amount of the low-melting-point compound in the bed material.

- In comparison with those from the tests at a lower gas velocity, much less amount of agglomerates were obtained from the experiments operating at a higher gas velocity, due to the higher disruptive forces present in the bed at a higher fluidizing gas velocity.

Finally the last part of this study aimed to investigate on the effects of K on the formation of liquid bridge/fusion between fluidized bed materials (silica sand particles) upon heating using synthetic biomass ash (of composition that of typical ash from biomass boilers), pure K compound (KOH), and a real biomass fly ash obtained from a biomass boiler in a Canadian pulp mill. The fusion tests were carried out on a custom-designed microscope equipped with a heating stage of a heating capacity up to 1100°C. The softening of the synthetic/real ash and the formation of liquid bridge between sand particles were photographed during heating of the mixture from room temperature up to 1100°C. Some conclusions were drawn from this work:

- For a synthetic ash sample, when increasing the  $K_2O$  content from 10.75 wt% to 29 wt% of the total ash, its fusion temperature decreases from ~767°C to ~679°C, which is as expected as alkali components, mainly potassium (K) and sodium (Na) form low-melting alkali compounds and may also react with the bed material forming low-melting alkali silicates.
- Pure KOH added to the silica sand particles started to melt at around 170°C, much lower than the standard melting point (360°C) of pure KOH, because the KOH used in this study absorbed moisture in air, resulting in great reduction in melting points. The melted KOH moves through the sand particles forming liquid bridges between them, causing agglomeration of the sand particles at ~180°C.
- The fusion of the high alkali salts-containing fly ash started to melt at as low as 634-679°C likely due to the much higher concentration of potassium and sodium in the real fly ash ( $K_2O$  19.93 wt%;  $Na_2O$  12.32 wt%).

From this MEng thesis it can be concluded that the critical amount of liquid causing bed agglomeration is likely 0.2-0.5 wt% (in relation to the weight of bed material loaded) and that approximately 1 wt% would cause severe channeling and very poor fluidization

conditions. It is expected that these results will be similar to the future experiments that will be performed in the coming year. These results will help pulp and paper mills develop new strategies to prevent bed agglomeration in BFB boilers

## 6.2 Recommendations

- Installation of another thermocouple in the fluidized bed located at Sarnia. As is well known the temperature profile inside the bed is another indicator of defluidization. In a well fluidized bed the bed temperature is very uniform, but when agglomerations occurs the difference between the bottom of the bed and other points above becomes larger due to poor mixing, the current bed configuration only has one thermocouple in the bottom of the bed.
- Modify the small furnace heating system for preheat the fluidization air, by packing steel balls in the air line or by changing the shape of the air line. With the current configuration the fluidization air do not have enough residence time, thus the system is losing efficiency.
- Study and determine the critical amount of liquid (molten ash) that would result in severe bed agglomeration and defluidization in BFB biomass boilers at high temperatures ( $\sim 800^{\circ}\text{C}$ ) first using different amounts of a mixture of KCl,  $\text{K}_2\text{SO}_4$ , NaCl and  $\text{Na}_2\text{SO}_4$  to simulate molten ash, and finally using real biomass.

## Appendices

### A Bubbling fluidized bed reactor description, modifications and operation procedures

This appendix describes the facility, the operation procedures and the modifications performed on the small pilot-scale bubbling fluidized bed (BFB) reactor located at Western Research Park (Sarnia). The operation procedures mainly include 3 stages of operation: warming up, steady-state operation and cooling down/shutting down. The modifications were implemented to better suit our proposed tests and in order to correct some design problems.

#### A.1 Facility description

The BFB column is made of stainless steel 316 L, 76 mm inner diameter and 1.75 m total height. A schematic of the reactor is shown in Figure A-1.

As is illustrated in Figure A-1 the facility is equipped with a screw feeding system (Ktron, model KMV-KT20), consisting of a twin screw feeder, a hopper, a 0.45 kw motor and a controller (Ktron model KCM) used to adjust the screw speed. The feeding capacity is 1-2 kg/hr of dry biomass. The screw feeding system is combined with a rotary airlock valve (Rotolok). A picture of the real fuel feeding system is illustrated in a photo presented in Figure A-2.

After passing through the rotary valve the feedstock is fed into the fluidized bed, assisted by a vibrator (Vibco model SPR-2) installed also in the feeding line. In the downstream from the free board of the BFB reactor, the system is equipped with a cyclone for removal and collection of small particles in the effluent gas (bed material, unburnt biomass/char and fly ash when combustion or gasification is carried out), a bag filter, a water-cooled condenser for tar removal, and a flue gas sampling port. The non-condensable gases are vented to the outside of the building and into the environment.

The reactor is equipped with a primary air inlet (fluidization gas) and a secondary air inlet (to assist volatile combustion when the reactor is used as a combustor for biomass). Both air inlets have flow meters to control the air flow rates, and before the flow meters there is a pressure regulator (0-160 psi) to regulate the air pressure coming from the air compressor.

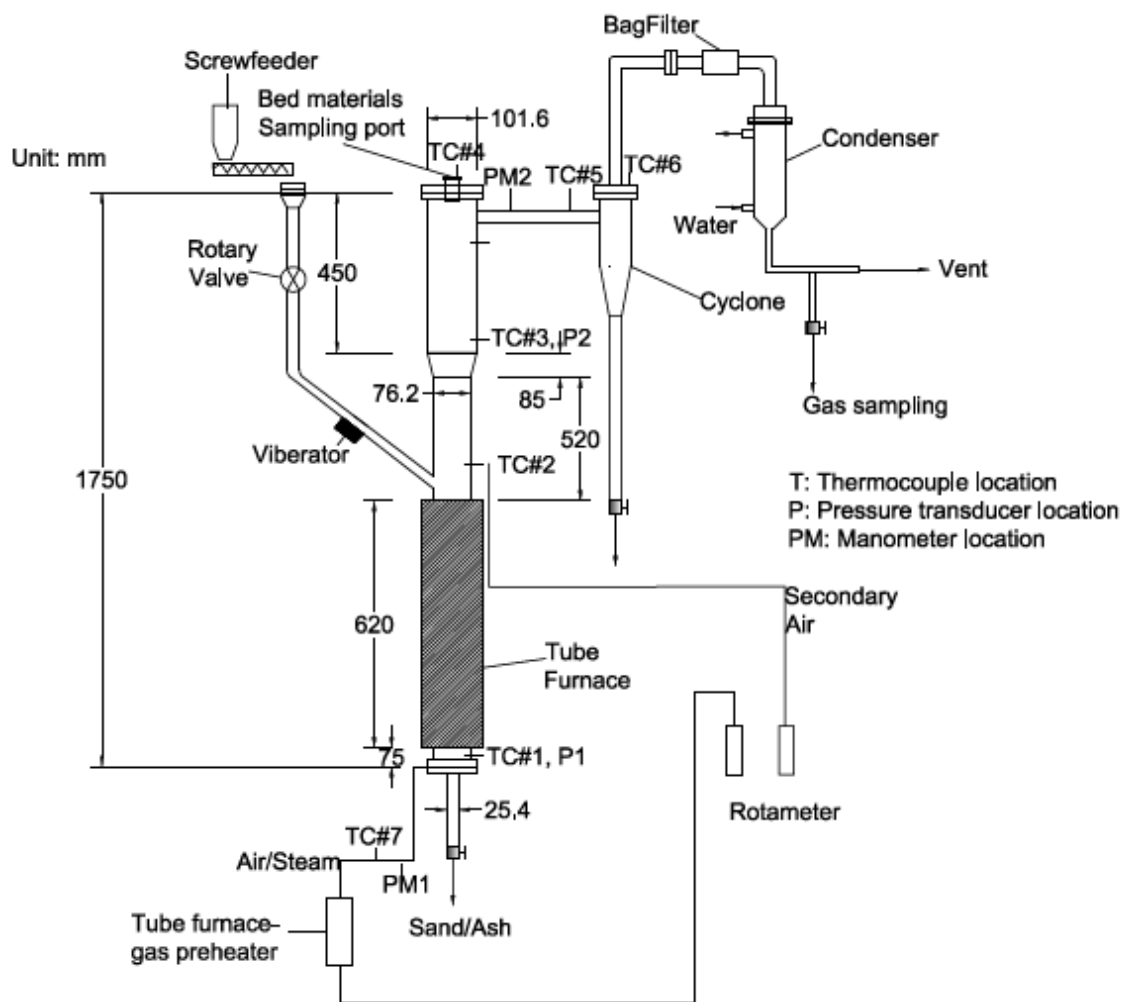


**Figure A-1: Schematic diagram of the bubbling fluidized-bed reactor system for biomass combustion, gasification or pyrolysis studies at the Industrial Bioproducts Lab in Western Research Park (Sarnia)**

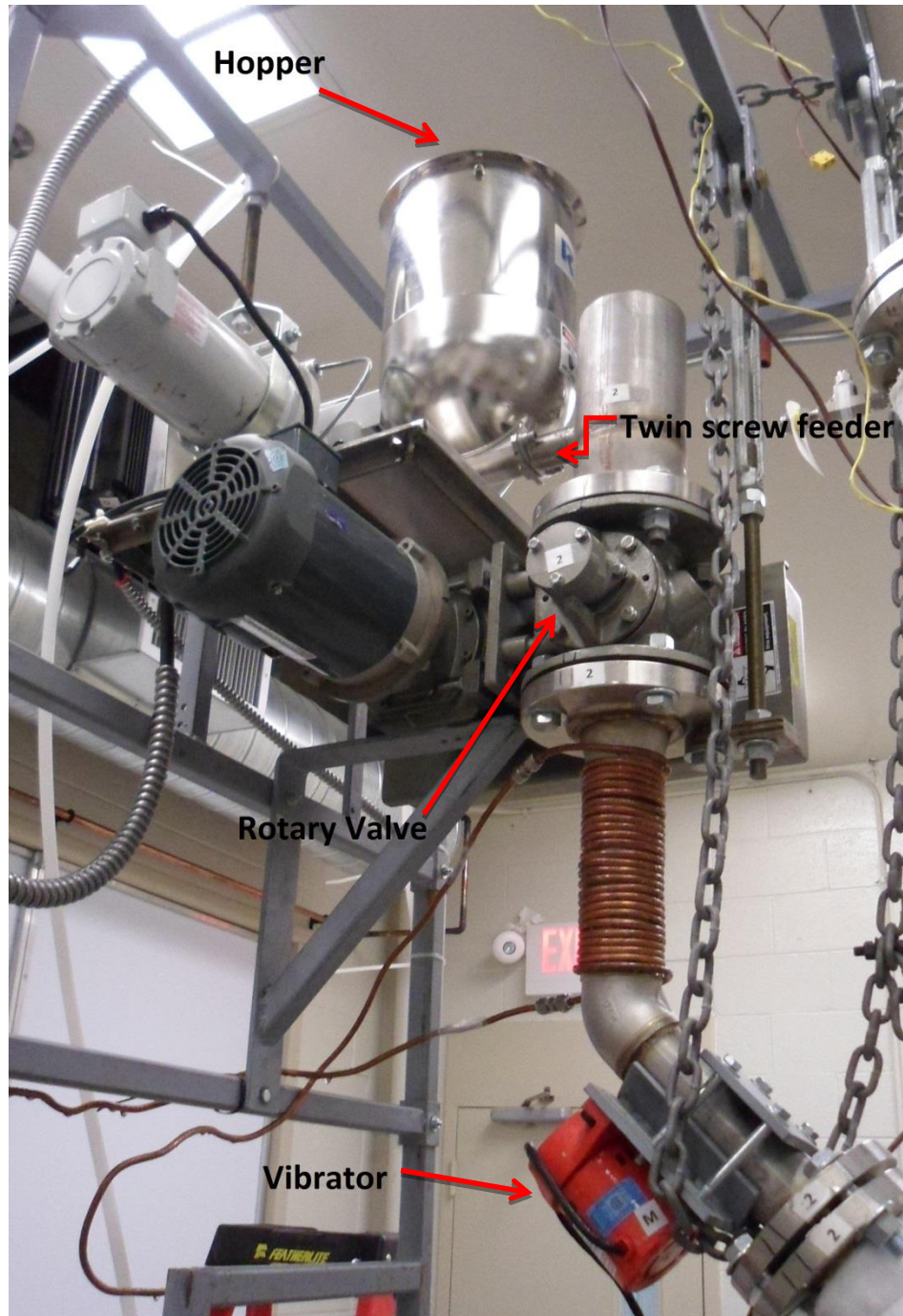


**Figure A-2: Photo of the feeding system**

Two furnaces with their corresponding controllers are used to heat the system, one to preheat the fluidization air and the other to heat the bed materials. The furnaces specifications are presented below:

- Air preheater: Thermcraft furnace, Model: SST-1.25-0-12-1C-D2155-C (1200 watts, Max T°:1200°C), with a Thermcraft controller Model: 1-1-20-120-Y11SP-C2278E-A;
- Bed materials heater: Thermcraft furnace, Model: SST-3.75-0-18-1C-D2155-BW (4900 watts, Max T°:1200°C) with a Thermcraft controller Model: 1-1-40-230-Y11SP-C2287-AP.

The reactor's instrumentation consists of 7 thermocouples, 2 pressure transducers and 2 pressure gauge located at different positions in the system (Figure A-1).

- The thermocouples are Omega, K type probe, 1/8 inch (3.2mm) diameter, 12 inch (300mm) length.
- The pressure transducers are Omega, model PX219-015G5V.
- The pressure gauges are Swagelok (0-15 psi).

The signals from the thermocouples and the pressure transducers are collected with an Omega data acquisition system, Model: OMB-DAQ-3005, 16bit/1mhz. The data acquisition system is connected by an USB port to a personal computer equipped with a custom-designed software developed by Mr. Yufei Wang – summer project student from Department of Software Engineering of Western University. Figure A-3 shows a screenshot of the software.

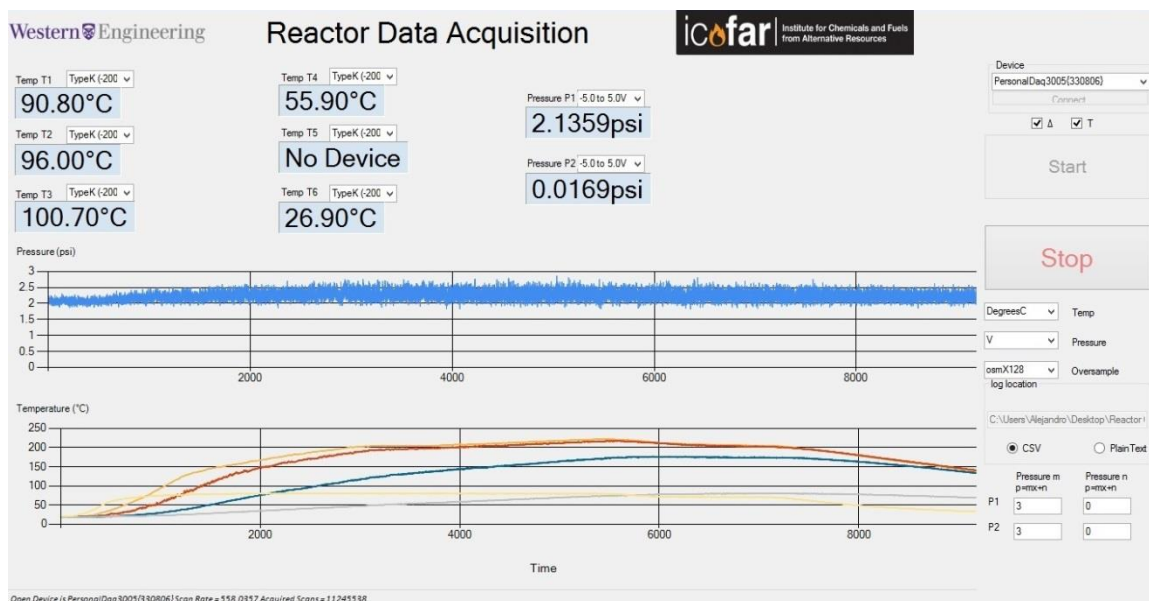


**Figure A-3: Data acquisition software developed for the BFB system**

## A.2 Modification of the gas distributor

The installation of the reactor was finished at the end of August 2013. After some trial tests were performed it was found that the air inlet used to fluidize the bed was always plugged with silica sand likely due to some problems with the originally designed gas distributor, cone shape distributor made of SS 316 L perforated sheets, as shown in Figure A-4.



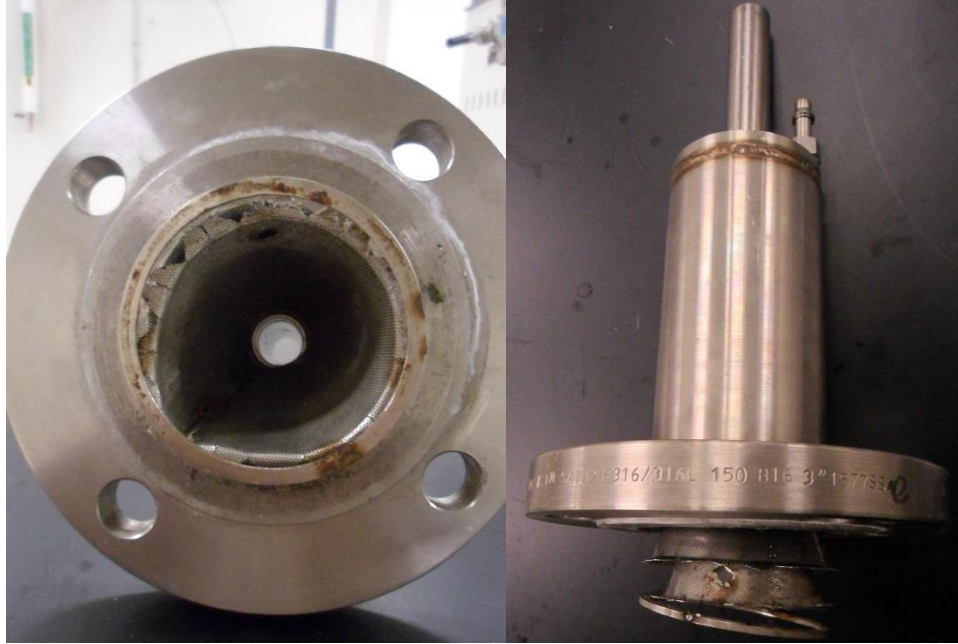


**Figure A-4: Original gas distributor**

As can be seen from Figure A-4, the distributor was made up of a set of perforated truncated cones each with different sizes of holes, and the truncated cones were placed one over the other to form the distributor. Between the set of truncated cones and the wall of the reactor (wind box) steel balls (to enhance gas distribution) were placed. The truncated cones were all connected at the bottom with a 1'' discharge line which was built with a ball valve to discharge the reactor materials. A 3/8'' air inlet was located at the bottom of the structure as can be seen in the right picture in Figure A-4. Figure A-5 shows the set of truncate cones used in the original design. As can be seen in Figure A-5 the cones were in a poor condition, some of which were broken and the sizes of the holes are not small enough to prevent the sand particles from entering into the wind box, which would cause the problem of plugging the gas line during the trial tests.

It was found that in each trial test the pressure in the air inlet increased dramatically despite the fact that after each test the reactor was completely discharged and the pressure line was unplugged. Figure A-6 shows how the wind box looked after a trial test and after removing the set of cones and some of the steel balls.

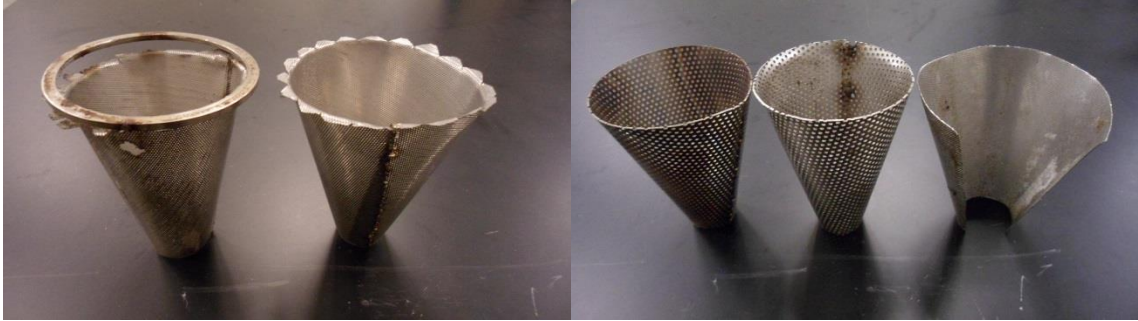


**Figure A-5: A set of perforated cones used for the gas distributor**



**Figure A-6: Wind box blocked with bed materials particles (silica sand)**

As clearly illustrated from the above photo (Figure A-6), the silica sand particles entered to the wind box, which eventually partially/completely plug the gas line. To resolve this problem, it was decided to modify the distributor by implanting a new design for the gas distribution. The new distributor design and pictures are shown in Figure A-7 and Figure A-8, respectively. The new distributor is made of SS 316 L and has an overall diameter of 3 inch. In its center there is a 1-inch diameter discharge port which is connected to a ball valve. Two inches from the center along the entire circumference there are 10 perforated plates (SS316L, 40  $\mu\text{m}$ ) with a diameter of 0.45 inch each through which the fluidization air flows (showed in orange color in Figure A-7). The distributor is embedded in a flange

of 7.5 inch diameter. A ¼-inch air inlet is located on the side of the flange structure. Detailed dimensions of the distributor are presented at the end of this Appendix.

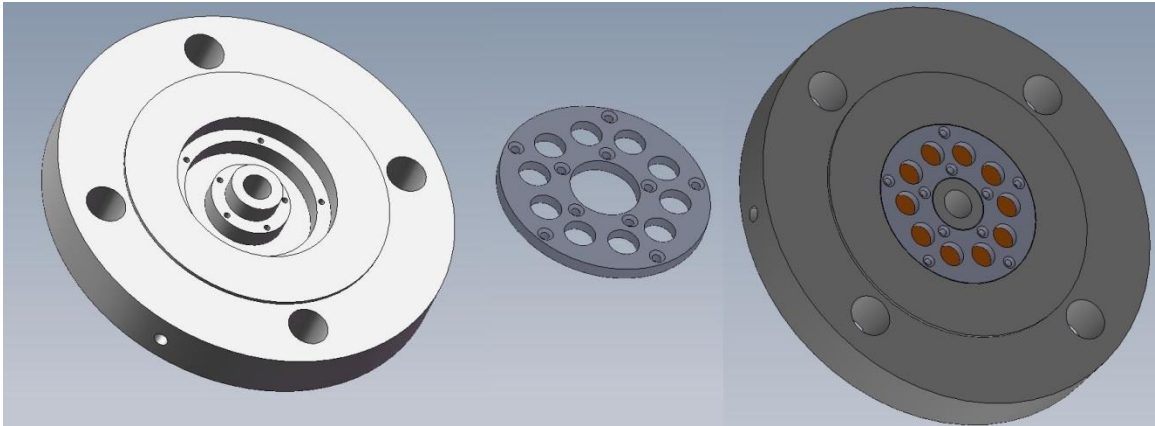


**Figure A-7: New gas distributor design**

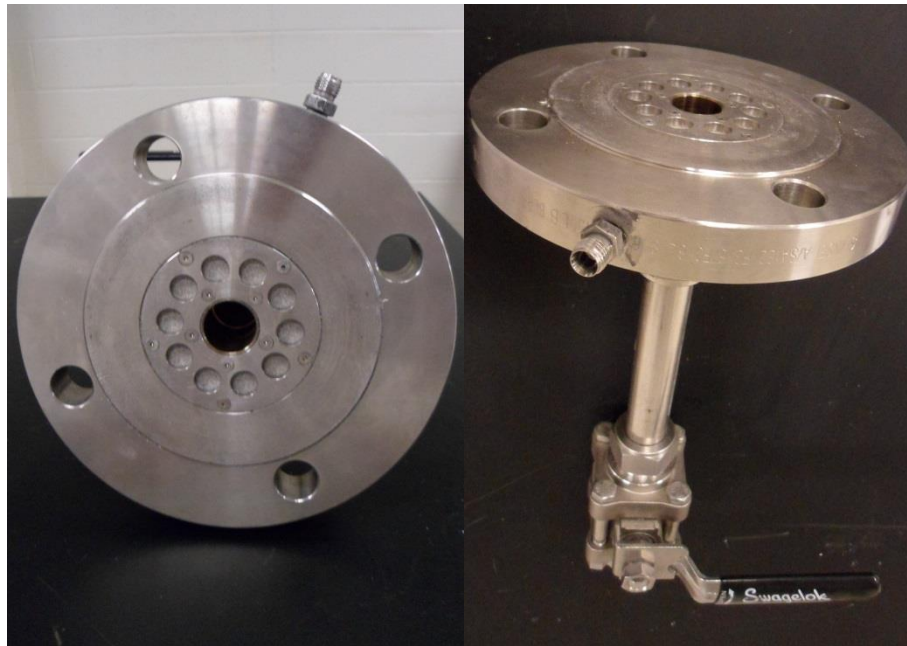


**Figure A-8: Picture of the new gas distributor**

### A.3 Fluidization air supply and flow rate control

In the original design of the BFB reactor, the primary air (fluidization air) is controlled with a rotameter of a range from 0 to 14 L/min. In order to ensure the range of the flow meter is sufficient to fluidize the bed materials (sand particles), the superficial gas velocity ( $U_g$ ) was calculated using the cross sectional area of the reactor and the flow meter readings, as listed below:

**Table A-1:** Air flow rates vs. superficial gas velocities ( $U_g$ )

Air flow rate (L/min)	$U_g$ (m/s)
0	0
1	0.0037
2	0.0073
3	0.0110
4	0.0146
5	0.0183
6	0.0219
7	0.0256
8	0.0292
9	0.0329
10	0.0365
11	0.0402
12	0.0439
13	0.0475
14	0.0512

As shown from Table A-1, the original flow meter (0-14 L/min) can provide  $U_g$  between 0 and 0.0512 m/s. In a BFB operation, the  $U_g$  is normally  $>2-4 U_{mf}$  to avoid channeling, defluidized zones or grid leakages, and to maximize the throughput. Thus, the minimum fluidization velocity ( $U_{mf}$ ) was calculated or measured to ensure that the flow meter was big enough to supply enough fluidizing gas to the reactor.

#### A.1.1 Minimum fluidization velocity

The  $U_{mf}$  for the silica sand bed materials can be calculated using empirical or theoretical correlations or measured by experimental approaches, as was explained preciously in Chapter 2.

### A.1.1.1 Theoretical Calculation of $U_{mf}$

The theoretical calculations for  $U_{mf}$  were performed using an empirical correlation and correlations based in Ergun's equation.

The most commonly used empirical correlations for  $U_{mf}$  prediction is Leva (1959)'s correlation:

$$U_{mf} = \frac{7.169 \times 10^{-4} (\rho_p - \rho_g)^{0.94} d_p^{1.82} g}{\rho_g^{0.06} \mu_g^{0.88}} \quad \text{A-1}$$

Where,

$\rho_p$  = particle density, kg/m<sup>3</sup>

$\rho_g$  = gas density, kg/m<sup>3</sup>

$d_p$  = volume-equivalent particle diameter (Sauter mean diameter in the case of multisize particles), m

$g$  = gravity constant = 9.8 m/s<sup>2</sup>

$\mu_g$  = gas dynamic viscosity, Pa.s

This correlations works well if  $Re_{mf} = \frac{\rho_g U_{mf} d_p}{\mu_g} < 30$ , when the particles are relatively small.

Correlations based on Ergun's equation are also widely used for theoretically estimate

$U_{mf}$  from the Reynolds number at the minimum fluidization ( $Re_{mf} = \frac{\rho_g U_{mf} d_p}{\mu_g}$ ):

$$Re_{mf} = \sqrt{C_1^2 + C_2 Ar} - C_1 \quad \text{A-2}$$

Where  $C_1$  and  $C_2$  are constants whose values are shown in Table A-2;  $A_r$  is the the

Archimedes number: 
$$A_r = \frac{\rho_g (\rho_p - \rho_g) g d_p^3}{\mu_g^2}$$
.

For the present air-sand particle fluidization system at room temperature (298 K), the given parameters are:  $\rho_p = 2650 \text{ kg/m}^3$ ;  $\rho_g = 1.18 \text{ kg/m}^3$ ;  $d_p = 204 \text{ }\mu\text{m}$ ;  $\mu_g = 1.8 \times 10^{-5} \text{ Pa}\cdot\text{s}$ .

The calculation results obtained are:

- From the Leva (1959)'s empirical correlation (Eq. A-1):  $U_{mf} = 0.033 \text{ m/s}$ .
- From the correlations based in Ergun's equation (Eq. A-2), the calculated  $U_{mf}$  values are in the range of 0.036-0.042 m/s, as shown in Table A-2.

**Table A-2:  $U_{mf}$  calculated with different correlations based in Ergun's equation**

Correlation	C1	C2	$Re_{mf}$	$U_{mf}$
Wen and Yu (1966)	33.7	0.0408	0.513	0.036
Richardson & Jeronimo (1979)	25.7	0.0365	0.600	0.042
Thonglimp et al. (1984)	31.6	0.0425	0.569	0.040

#### A.1.1.2 Experimental Measurement of $U_{mf}$

As well known,  $U_{mf}$  can be determined experimentally from  $\Delta P$  vs  $U_g$  plots. The plots were recorded, starting with a well-fluidized bed and gradually decreasing the gas velocity while measuring the bed pressure drop. The  $U_{mf}$  is the velocity at which the Ergun equation becomes valid.

Figure A-9 shows the experimental results of the  $\Delta P$  vs  $U_g$  plots obtained under conditions of both increasing and decreasing  $U_g$ .

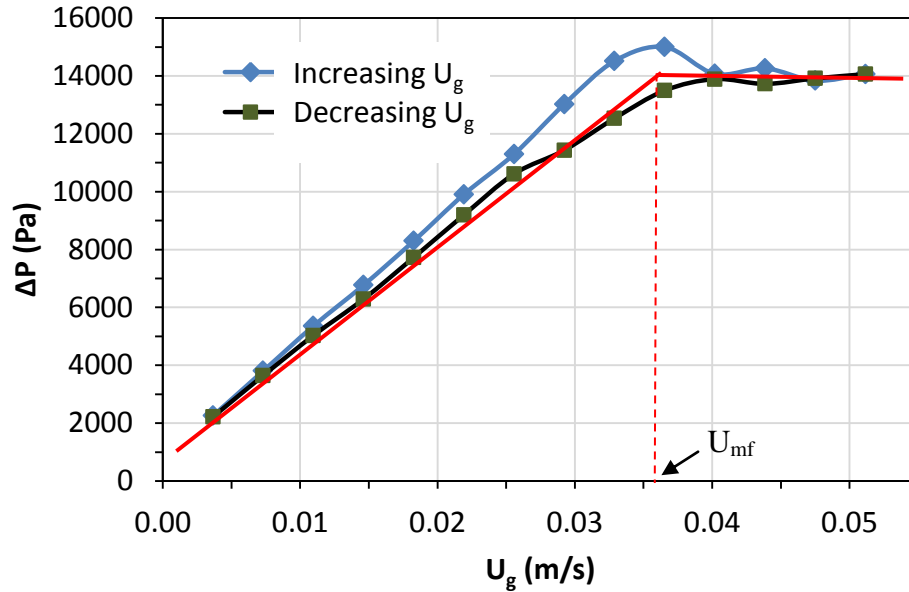


**Figure A-9: Experimental measurement of  $U_{mf}$**

It can be seen from Figure A-9 that the measured  $U_{mf}$  is around 0.036 m/s, in a good agreement with the theoretical calculations (0.033-0.042 m/s), in particular with that ( $U_{mf} = 0.036$  m/s) predicted by Wen/Yu (1966). Thus, Wen/Yu (1966)'s correlation can be used for prediction of  $U_{mf}$ , as similarly concluded by Thonglimp et al. (1984).

Comparing the value of  $U_{mf}$  calculated or measured with the values of  $U_g$  presented in Table A-1, it was found that the original 0-14 L/min flow meter can obtain a maximum superficial gas velocity of approx.  $1.4 U_{mf}$ , which is not high enough to avoid channeling, defluidized zones or grid leakages. As such, it was decided to install in parallel (with the old flow meter) a new flow meter (Panel-Mount flow-meter, 15-180 Scfh) that allows a wider gas flow rate range to obtain  $U_g = 0 \sim 10 U_{mf}$ .

## A.4 Reactor Heating and Insulation

The reactor was built to perform high temperature experiments. In order to achieve a high temperature of the reactor, the heating and insulation configurations of the reactor were tested.

To examine the heating performance of the BFB reactor without insulation, the fluidized bed column was filled with silica sand (7.37 kg), both the air pre-heater and the bed materials heater were set at 850°C. Figure A-10 shows the bed material temperature measured against heating time.

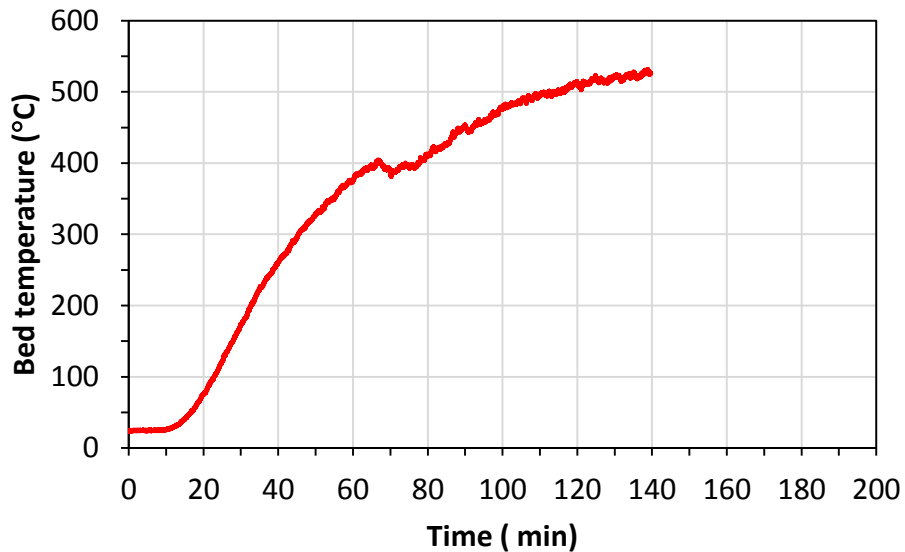


**Figure A-10: Bed temperature measured without insulation**

It can be seen from Figure A-10 that after 140 min of heating the temperature of the bed materials only attained approximately 550°C, well below the desired temperature (700-800°C).

The same experiment was repeated but now using glass fiber insulation material (Knauf Earthwool 1000 Pipe Insulation), and the bed temperature was measured and displayed in Figure A-11.



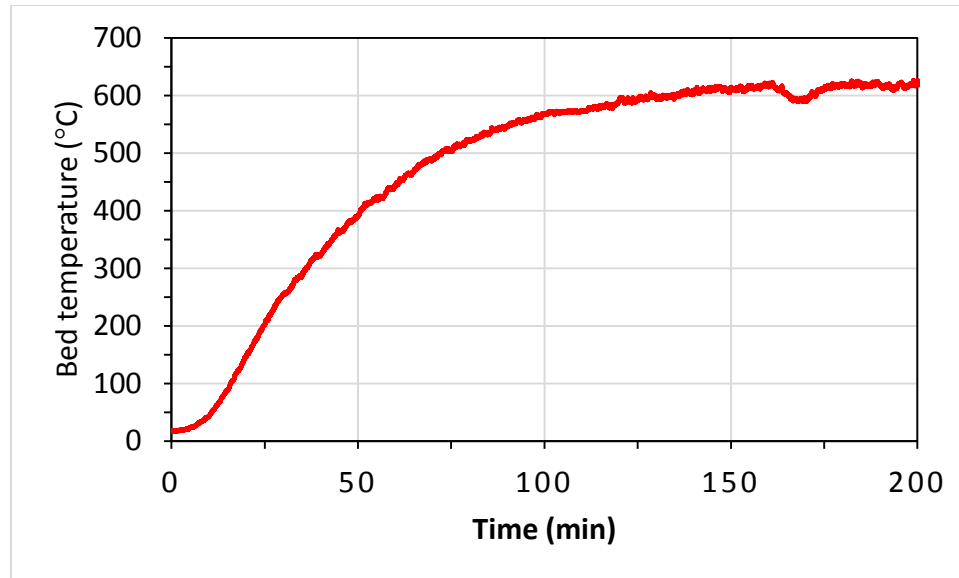


**Figure A-11: Bed temperature measured with glass fiber insulation material**

As shown in Figure A-11, the final bed temperature ( $\sim 600^{\circ}\text{C}$ ) measured after 140 min heating of the reactor system with glass fiber insulation was about  $50^{\circ}\text{C}$  higher than that obtained without insulation (Figure A-10). However, this final bed temperature is still below the desired temperature for biomass combustion and gasification ( $700\text{-}800^{\circ}\text{C}$ ).

**Problems detected:**

- 1) The bed temperature was being measured using the thermocouple TC#1 (Figure A-1), which was placed 2.5 inch above the distributor and outside of the heater. Because the thermocouple was very close to the distributor, the fluidization air coming from the air pre-heater at a lower temperature could cool the thermocouple and as a result the measured bed temperature was not accurate;
- 2) The temperature of the pre-heated air at the exit of the pre-heater was not monitored;
- 3) The fibre glass insulation material does not seem to be much effective. Other insulation materials shall be tested.

In order to fix the above problems, it was decided to do the following modifications:

- Bending TC#1 as is shown in Figure A-12, to position the tip of the thermocouple inside the heater's heating zone and farther away from the distributor (approx. 5.5 inch above the distributor);
- Installing a new thermocouple (indicated as TC#7 in Figure A-1) at the exit of the air pre-heater;
- Installing ceramic fiber insulation material.

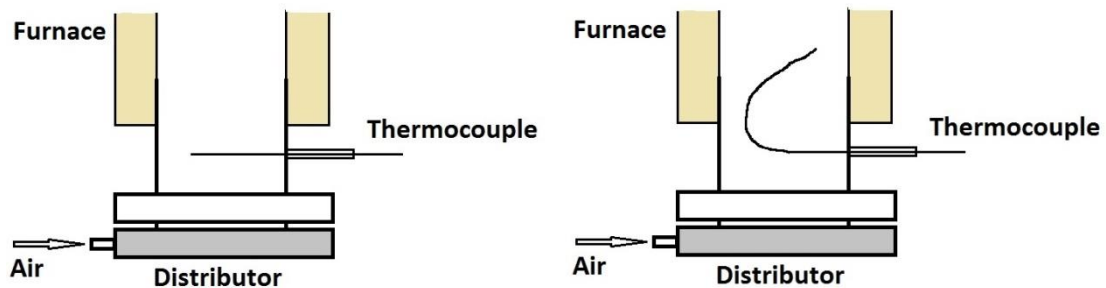


**Figure A-12: Bed material temperature measurement**

Figure A-13 shows the temperatures of the bed materials and the pre-heated air at the exit of the air pre-heater after the abovementioned modifications were done. It can be seen from Figure A-13 that after 110 min of heating the bed material attained approximately 765°C and the fluidization air at the exit of the pre-heater went up to approximately 350°C. These results show that the modifications performed to the reactor were successful and the bed materials could be successfully heated up to the desired temperature range (700-800°C) within 2 hours.

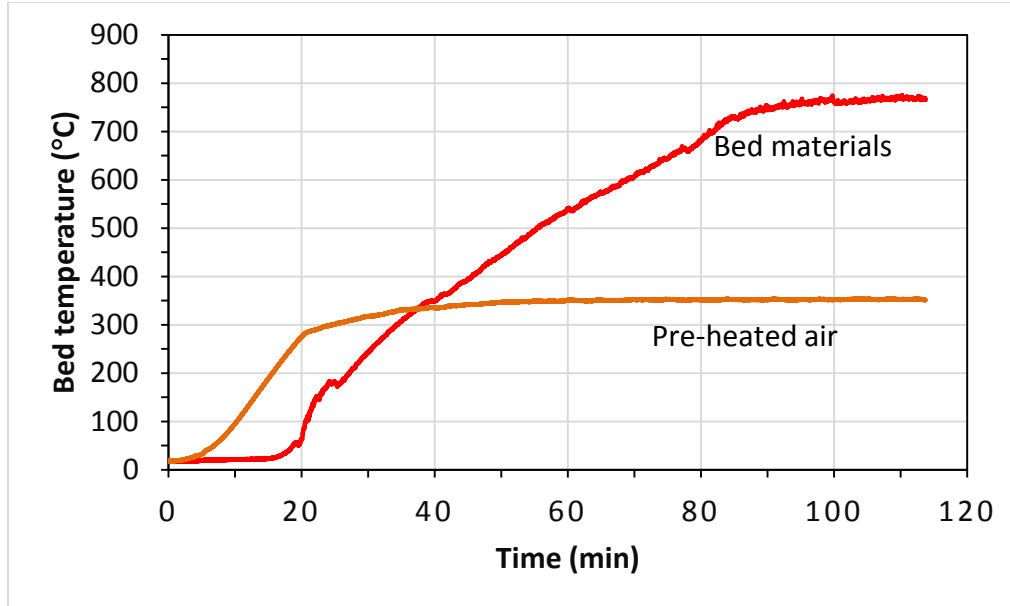


**Figure A-13: Bed material temperature with ceramic insulation and fluidization air temperature at the exit of the small furnace**

## A.5 Operation Procedures

The following operation procedures describe the main steps followed in the experiments presented in Chapter 4 and include mainly 3 stages of operation, warming up, steady-state operation and cooling down/shutting down (taking as a supposed that the reactor is clean):

*Warming up:*

Step 1: Select the static height of the bed.

Step 2: Charge the reactor with the selected bed material in order to achieve the selected static height of the bed using the feeding system.

Step 3: Charge the feeding system with the synthetic ash compounds or the biomass feedstock, depending on the tests conditions. It shall be noted, in the tests as reported in Chapter 4 the synthetic ash compounds (e.g., KOH) were pre-mixed

with the bed materials and were fed into the reactor directly from the ash sampling port at the top of the freeboard zone due to the operational challenges caused by the synthetic ash compounds (becoming cohesive while absorbing moisture) and the very small addition amounts in the tests.

Step 4: Turn on, the screw feeder, the rotary valve and the vibrator, to feed the materials into the bed column.

Step 5: Open and set the pressure regulator at around 50 psi (keeping in mind the maximum pressures at which the flow meters can be exposed) that supplies air to the flow meters. Open the flow meter and set the corresponding gas flow rate according to the desired superficial gas velocity. Check all the pressure gauge and make sure that the pressure is stable, without increasing continuously.

Step 6: Turn on the cooling water system. This protects the rotary valve and when biomass combustion or gasification tests are operated, this will allow to condensate the tar in the condenser.

Step 7: Start the data logging program to record the temperatures and pressures on the computer.

Step 8: Turn on the air pre-heater furnace and the main heater for the bed material, set the set-points for both temperature controllers according to the experimental conditions, in order to warm up the reactor.

*Steady-State operations:*

Step 1: Record the time when the desired temperature is reached and stabilizes.

Step 2: Monitor the temperature and pressure readings in the computer software and on the pressure gauges.

*Cooling down/shutting down*

Step 1: Set the set-points of both temperature controllers at room temperature. Do not turn off the controllers because it can affect the thermocouples reading.

Step 2: Open the secondary air inlet and set it in the maximum flow.

Step 3: Open the furnaces (both are split-hinge tube furnaces) to speed up the cooling, when the temperature is less than 250°C.

Step 4: Discharge the bed materials from the column into a container when the bed temperature drops to the desired temperature that is considered safe for the container. (For example for the LDPE containers, the maximum temperature is around 50°C)

Step 5: Collect the entrained fine particles in the cyclone and weigh the collected particles.

Step 6: Increase the primary air flow rate to 120 scfh.

Step 7: Turn off the temperature controllers of the tube furnaces, the cooling system, and the data acquisition system.

Step 8: Shut down the air supply, close the flow meters, and lose the pressure regulator.

Step 9: Sieve and weigh the bed material to evaluate the agglomerates of the bed materials.

The above operation procedures can also be applied for combustion/gasification experiments, but with little modifications in the feeding, and management of the air inlets.

## A.6 References

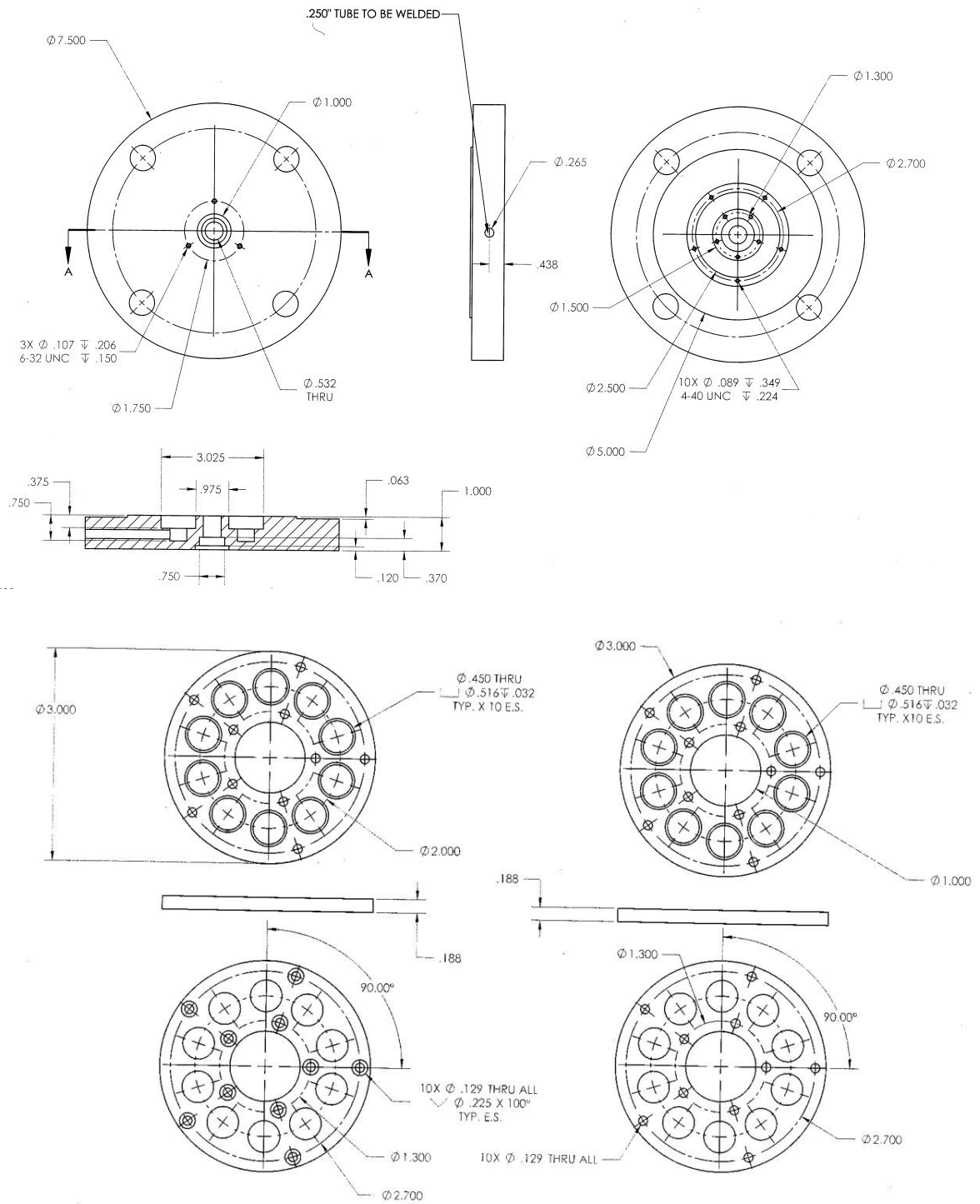
Leva, M. (1959). *Fluidization*. New York: McGraw-Hill.

Richardson, J., & St Jeronimo, M. (1979). Velocity-voidage relations for sedimentation and fluidization. *Chemical Engineering Science*(34), 1419-1422.

Thonglimp, V., Hiquily, N., & Lagueira, C. (1984). *Powder Tech*, 233-253.

Wen, C., & Yu, Y. (1966). A generalized method for predicting the minimum fluidization velocity. *AIChE Journal*(12), 610-612.

## A.7 Distributor Dimensions



## Curriculum Vitae

- Name:** Alejandro Montes
- Post-secondary Education and Degrees:** University of Chile  
Santiago, Chile  
1998-2005 B.E.Sc, Chemical Engineering.
- University of Chile  
Santiago, Chile  
1998-2005 B.E.Sc, Biotechnological Engineering.
- The University of Western Ontario  
London, Ontario, Canada  
2012-2014 M.E.Sc.
- Honours and Awards:** Western Graduate Research Scholarship  
Faculty of Engineering, Western University.
- Related Work Experience** Graduate Research Assistant  
Institute for Chemical and Fuels from Alternative Resource  
The University of Western Ontario  
2012-2014
- Publications:**  
Cifuentes, L.; Montes, A.; Crisóstomo, G. (2011), Corrosion behaviour and catalytic effectiveness of Pb-Ca-Sn, RuO<sub>2</sub>-IrO<sub>2</sub>/Ti and IrO<sub>2</sub>-Ta<sub>2</sub>O<sub>5</sub>/Ti anodes for copper electrowinning Source: Corrosion Engineering, Science and Technology
- Montes, A; Hamidi, M; Briens, C; Berruti, F; Xu, C; Tran, H; “Study on the critical amount of liquid for bed materials agglomeration in a bubbling fluidized bed”, To be submitted to Chemical Engineering Science journal
- Montes, A; Xu, C; Tran, H; Study of bed materials agglomeration in a heated bubbling fluidized bed (BFB) using silica sand as the bed material and KOH to simulate molten ash
- Conference presentations:**  
Increasing energy and chemical recovery efficiency in the kraft process – III. November 6 - 8, 2012



Increasing energy and chemical recovery efficiency in the kraft process – III. November  
5 - 7, 2013